University of London

SENATE HOUSE MALET STREET WC1E 7HU

Tel. 071- 636 8000 • Fax 071- 636 5874

With the compliments of

Examinations Division

PREPARATION OF ALLOYS FOR GLASSY METAL PRODUCTION

BY

Mohammad Ali MESHKOT

A THESIS SUBMITTED FOR THE DEGREE OF DOCTOR OF PHILOSOPHY OF THE UNIVERSITY OF LONDON AND FOR THE DIPLOMA OF IMPERIAL COLLEGE.

Department of Materials Science
Imperial College of Science, Technology and Medicine
London SW7.

MARCH 1991

ABSTRACT

Glassy metals are metallic materials with an amorphous structure. They can be produced by alloying transition metals with semi-metal (metalloid) elements and cooling from the melt at rates in excess of 10^6°C/s. Glassy metal alloys are commonly prepared by melting together elements in the required proportions or by diluting a mother alloy prepared in this way.

The aim of this work has been to prepare glassy metal alloys (metallic glass) more efficiently and more economically by the reduction of metalloid oxides to their elements and dissolution of the metalloid into the melt by a single step process involving submerged powder injection.

To achieve this aim three powder mixtures were used to investigate the preparation of Fe-B-Si alloys with boron and silicon components below 5%. The three powders being mixtures of silicon-carbide/boron-oxide, ferrosilicon / boron-oxide and aluminium/boron-oxide.

For preliminary experiments to investigate the feasibility of the process and to obtain working parameters for injection experiments, an induction furnace with 300 cm^3 charge capacity, a working temperature of 1600°C and controllable atmosphere was designed and built. For the injection of powders into molten iron, a simple high pressure batch type powder feeder capable of variable rate delivery to a depth of up to 0.5 m was designed and built.

The said powders were plunged as 50 g packets and injected at carrier-gas flow rates of 10 and 20 l/min into 1.5-2 kg of molten iron at various depths.

TABLE OF CONTENTS

ACKNOWLEDGEMENT

I am very grateful to my supervisor Professor Paul Grieveson for his valuable guidance and support throughout this project.

I would also like to thank Dr B. S. Terry for his advice during my first year and Mr A. J. Tipple for his practical advice on the use of high temperature materials. Thanks are due to Mr A. P Willis for his help with some of the final experiments.

Borax Holdings Limited partly supported this SERC CASE award for which I am grateful and to Dr. W. J. Rosenfelder for his visits.

I thank Foseco International Limited for supplying the experimental powders and for their help with the chemical analysis.

LIST OF FIGURES

LIST OF TABLES

LIST OF GRAPHS

1. INTRODUCTION

Amorphous Metals are metallic materials similar in electrical conductivity and sheen to a typical metal and at first sight there is no apparent difference between a piece of amorphous metal and a normal metal of the same composition and shape. Yet amorphous metals lack long range atomic order similar to oxide glasses. Amorphous metals are metallic non-crystalline solids lacking long-range periodicity of the atomic arrangement.

Amorphous metals may be produced by many methods such as the following:

1) Evaporation - Direct evaporation by heating of metal or alloy onto a substrate.

2) Sputtering - Condensation onto a substrate of secondary cathodic emission caused by ionic bombardment of a cathode

3) Chemical Vapour Deposition (C.V.D.) - Condensation of gases or vapours from a carrier gas onto a substrate on which controlled chemical reactions or atomic combination may take place to produce an alloy.

4) Rapid Solidification - Cooling of metals or alloys from the molten state to the solid state by quenching at rates of greater than 10^4 degrees per second.

Production of glassy metals by rapid solidification yields the highest rate and amorphous metals produced by such high volume fast quenching techniques are distinguished from the product of other methods, such as those described in 1, 2 and 3 above, by using a different name. Amorphous metals produced by quenching from the melt are called Metallic Glass.

This project is concerned with the preparation of Metallic Glass type amorphous metals, and in particular those iron-based alloys which exhibit interesting magnetic properties and which can be produced in commercially usable forms such as ribbons, strips or wires. The technique developed during this project may also be applicable to other amorphous metal alloys.

One consequence of amorphous metal production by rapidly quenching the melt is that the high rates of cooling required necessitate at least one dimension of the quenched product to be small in relation to the other two. Hence thin strips, wires, flakes and such shapes are produced with typical dimensions being 30-50 microns thick and 5-10 cm wide. At least one dimension has to be small in order to facilitate rapid cooling.

Metallic glasses in a usable form are a recent development with respect to other industrial materials, with properties that set them apart from other materials. Their atoms are bound by long-range metallic bonding which, unlike covalently bound silicate glasses, gives them malleability and sheen with electrical conductivities similar to that of liquid metals. They are not brittle like silicate glasses and they exhibit considerable ability to deform plastically.

A non-crystalline solid may be expected to exhibit far lower densities than the crystalline solid of the same composition, yet metallic glasses have densities comparable to that of their crystalline form. Iron-based glasses are as hard as steel, yet unlike steel they are extremely soft ferromagnets, and this ability to conform magnetically to an applied external magnetic field is one of their most important properties which has made them commercially important.

Since metallic glasses are free from grain boundaries and some are exceptionally soft magnetic materials, they are ideal candidates for use in transformers, motors, generators and other electromagnetic devices.

The Allied Corporation of the United States was the first to produce commercially available metallic glass under the trade name of METGLAS. This corporation has been one of the world leaders in this field since the 1970s with over 100 U.S. patents in its name.

The major work on METGLAS products have been the development of new compositions, characterization and assessment of their properties.

In recent years, iron-based metallic glass alloys with composition in the range Fe-B-Si with metalloid atoms making up greater than 15% of the total weight have given rise to a great deal of interest in the power industries. This is chiefly due to the superior magnetic properties of these materials and the energy saving that can be achieved by using them.

In the United States alone over 100 bn KWh of electricity per year are attributed to core losses in major power generation and consumption equipment. The industry believes that at least 75% of this costly loss can be eliminated by the use of metallic glass for core materials (Rosenfelder, W. J. 1986).

The most common composition of metallic glass magnetic alloy is 92% Fe - 3% B - 5% Si (by weight) (Rosenfelder 1983). This is produced from high purity Ferroboron (FeB), Ferrosilicon (FeSi) and electrolytic iron (Fe). The components may be heated in a submerged electric arc furnace to yield the desired composition. It is estimated that the production of this type of alloy was 20,000 tons/annum for 1986 rising to 400,000 tons/annum by 1994 (Rosenfelder, W. J. 1983).

The present day use of these magnetic alloys is restricted by their cost. Although energy saving, metallic glass magnetic core materials cost about 4 times more than the traditional grain orientated 3% Silicon steel, with the bulk of this cost being attributed to the FeB component of the material.

The industrial emphasis at present is to reduce the cost of these alloys by half so that metallic glass alloys become a more viable product.

The aim of this project was to investigate the reduction in cost of magnetic metallic glass alloy production by achieving the desired composition via other routes. It is proposed that the Fe-B-Si alloy composition be prepared by direct Carbothermic, Aluminothermic or Silicothermic reduction of Boron oxide into an iron melt by following one of the these reactions:

$2\ B_2O_3$ (Slag) +	3 C (%)	=	4 B (%) +	$3\ CO_2$ (g)	(1.1)
$2\ B_2O_3$ (Slag) +	3 Si (%)	=	4 B (%) +	$3\ SiO_2$ (Slag)	(1.2)
$2\ B_2O_3$ (Slag) +	2 Al (S)	=	4 B (%) +	Al_2O_3 (Slag)	(1.3)
$3\ SiO_2$ (Slag) +	4 Al (S)	=	3 Si (%) +	$2\ Al_2O_3$ (Slag)	(1.4)

Hence the boron and silicon may be dissolved interstitially into the iron.

Two operational methods are proposed for these reactions:

(1) Injection of particles into the iron melt using a carrier gas. The particles will contain a core of the reducing element covered by a layer of B_2O_3, such that on reaching the iron melt, the rise in temperature will cause the reduction of B_2O_3 to take place before the reductant comes into contact with the melt.

(2) Plunging packets of the (B_2O_3 + reducing-agent) mixture into molten iron so that reduction of the B_2O_3 takes place before the packet of powder is dispersed. The reductant may also be contained in the melt or in a slag, where it is made to reduce the B_2O_3 by providing the appropriate temperature and stirring to produce the desired dissolution of boron into the melt.

An important part of this project has been the practical aspect of overcoming experimental difficulties involved in powder injection and packet plunging. An apparatus suitable for injection of powders into molten iron was designed and built so that reduction with various powder compositions could be investigated.

2. SUBJECT REVIEW

2.1 > BACKGROUND

The interest following the advent of a new class of material together with commercial forces have given rise to an exceptional growth in the publication of literature relating to amorphous metals over the last two decades with over 1000 publications on this subject each year. It is not the aim of this section to review the available literature on the subject of metallic glass, but merely to give a brief insight into the main areas and to show some of the important properties.

Normal quenching of crystalline materials from the melt produces metastable phases. This principle is widely used by metallurgists and the best known example is the achievement of hardness in Carbon steels where the formation of the equilibrium phases of carbon are prevented by quenching.

In January 1960 Professor Pol Duwez (Duwez 1960) and his co-workers reported the preparation of metastable phases in Copper-Silver alloys by quenching from the melt onto a rotating Copper surface. A solid surface was used because liquid quenching produces a gas layer of poor thermal conductivity which hinders heat loss, and the target was rotating to improve contact between the melt and the cooling surface by centrifugal force. A United States Patent awarded to R. B. Pond in 1958 also describes improved contact with the substrate by the use of centrifugal force.

During September of 1960 the same group of workers (Klement, W. et al, 1960) reported amorphous gold-silicon alloys produced by a 'gun' technique described by them elsewhere (Duwez, P. et al, 1963) in which molten metal is ejected from an orifice by a shock wave.

In 1972 H. Chen and D. E. Polk (U.S. Patent 3 845 805) of the Allied Chemical Corporation reported making the first ductile glassy ribbon of ferrous alloys. Since then the advantages of metallic glass have been recognized leading to a growing number of international conferences on the subject (Rapidly Quenched Metals, 1978; Metallic Glasses Science and Technology, 1980; Rapidly Quenched Metals, 1984).

2.2 > GLASS FORMING SYSTEMS

Extensive work on amorphous metals has shown that alloying results in easier glass formation and more stable glasses. A review of amorphous metal structures and their formation is conducted by S. Takayama (1976) which includes a comprehensive list of glass forming compositions. T. Massumoto and R. Maddin (1975) published a representation of the glass forming compositions based on the periodic table, and H. Jones (1983) categorizes such compositions into three groups. The grouping of Donald E. Polk and C. Giessen (1976) is slightly different and is represented in table 2.2.1.

The Fe-B-Si alloy that this work concentrates on, is a member of the first major system according to the classification of table 2.2.1, the T^2+X group, where T^2 is a late Transition metal and X is a metalloid(s). In the case of Fe-B-Si two metalloids are used and Anantharaman (1984) confirms the use of a second metalloid to improve glass-forming ability and to increase the composition range.

2.3 > STRUCTURE

The very nature of amorphous metals makes structure determination of such materials a difficult task. Diffraction and Electron Microscopy are the major tools for direct structure determination, yet inherent in these techniques is that smaller grain size produces a more diffuse diffraction maxima such that it becomes difficult to distinguish between microcrystalline and amorphous structures (Sinha, A. K. and Duwez, P., 1971)

Three structural models have been proposed for metallic glass structures. The first is microcrystalline (Cargill III, G. S., 1975) consisting of microcrystals identical in atomic configuration to that of a small volume from a normal three dimensional crystal and with amorphous matter in between. The orientation of these small crystals and often the boundary layer structure is not defined. In order to avoid confusion of the term Microcrystalline here with that commonly used in metallurgy, it is proposed (Polk, D. E. and Giessen, B. C., 1976) that the term nano-crystalline be used for the 10 Angstrom range into which metallic glass falls.

The "Continuous Random" structure model is not a new idea and this model is also covered by Cargill (1975). This is the Dense Random Packing of Hard Spheres (DRPHS) which is the basis for amorphous metal structure models. Statistically the structure is said to be homogeneous on the 10 Angstrom scale and so this avoids the boundary region of the above model.

The third model, "Noncrystallographic Cluster" (Davis, L. A., 1976) consists of highly ordered discrete regions as in the first model, but in this case the ordered regions have symmetrical elements especially five fold rotation axis which prevent them from forming long range order.

The metal-metalloid system, which includes Fe-B-Si metallic glass alloys with about 80 atomic % metal, are proposed (Polk, D. E., 1970) to consist of a Bernal (DRPHS) structure with the metalloids filling some of the larger holes inherent in random packing, hence resulting in the stabilization and increased density of the amorphous structure.

2.4 > PREPARATION OF METALLIC GLASS

A brief description of the industrial process for making the Fe-B-Si composition has been given in section 1 and elsewhere (Rosenfelder, W. J., 1983). Chen et al. (1974) describe a three stage process in a U.S. patent whereby one metalloid is sintered with the iron, then melted in vacuum and the second metalloid addition is made. This alloy is re-melted for homogeneity before rapid cooling.

Having achieved the desired composition through melting of the constituent pure elements together or by reducing the metalloid component from its oxide, the next stage in the production of metallic glass is rapid solidification of the alloy. Many techniques have been described elsewhere for rapid solidification (Jones, H., 1983 and Davis, L. A., 1980). A few industrial processes which produce useful shapes will be discussed below.

A) The twin roller technique described by Chen and Miller (1970) (see figure 2.4.1A) was the first process capable of producing continuous ribbons. In this process a stream of molten metal is fed through the nip of two rollers rotating rapidly in opposite directions. The rollers rapidly cool the melt and can form continuous ribbons or sheet from the solid.

B) Melt Spinning covers a whole range of processes which are used for producing wire of ribbon at output rates of 100's of meters per minute. The principles of and variations in this group of processes have been adequately described elsewhere (Pond, R. and Maddin, R., 1969; U.S. Patent 3 845 805; Schile, R. D., 1970). Essentially a stream of molten metal is directed at a fast moving substrate to produce ribbons or wires 20-30 microns thick (see figure 2.4.1B).

C) Melt Extraction (Maringer & Mobley, 1974; Nakagawa and Suzuki, 1977) is a process whereby the circumference of a rotating disc is immersed into a molten bath of alloy (Figure 2.4.1C). The disc rotation causes a stream of metal to be extracted from the melt which solidifies into a continuous wire or strip form depending on the disc profile at the circumference and its width.

D) Three similar methods of producing metallic glass ribbons are the Pendant Drop method (Maringer & Mobley, 1976) (see figure 2.4.1D), the Melt Drag method (Hubert et al. 1973) and the Planar Flow Cast (PFC) process (Narasimhan, 1979) (figure 2.4.1E). In these techniques a moving substrate removes and solidifies a molten drop or meniscus from the tip of a nozzle held close to it. PFC is a more modern process whereby the melt is forced onto the substrate by gas pressure. This technique has been further improved by automation recently (Vogt, 1986).

In all liquid quenching techniques the cooling rate is of prime importance since it determines whether or not a particular amorphous metal can be produced. The cooling rate is a difficult factor to measure considering the process speed and the small volume of material being cooled at any one time. It is susceptible to fluctuations at any point and variations along the dimensions of the shape being produced.

Theoretical predictions have been made on the cooling rates (Jones, H. 1973) but in reality the cooling rate is very much dependent on the heat transfer coefficient which is affected by such factors as trapped gas, adhesion to substrate and oxide film formation. The cooling rate of metallic glass also effects its properties which are discussed in the next section.

2.5 > PROPERTIES

Many aspects of amorphous metal properties have been investigated for various compositions of possible commercial interest. In this section the basic thermal, mechanical and magnetic properties will be briefly discussed. More attention will be given to Fe-B and Fe-B-Si compositions and their magnetic behaviour will be discussed more fully.

By way of introduction tables 2.5.1 and 2.5.2 from Anantharaman (1984) give a general overview of the properties. Table 2.5.1 gives a qualitative comparison between metals, oxide glasses and metallic glasses, while table 2.5.2 compares the mechanical properties.

2.5.1 >> THERMAL PROPERTIES

Glass is a metastable state which has a tendency to crystallize. The crystallization temperature (T_x) of a specific glass will depend on its internal energy. The higher this internal energy, the greater is the tendency to crystallize. Composition and cooling rates are the main factors effecting the internal energy.

The Glass Transition Temperature (T_g) is the temperature at which plastic deformation of amorphous metals can occur and this temperature may be above or below the crystallization temperature depending upon the cooling rate and composition of the material.

A more stable metallic glass will show viscous flow before the onset of crystallization ($T_g < T_x$). The parameter ($T_x - T_g$) can be used as a measure of the stability of metallic glasses. Metallic glass crystallization temperatures range from 100-700°C with typical values being around 400°C. The crystallization temperature can be increased by the "Confusion" principal which means increasing the number of components in order to prevent crystallization and induce stability. This principal has lead to such compositions as $W_{35}M_{20}Cr_{15}Fe_5Ni_5P_6B_6C_5Si_3$ (Anantharaman, 1984) with a crystallization temperature of 1225 K.

Iron-boron metallic glass is one of the more stable compositions in which spherulitic crystallization has been observed to take place between 300 and 450°C (Koster et al., 1978 and Davis et al., 1976). This composition is important for its magnetic properties and to enhance these properties the material is stress relieved at 200-250 °C (Davis et al., 1976). This relaxes the structure, causes an increase in the density and reduces the defect concentration, but it also leads to embrittlement (Jones, H. 1983).

2.5.2 >> MECHANICAL PROPERTIES

Metallic glasses have high strength, some higher than any ferrous metal, they are hard with a high flow stress and do not work-harden since there are no grain boundaries. Mechanical properties of metallic glass are reviewed elsewhere (Massumoto, 1976 and Davis, L. A., 1977).

Iron-boron metallic glass has equivalent shear and yield stress, the yield stress being as high as 3.7 GPa (Davis et al., 1976). Table 2.5.2.1 shows a comparison between mechanical properties of some commercially available metallic glass compositions, and it can be seen from this table and table 2.5.2 that Fe-B compositions are more than twice as hard and almost twice as strong as steels.

2.5.3 >> MAGNETIC PROPERTIES

A ferromagnetic material will respond to the application of an external magnetic field by the alignment of its magnetic domains along the direction of the applied field. The Hysteresis curve of figure 2.5.3.1 shows how a typical ferromagnetic material may respond. As the external field strength H increases, the material reaches a saturation flux density B_s when all its domains are aligned with the external field direction. When the external field is removed, a residual magnetization flux B_r remains. To remove this residual magnetization, an external field in the opposite direction must be applied of strength $-H_c$, hence H_c is known as the Coercive force of the material.

Metallic glasses of differing compositions can be made Ferromagnetic (when all the magnetic domains point in the same direction), Diamagnetic (magnetization in the opposite direction to the applied magnetic field) or Anti-ferromagnetic (alternate magnetic domains pointing in opposite directions) (Gilman, 1975).

A soft magnetic material is one that is magnetized and demagnetized easily, that is, using a low external field strength. Eghami et al. (1975) were the first to give evidence of soft magnetization in amorphous metals, and this behaviour is attributed to the lack of grain boundaries in the structure which would otherwise 'pin-down' magnetic domain boundaries making realignment difficult. Luborsky et al. (1975, 1976A) investigated the influence of stress relief and found that a typical annealing of one hour at 300 °C would improve magnetic properties. As a side effect this was found to induce embrittlement (Ast et al., 1976; Luborsky et al., 1976B; Davis et al., 1976; Pompillo et al., 1978). F. E. Luborsky (1980) has discussed the ferromagnetic properties of metallic glass and P. Duwez (1967) that of iron-rich amorphous metals.

Iron-boron and Fe-B-Si compositions are ferromagnetic with a typical Curie temperature of about 380 °C. They can achieve 80% of the magnetization of pure iron with the advantage of a low coercive force H_c (Stewart, 1983).

The addition of carbon to the iron-boron composition was investigated (Hatta et al., 1978) in order to increase B_s at room temperature, but this addition was found to cause thermal instability in the $Fe_{86}B_8C_6$ metallic glass. Instead replacement of the boron by silicon was found to increase B_s at room temperature when the iron content is 80 at.% (O'Handley, 1979 and Luborsky, 1979).

The relationship between cooling rate and magnetic properties of Fe-B alloys were investigated by P. Vojtanik et al. (1980) and show a large influence of cooling rate on magnetic susceptibility. Although direct evidence has not been found, this influence is expected to be much weaker for Fe-B-Si alloys due to the confusion principle.

Table 2.5.3.1 gives a comparison between magnetic properties of metallic glasses and some crystalline alloys. For metallic glasses the saturation magnetization is reasonably high although lower than crystalline alloys. The Curi temperatures are lower due to the disordered arrangement of the atoms, and the high electrical resistivity reduces eddy current losses.

GROUP (a)	REPRESENTATIVE SYSTEM	TYPICAL COMPOSITION ATOMIC %	PREPARATION METHOD
Major Systems			
T^2 (or noble) metal + metalloid (X)	Pd-Si, Co-P, Fe-P-C, Ni-P-B	15-25 X	LQ, ED
T^1 metal + T^2 metal	Zr-Cu	30-65 Cu	LQ, SP
(or Cu)	Y-Cu, Ti-Ni	30-40 T^2, Cu	LQ
	Nb-Ni, Ta-Ni	30-65 Ni	LQ, SP
Miscellaneous systems			
A metal + B metal	Mg-Zn	25-35 Zn	LQ
T^1 metal + A metal	(Ti-Zr)-Be	20-60 Be	LQ
Actinide + T^1 metal	U-V, U-Cr	20-40 T^1	LQ

A metal = Li, Mg groups
B metal = Cu, Zn, Al groups
T^1 metal = early transition metal (Sc, Ti, V groups);
T^2 metal = late transition metal (Mn, Fe, Co, Ni groups)
metalloid = B, C, Si, Ge, P
LQ = liquid quenching, ED = electrodeposition, SP = sputtering.

TABLE 2.2.1 : Alloy systems that form metallic glasses by liquid quenching, based on chemical classification of constituents. (Polk, D. E. and Giessen, B. C. 1976)

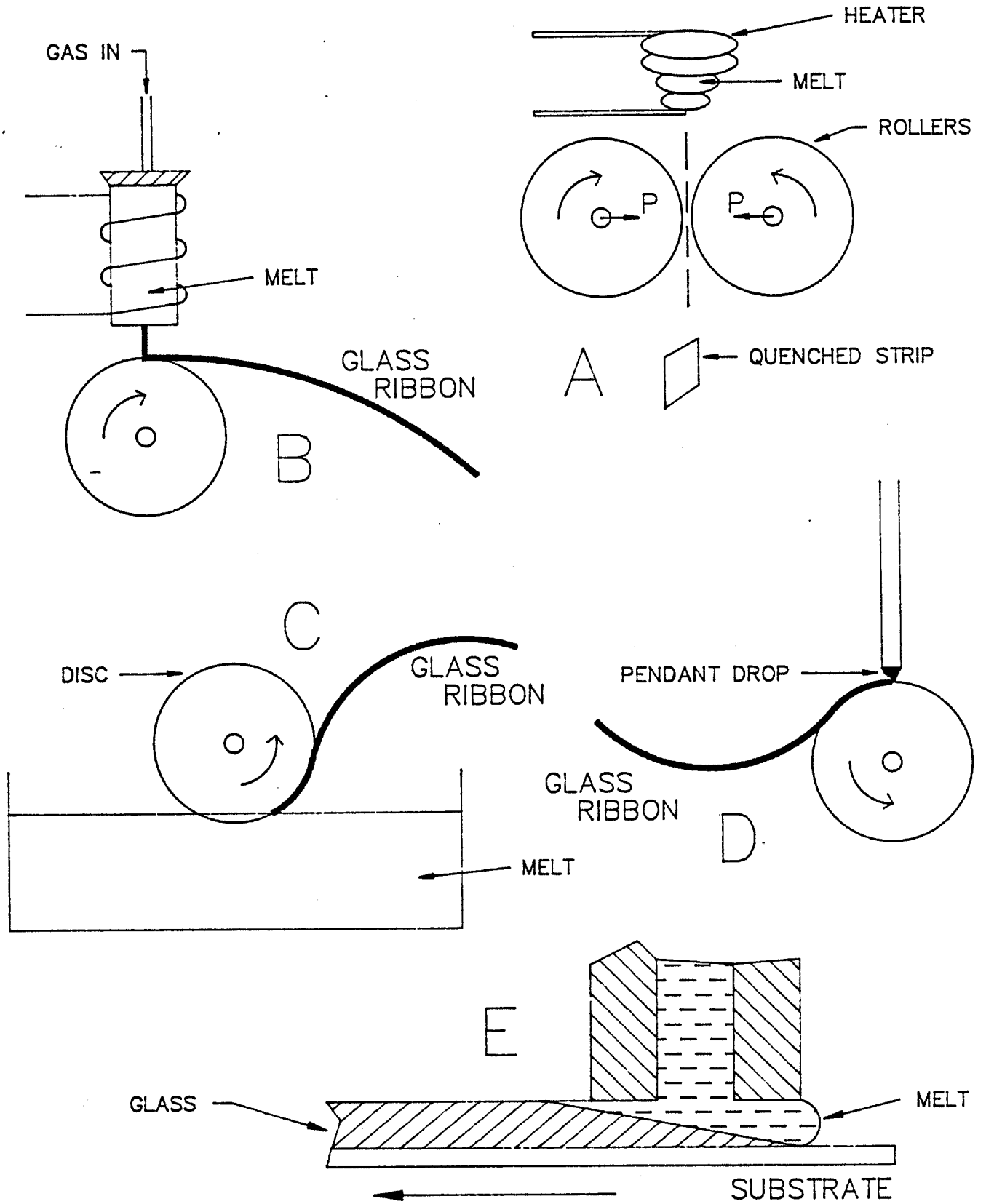

FIGURE 2.4.1 : Common methods of metallic glass production
A : The twin roller technique
B : Melt Spinning
C : Melt Extraction
D : The Pendant Drop method
E : Planar Flow Casting (PFC).

PROPERTY	TRADITIONAL METAL	TRADITIONAL GLASS	METALLIC GLASS
structure	crystalline	amorphous	amorphous
bonding	metallic	covalent	metallic
yield stress	non-ideal	almost ideal	almost ideal
workability	good, ductile	poor, brittle	good, ductile
hardness	low to high	very high	very high
UTS	low to high	low	high to v. high
optical transmission	opaque	transparent	opaque
thermal conductivity	very good	poor	very good
elec. resistance	very low	high	very low
corrosion resistance	poor to good	very good	very good
magnetic properties	various	non-existent	various

TABLE 2.5.1 : Comparison between traditional metals, oxide glasses and metallic glasses. (Anantharaman, T. R., 1984)

Alloy	Vickers Hardness ($kgmm^{-2}$)	Yield Strength ($kgmm^{-2}$)	Density (gcm^{-3})	Specific Strength (m)
METALLIC GLASSES				
$Pd_{77.5}Cu_6Si_{16.5}$	500	160	10.30	15200
$Zr_{50}Cu_{50}$	580	180	7.33	24700
$Ti_{60}Be_{35}Si_5$	805	253	3.90	65000
$Fe_{80}P_{16}C_3B_1$	835	250	7.30	34100
$Fe_{80}B_{20}$	1100	370	7.40	50000
$Co_{60}W_{30}B_{10}$	1600	360	-	-
$Fe_{60}Cr_6Mo_6B_{28}$	-	490	-	-
STEELS				
AISI 4340 [1]	450	170	-	-
18% Ni[2]	600	205	8.0	25600

TABLE 2.5.2 : Mechanical properties of metallic glasses compared with those of commercial steels (Anantharaman, T. R., 1984).

Alloy	Hardness H (kg/mm^2)	Yield stress Y_s (kg/mm^2)	H/Y_s	Young's Modulus E $x10^3$ (kg/mm^2)	E/Y_s
METGLAS 2605 $Fe_{80}B_{20}$	1100	370	2.97	16.9	45
METGLAS 2615 $Fe_{80}P_{16}C_3B_1$	835	249	3.35	13.8	55
METGLAS 2826B $Ni_{49}Fe_{29}P_{14}B_6Si_2$	792	243	3.26	13.4	56

TABLE 2.5.2.1 : Mechanical properties of some metallic glasses.

FOOTNOTES

1 0.42% C, 0.78% Mn, 1.79% Ni, 0.8% Cr, 0.33% Mo .

2 18% Ni, 8% Co, 3% Mo, 0.2% Ti, 0.1% Al .

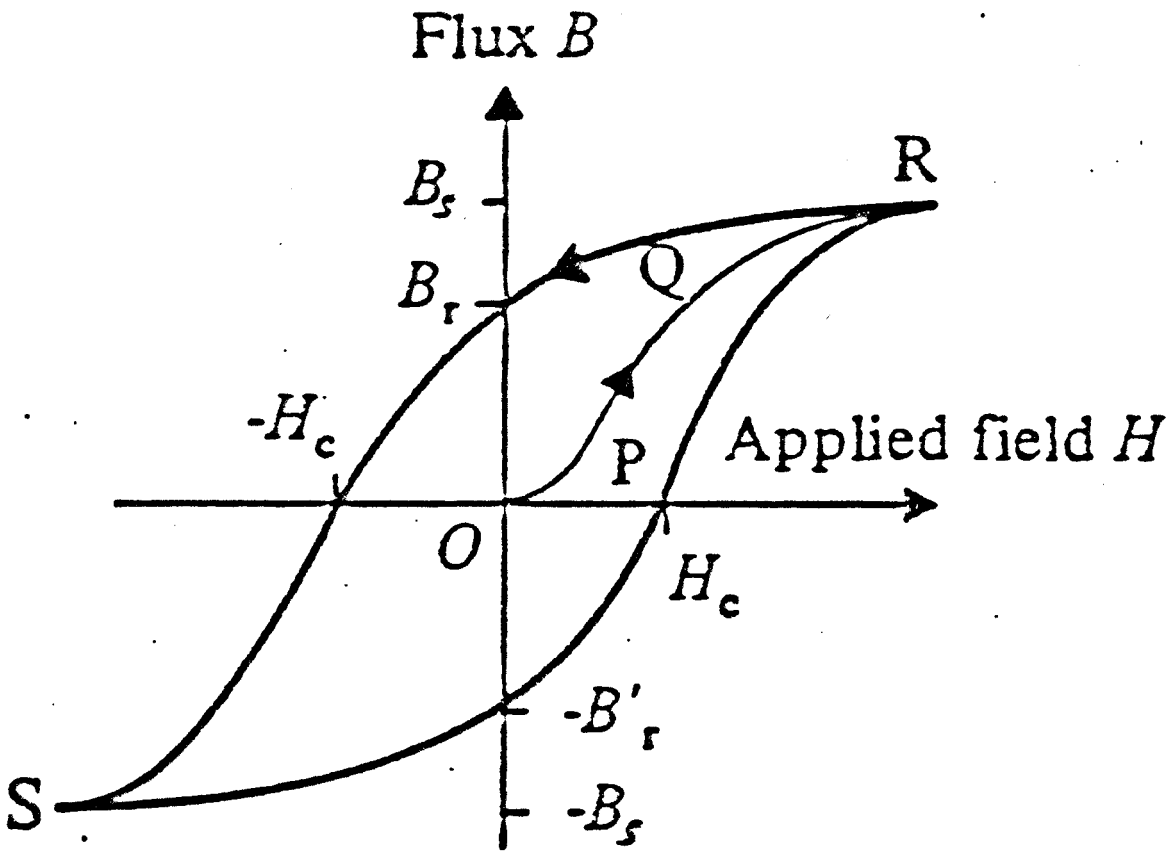

FIGURE 2.5.3.1 : The response of a typical ferromagnetic material to an external magnetic field.

ALLOY	B_S(kG)	T_C(K)	H_C(Oe)	Rho
metallic glasses				
$Fe_{80}B_{20}$	16	374	0.04	140
$Fe_{62.5}Ni_{15.5}Si_8B_{14}$	13.1	460	0.006	-
$Fe_{40}Ni_{40}P_{14}B_6$	8.3	250	0.007	180
$Co_{70}Fe_5Si_{15}B_{10}$	6.7	430	0.006	134
crystalline alloys				
Deltamax[3]	16	480	0.10	45
Square Permalloy[4]	18.2	460	0.028	55

B_S : saturation magnetization (kilo Gauss)
T_C : Curie temperature (Kelvin)
H_C : Coercivity (oersted)
Rho : Resistivity (micro Ohm cm)
where
1 kilo Gauss = 0.1 Tesla = 0.1 Weber m^{-2}
1 Weber = 1 Vs (JsC^{-1}) and
1 oersted = 79.58 Am^{-1} or 10^{-4} Tesla in vacuum

TABLE 2.5.3.1 : Magnetic properties of metallic glasses and crystalline magnetic materials (Anantharaman, T. R., 1984).

2.6 > APPLICATIONS

Many applications have been proposed for metallic glass compositions, but the most economic proposals must be those which find their way into production and sales. Metallic glasses of certain compositions (Hasegawa et al., 1978) deform elastically when an external magnetic field is applied to them (Magnetostriction), hence they are used as high frequency transducers.

---

[3] Deltamax : Fe-50%Ni

[4] Square Permalloy: Ni-16%Fe-4%Mo

Crystalline brazing rods for critical joints are brittle and can not be 'fitted' into the joint before heating. Metallic glass ribbons overcome this problem by their ductility and eliminate the use of paste or polymeric tapes.

Owing to their high strength, metallic glasses are used for replacement flywheel applications. They have high chemical and corrosion resistance due to their amorphous structure.

The following section describes how the desired amorphous alloys may be prepared by a single-step reduction and dissolution of the metalloid into the metal.

2.7 > THE PROPOSED METHOD

The basic process to be followed for obtaining the Fe(92)Si(5)B(3) (weight %) composition from the raw materials of iron and metalloid oxides is as follows:

Metalloid Oxide (in slag)	+ Reducing Agent (in slag/melt)	=	Metalloid (in iron)	+ Oxide of Reducing Agent (in slag)

.....Equation (2.7.1)

The most convenient and cost effective reducing agents for this process are carbon, silicon and aluminium, the reactivity of which will depend upon the experimental conditions. The use of each of these reducing agents will now be examined in turn.

The reader should bear in mind that the reactions discussed in this section are at high temperatures (above 1400 °C) and involve a molten bath of iron.

2.7.1 >> USING CARBON AS THE REDUCING AGENT

As discussed in section 2.5.3 the presence of carbon in the final alloy composition reduces the room temperature stability of the metallic glass of interest. Hence if carbon is to be used as a reducing agent, all traces of it must be removable from the alloy.

Substitution of carbon in the form of Graphite or Coal into equation 2.7.1 gives the following equation:

Metalloid Oxide (in slag) + C (s) = Metalloid (in melt) + $CO(g)/CO_2(g)$ ...(2.7.1.1)

Whether carbon Monoxide is produced as a product or carbon-dioxide depends mainly on the reaction temperature.

The metalloid oxides to be used for this reaction (B_2O_3, SiO_2) are solids and so the forward reaction rate is reduced by the presence of two solid reactants. This rate can be expected to increase substantially if an intermediate reaction is caused to occur which results in gaseous intermediate compounds as follows:

SiO_2 (s) + C (s) = SiO (g) + CO (g) .....(2.7.1.2)

then

SiO (g) + C (s) = Si % + CO (g) .....(2.7.1.3)

In this case the rate of formation of silicon monoxide becomes important. The other metalloid oxide B_2O_3 melts at about 730 K which is far below the melting point of iron at which most of these reactions are expected to take place.

2.7.2 >> USING SILICON AS A REDUCING AGENT

Silicon can be used as a reducing agent when it is dissolved or stirred into the iron. Ferrosilicon (70-80% Si) is a readily available industrial product. The reaction by which the second metalloid in introduced into the melt may be as follows:

$2B_2O_3 + 3\ Si\% = 4\ B\% + 3\ SiO_2$ .....(2.7.2.1)

It is possible to obtain the metallic glass composition Fe(92%)-Si(5%)-B(3% by wt.) by a two step process whereby in the first step iron with excess silicon is used to reduce the boron oxide, and in the second step more iron is added to achieve the desired composition.

To achieve the metallic glass composition by a one step process requires either a low silicon solute concentration or the removal of excess silicon at the end of the reduction process. If excess silicon is not used, then the low silicon concentration will lower the reduction rate. This may then be remedied by either causing turbulence in the melt (bubble stirring with an inert gas) or by injection of boron oxide into the melt so as to increase the contact between B_2O_3 and the silicon in solution. It would be more desirable to use a one-step process.

A more efficient method still, would be the simultaneous dissolution of silicon and boron into the melt by using a powder mixture of SiC and B_2O_3 so that in a one step process CO/CO_2 is formed and both silicon and boron are dissolved in the iron as follows:

$3\ SiC + B_2O_3 = 3\ Si\% + 2B\% + 3\ CO$ .....(2.7.2.2)

2.7.3 >> USING ALUMINIUM AS A REDUCING AGENT

If Aluminium is used to reduce boron oxide and silicon, then it must be removable from the melt to as low as 0.01% by weight, since greater concentrations of aluminium would be detrimental to the magnetic properties of the final product (Rosenfelder, 1983).

Using aluminium metal would have two inherent problems. First it would oxidize in air to form a protective film which prevents exposure of the aluminium. Second, aluminium has a high affinity for iron, such that if it is dissolved in iron its ability to reduce the metalloid oxides is considerably diminished.

To overcome these problems it is proposed that powders developed by Foseco International Ltd. of Birmingham are injected into the iron melt using an inert carrier gas. These powders (particle size less than 1 mm) are made such that each particle contains a core of aluminium metal surrounded by a crust of boron oxide. When this powder is injected into a molten iron bath it is expected that the particle core will react with its crust before the aluminium comes into contact with iron as follows:

$$2\,Al + B_2O_3 = 2B\% + Al_2O_3\,(slag) \quad .....(2.7.3.1)$$

It is interesting to note that the melt silicon concentration problems encountered when using silicon as a reductant can be solved by injecting similar powders into the melt, but with a ferrosilicon core instead of aluminium.

Such powders with aluminium and ferrosilicon cores were received and both were injected into a molten bath of iron.

2.7.4 >> OTHER WORK IN THIS FIELD

A process for the attainment of Fe-B-Si alloys for the production of amorphous metals was described by R. C. Sussman and L. G. Evans (1986A and 1986B). This process most resembles the present work in that the inventors aim to produce the alloy by reduction of boron compounds such as B_2O_3 from the slag using reducing agents such as silicon, aluminium and carbon dissolved in the iron melt. In this case the melt and slag are mixed vigorously using Argon injection.

K. Seki et al. (1986) have described improvements to the electric arc furnace whereby iron-boron alloys are produced for metallic glass production. The improvements are concerned with better process control and improved purity of the end product.

In 1986 Hamada et al. disclosed a method of producing Fe-B-Si mother alloy which gives the desired Fe-B-Si metallic glass composition when the mother alloy is dissolved in iron. Their method of producing this alloy involves injecting iron ore and boron oxide powders into a coke-packed furnace using a carrier gas.

2.7.5 >> SCALE OF THE INJECTION EXPERIMENTS

If a process efficiency of 50% is assumed, then 6 g of boron would be required for each 100 g of iron. The various powders to be injected into molten iron contained boron oxide or Boric Acid in varying proportions ranging from 35% to 64% by weight. Boron oxide contains 31% boron by weight hence 60 g of powder would be required for 6 g of boron. The specific volume of a typical experimental powder based on the volume of a container it takes up, was about 1.5 ml/g, so that 60 g would take up 90 ml.

The powders to be injected contained a small percentage of boron, so a large volume of powder was required.

Because of the low boron content and the high volume of the supplied powders, it was most desirable to confine the iron mass for alloying to a small scale. On the other hand, the nature of the injection process dictates that a large experimental scale be used in order to achieve the desired depth of metal for the process, to prevent reaction between the crucible and the powders and to minimize the effect of metal loss from the crucible by splashing.

Table 2.7.5.1 shows details of the powders received.

POWDER	COMPOSITION	SIZE AND TREATMENT
SiC Mix	64.4% SiC 28.3% B_2O_3 7.3% H_2O	60-700 microns[5] sintered at 400 °C for 4 hours.
FeSi Mix	32.7% Si 10.6% Fe 31.9% B_2O_3 13.5% H_2O 9.1% CaF_2 2.2% unknown	125-800 microns sintered at 400 °C for 4 hours.
Al Mix	42.2% B_2O_3 27.9% Al 19.9% H_2O 7.2% CaF_2 2.8% unknown	125-800 microns sintered at 400 °C for 4 hours.

TABLE 2.7.5.1 : Showing the composition of each powder received and used in experiments.

5 63-150 mic.: 20%, 150-180 mic.: 20%, 180-710 mic.: 60%

3. EXPERIMENTAL

3.1 > APPARATUS

Two units of apparatus were designed, built and used. The first was a general purpose induction furnace and this was used to carry out initial experiments from which information about the injection and plunge processes were gained. The second unit was a powder feeder designed for submerged powder injection into molten iron.

During the design process, the following factors were a constant aim:

a) Simplicity of design

b) Safety in use

c) Low cost of building based on the use of readily available materials

d) Versatility to accommodate changes based on unforeseen problems

e) Practicality of construction so that it could be self made

3.1.1 >> INDUCTION FURNACE

The induction furnace is basically an elaborate heating chamber with a an induction heating coil around it (see figure 3.1.1.0). The water-cooled coil is connected to a high frequency generator to produce heat in a susceptor within the chamber by induced current.

The heating chamber in this case is a silica tube of 100 mm ID and 400 mm height with a water-cooled flange at each end. The heating coil is placed central and external to this tube. Below the lower flange is a base plate mounted on a trolley and above the upper flange is a Pyrex hood (see figure 3.1.1.1) containing a viewing port, two gas ports and two reactant ports. One of the gas ports is connected to a manometer and the other is used to carry away exhaust gases. Above the Pyrex hood is a split plate which can be set to exert a downward force on the hood in case experiments need to be done at positive pressures. The weight of the upper flange is supported by a platform which is held up using four support rods around the chamber and rising from the base plate. The same rods pass through the split plate for a compressive action. Figure 3.1.1.2 shows the split plate, the upper flange supporting platform and the support rods.

Gas input and vacuum facilities are housed below the base plate. Originally the manostats and regulators described in figure 3.1.1.3 were designed for use with this furnace, but a calibrated rotameter was found to give adequate accuracy. A needle valve controls the gas input rate and the chamber may be evacuated from below if required. A further port through the base plate is included as spare. Figure 3.1.1.4 shows the underside of the base plate below the reaction chamber.

The furnace is designed to withstand a temperature of 1800 °C with a working temperature of 1600 °C. The water-cooled cylindrical flanges were designed with safety in mind and their design is such that they contain no soldered parts which could come apart if there was over-heating. Also there is no direct groove or joint through which water could leak into the heating chamber. Figure 3.1.1.5 shows a cross-section of the lower flange and figure 3.1.1.6 shows the upper one. The two flanges are similar except for the base plate connections to the lower flange which slightly alter the shape of the water chamber.

The temperature was measured by means of a Pt/Pt-13%Rh thermocouple protected by a close-ended alumina rod and protruding from under the crucible platform. The thermocouple rod is introduced into the chamber through a gas tight connector at the centre of the base plate. The temperature is controlled by means of the coil current generator controls.

Gas pipe connections to the base plate and underside of the chamber are made using conventional domestic plumbing connectors for copper pipes. The connectors were modified for gas use by replacing the normal olive with a specially made olive and a rubber o-ring to make them impermanent and gas tight. Figure 3.1.1.7 shows how the plumbing connectors were modified.

Appendix A lists the operational steps required to use the furnace.

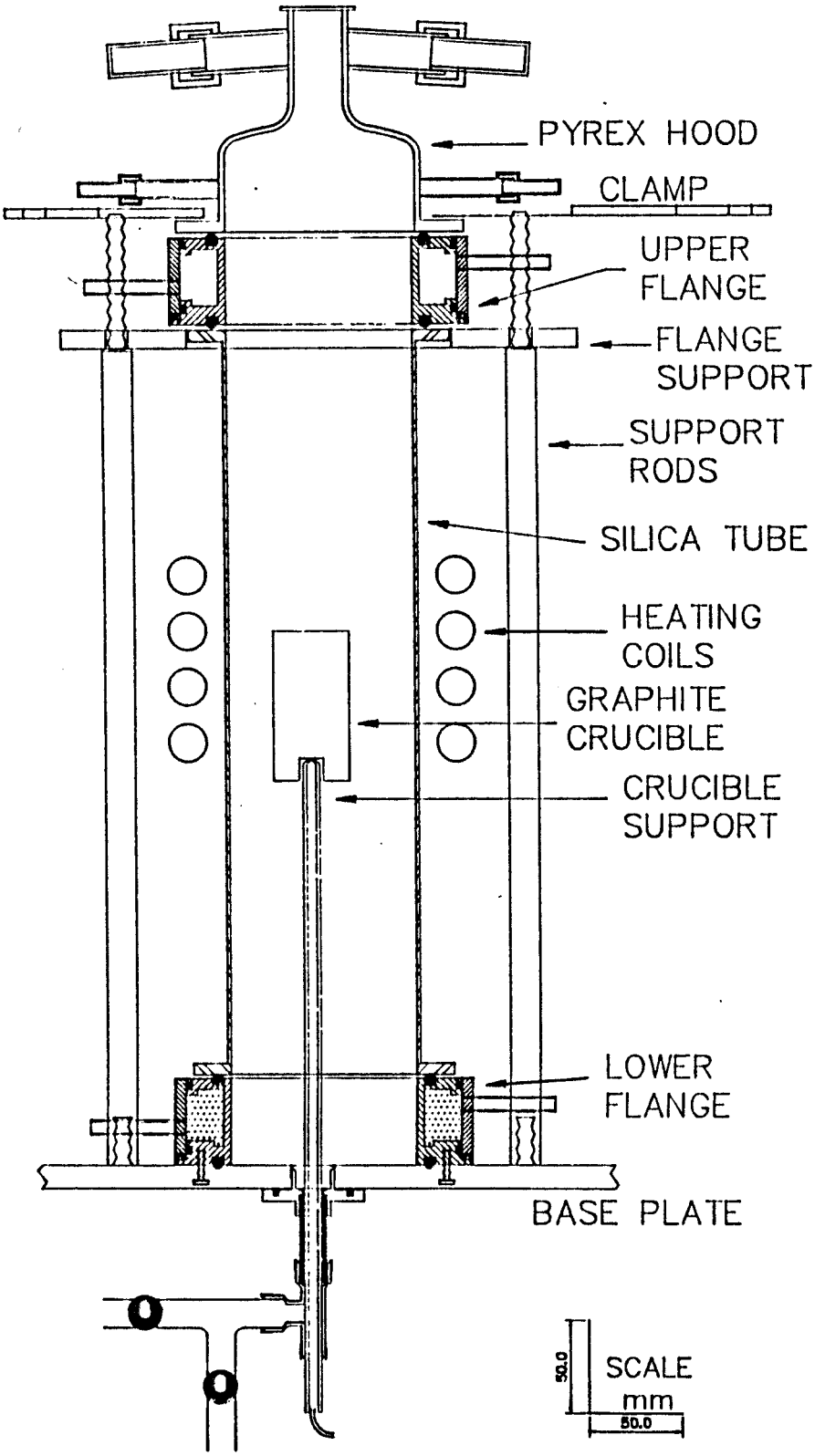

FIGURE 3.1.1.0 : The induction furnace, designed and built for a maximum working temperature of 1600 °C.

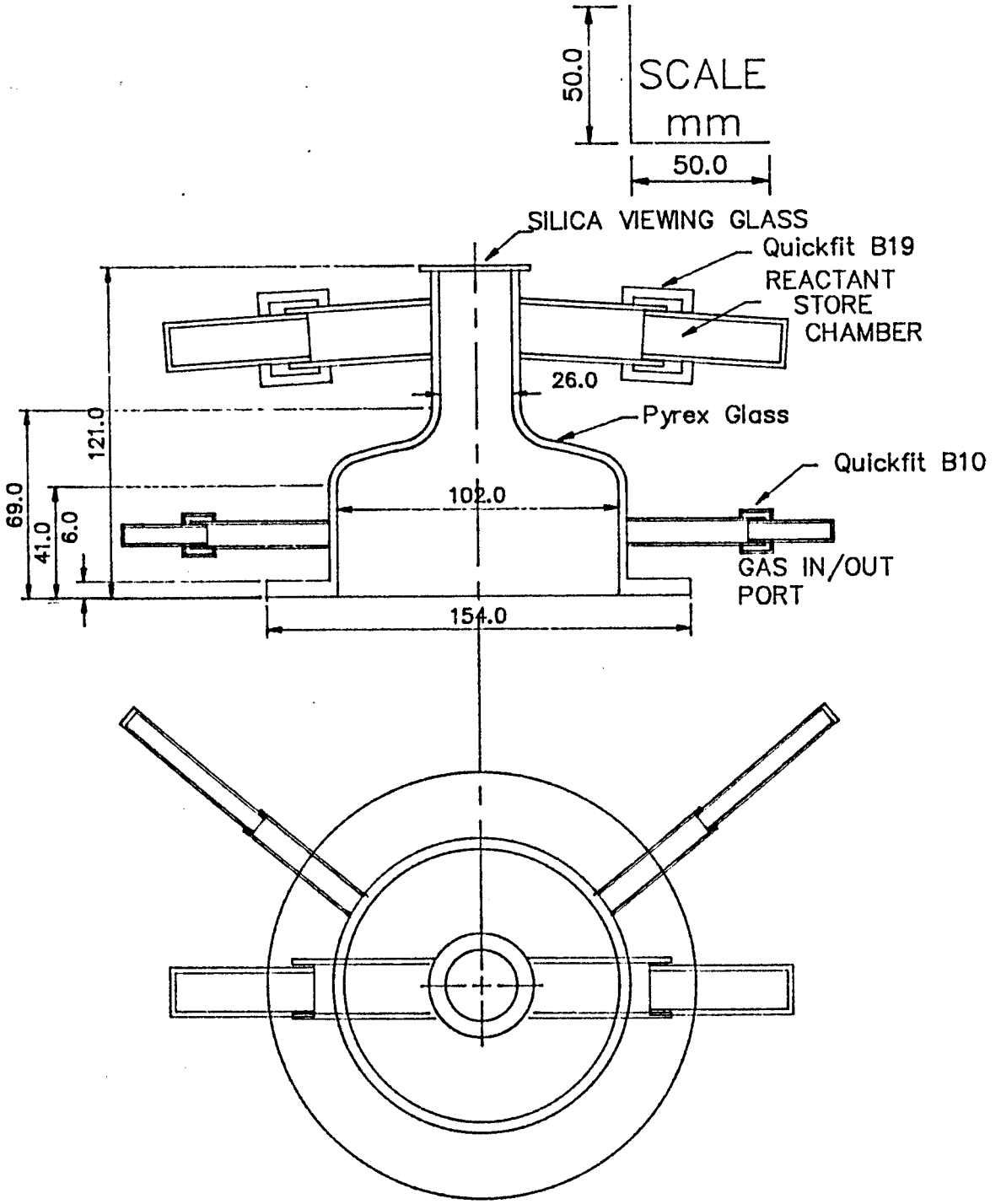

FIGURE 3.1.1.1 : Side view and plan of the Pyrex hood designed for the induction furnace showing gas input/output ports, sample chambers and viewing port.

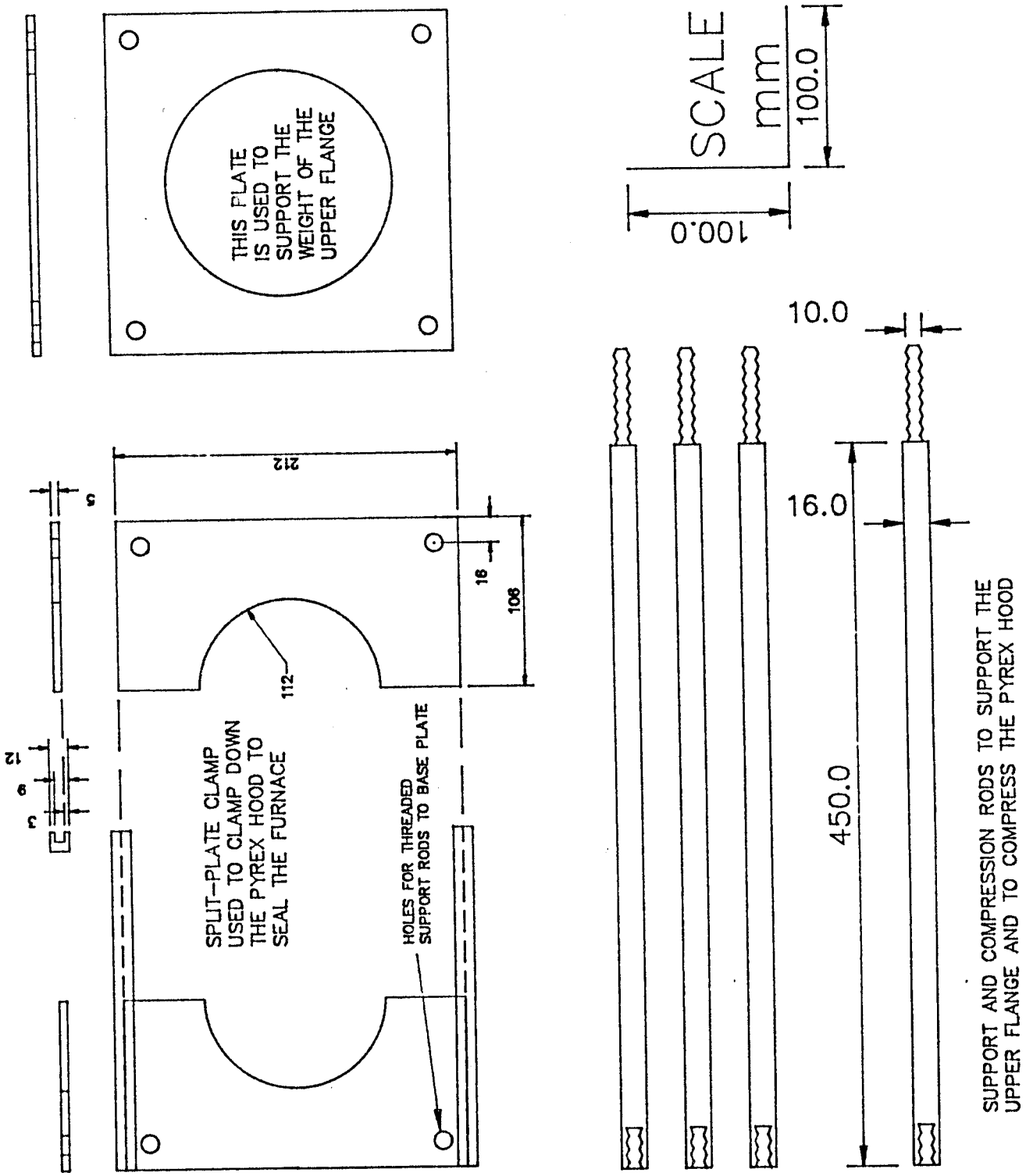

FIGURE 3.1.1.2 : Hood clamping (split) plate, the upper flange supporting platform and the support rods.

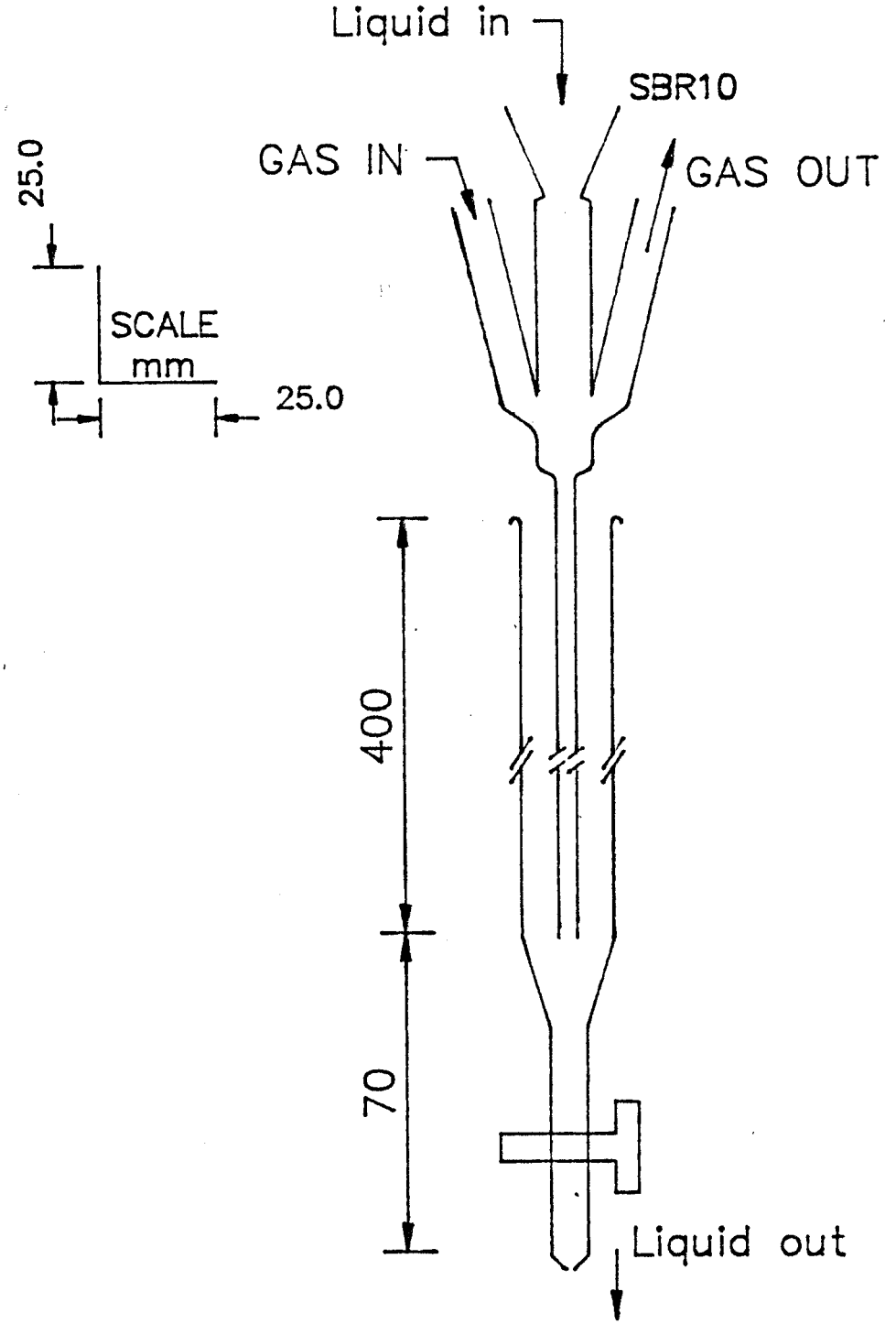

FIGURE 3.1.1.3 : Original bubbler designed for use with the induction furnace

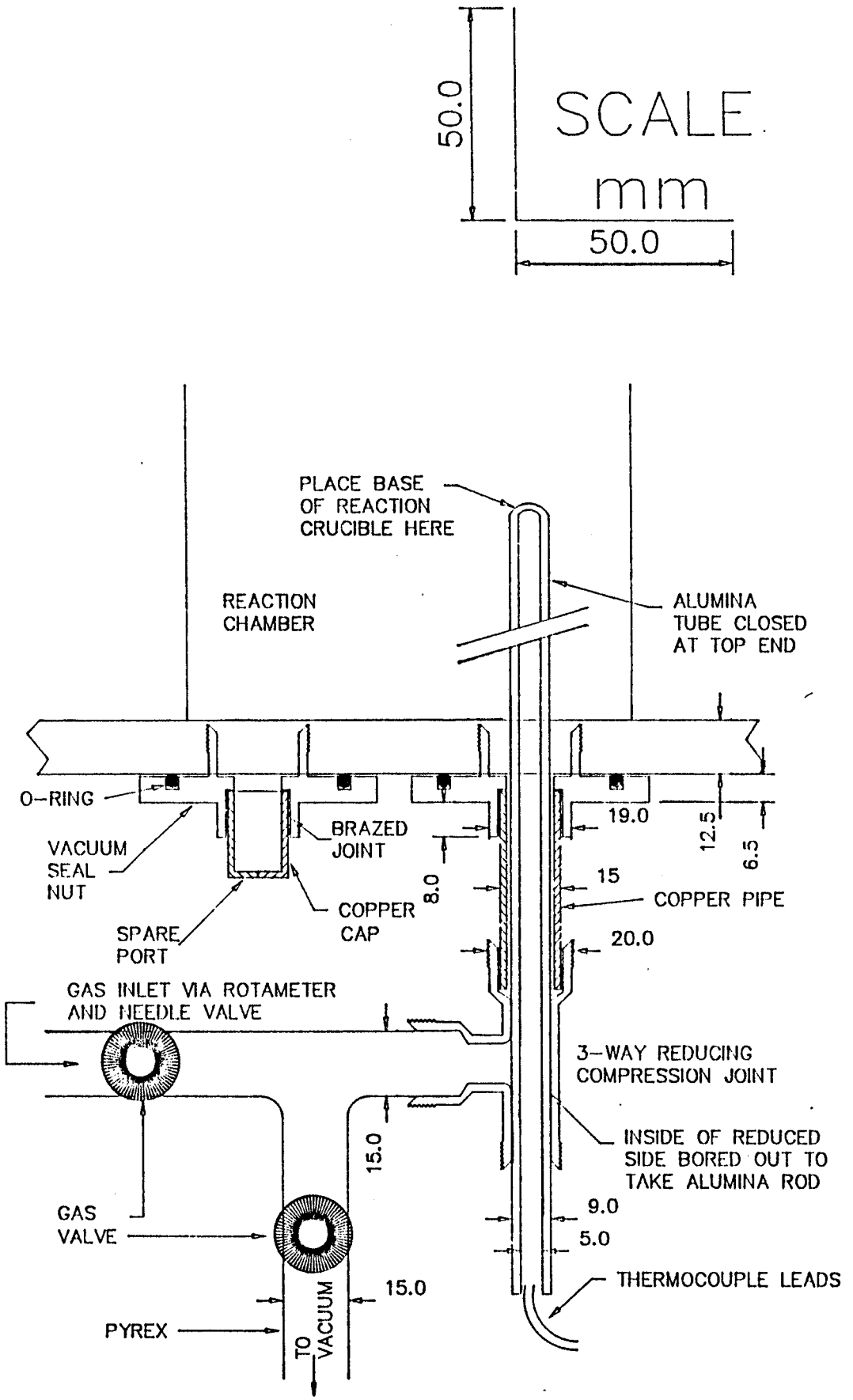

FIGURE 3.1.1.4 : Underside of the induction furnace base plate, below the reaction chamber.

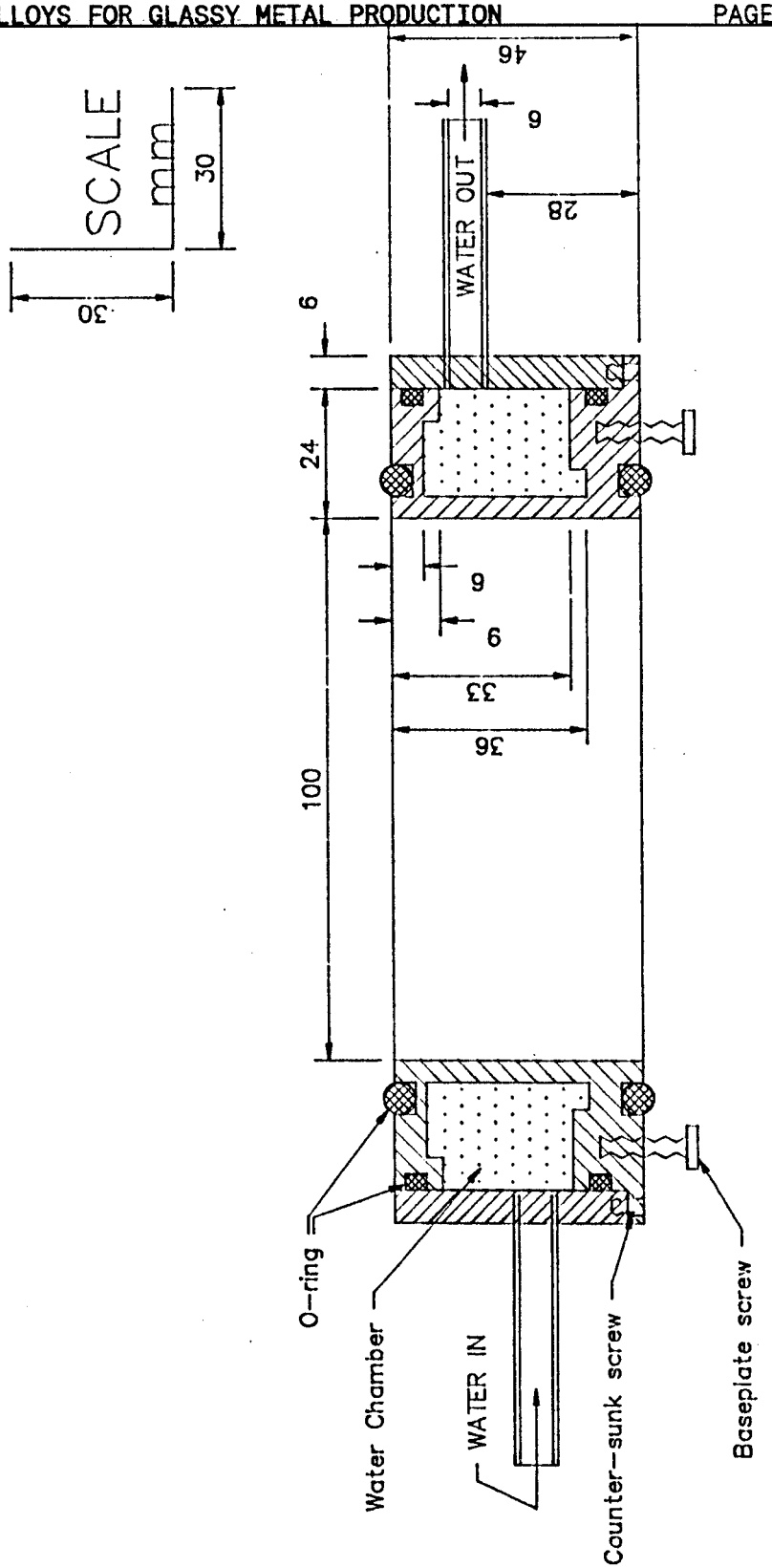

FIGURE 3.1.1.5 : Cross-section of the lower flange which is made of brass and water-cooled.

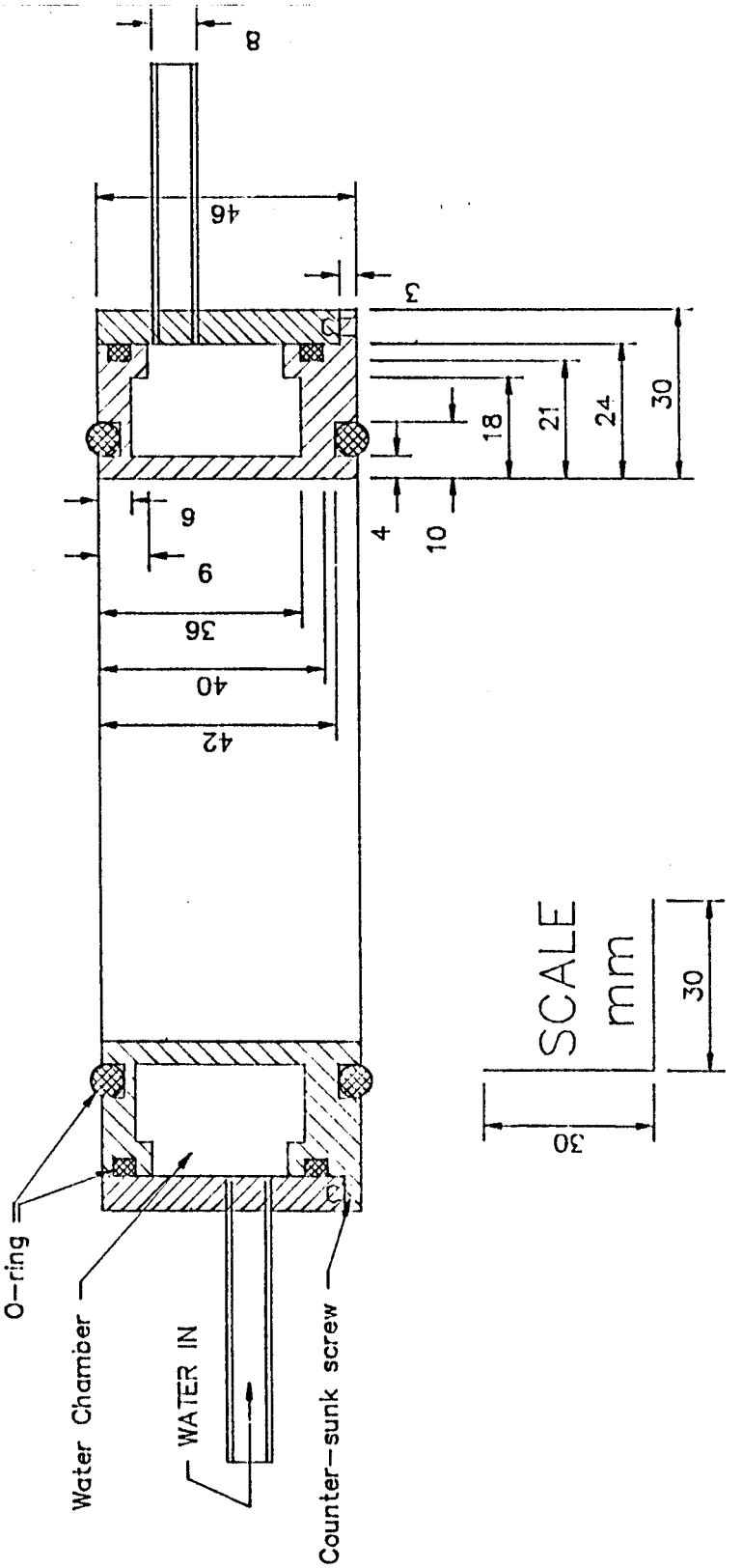

FIGURE 3.1.1.6 : Cross-section of the upper flange which is made of brass and is water-cooled.

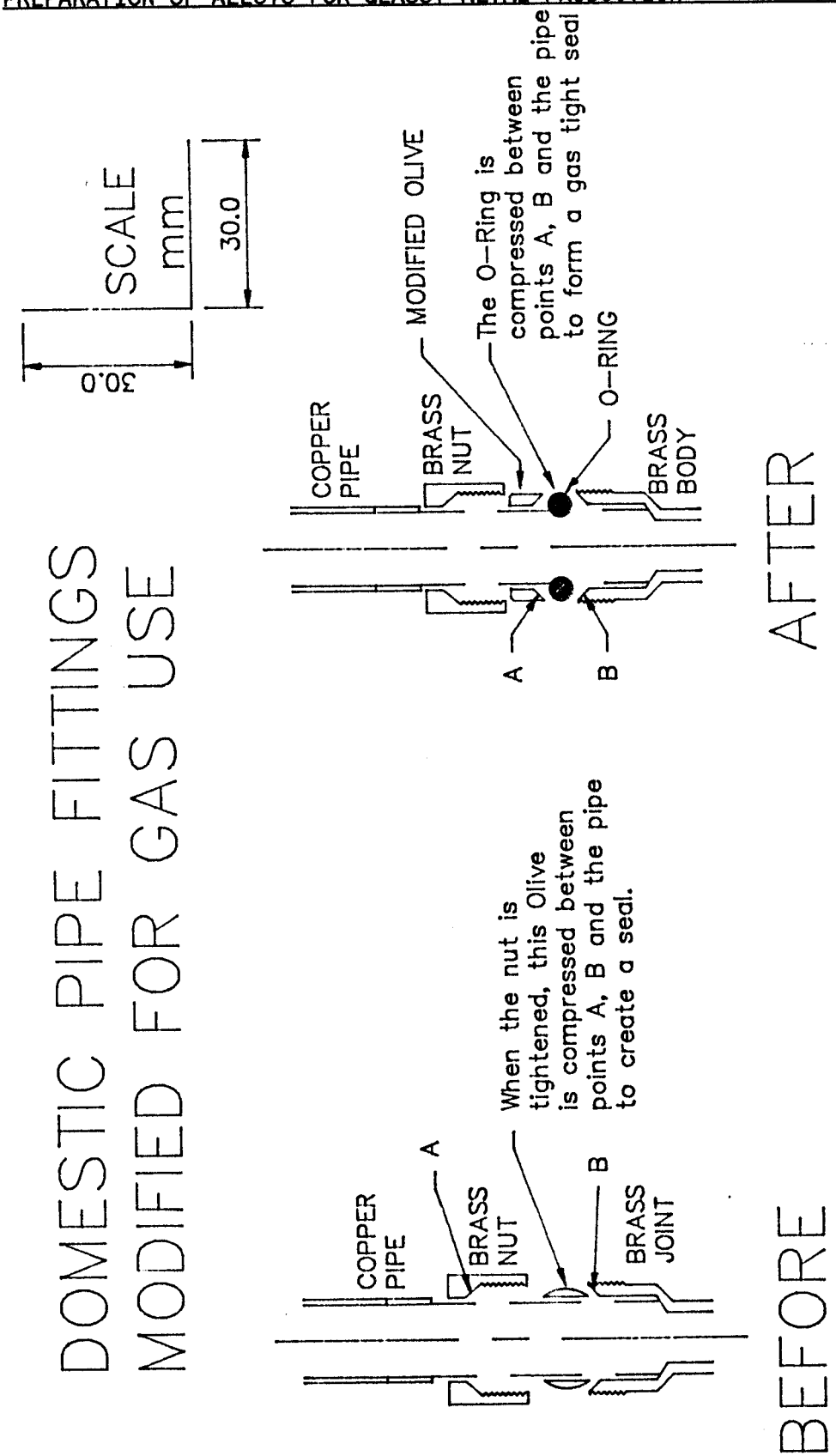

FIGURE 3.1.1.7 : Modification of domestic plumbing connectors for gas use.

3.1.2 >> POWDER INJECTION APPARATUS

The principle of the powder feeder is that an inert gas, in this case Argon, is used to carry a powder into molten iron. A refractory tube must be used at the hot end, and at some point the powder must be mixed into the carrier gas. There are numerous methods of mixing gas with powder including a fluidized bed. In this case however, there must be independent control of the powder feeding rate, carrier gas flow rate and pressure. In addition, the apparatus must be air-tight and able to withstand static pressures below the melt surface. Appendix B shows how the static pressure of molten iron increases with the depth of injection in various units of pressure.

A powder feeder can be of a batch or continuous type. Since a continuous feeder would require an air/argon interface for a large pressure range, this system was ruled out in keeping with the primary aim of simplicity.

Argon gas from a cylinder must enter a unit and exit that unit carrying a powder for injection. The following two paragraphs describe how the pressure inside this unit must be just above the static pressure below the liquid surface at the injection depth, and what the effect of the lance diameter will be, provided boundary effects such as capillary action are not considered.

At a certain depth below a liquid surface, there will be an excess static pressure P above the atmospheric pressure. Now consider a tube of diameter d1 being immersed into a liquid to a depth l (see figure 3.1.2.1). The level of liquid inside the tube will be the same as that on the outside if the powder mixing unit is at atmospheric pressure. As the pressure inside the unit is increased, so the level of liquid inside the tube decreases until when the powder unit is at pressure P, the liquid level inside the tube will be at the immersion depth. Therefore the powder mixing unit must be able to withstand a minimum internal pressure P for injection equivalent to the static pressure at the injection depth.

In order for the gas to carry the powder into the melt, it must form bubbles at the injection depth and to do this, it must overcome the static pressure at the injection depth. Appendix B shows how the static pressure below the surface of molten iron changes with depth. The pressure required to form a bubble below the melt surface also depends on the diameter of the tube forming it. In general, the larger the diameter the greater the pressure required to form a bubble.

When designing the apparatus, an internal lance diameter of 5 mm was envisaged because of the powder particle size and the gas flow needed to carry it. An internal lance diameter of less than 5 mm increases the risk of blockages. If the lance diameter is much more than 10 mm then the increase in flow rate needed to carry the powder would cause turbulence and loss of metal during injection, therefore a balance is required between these opposing factors.

In practice, tests were done with refractory tubes of internal diameter between 5 and 20 mm and it was found that a tube (lance) diameter of 12 mm was suitable for a carrier gas flow rate of 10 l/min and a diameter of 6.5 mm was suitable for a flow rate of 20 l/min.

In keeping with the aim of versatility, it was decided to make the gas/powder mixer an enclosed pressure unit within which any powder dispenser could be placed for batch feeding of powders. Since powder feeders are prone to blockages it was important that this pressure unit be optically clear so that the powder behaviour within it could be observed during operation. This unit would require a gas input port, a gas/powder output port, some means of measuring the internal pressure and at least one excess pressure safety valve in case the injection lance was blocked.

In careful consideration of all the primary aims it was decided to select a simple inverted bell-jar for the pressure unit with a lid to contain the pressure and an output port at the base. Figure 3.1.2.2 shows the bell-jar with its output port and figures 3.1.2.3 and 3.1.2.4 show the plan and side view of the lid respectively. The lid is clamped onto the inverted bell-jar by four compression rods to make a gas tight seal. Modified domestic water tank and plumbing connectors were again used here as with the designed induction furnace. Figure 3.1.1.7 shows how a standard plumbing connector was modified for gas use.

In a previous powder injection experiment (Ohguchi, S. 1983), powder flow rates of 7-10 g/min were used, however the previous discussion (section 2.7.5) indicated that a much higher flow rate was required for the injection of the present powders (see table 2.7.5.1 for the powders). Previous experience (Meshkot, M. A. 1985) with the flow of powders was used here to introduce the simplest, cheapest and most versatile powder dispenser, the Flow-Cone. The flow-cone has an interchangeable orifice which enables different flow rates of the powder to be used. The orifice found to be most suitable for the boron containing powders was 4.8 mm . Figure 3.1.2.5 shows the flow-cone, its small orifice adaptor, the 4.8 mm orifice and the flow control mechanism discussed below.

A simpler (magnetic) mechanism for the control of powders through the orifice (equivalent to an on/off switch) was found to be impractical due to the curvature of the bell-jar. Instead an electric solenoid was used with a spring return, such that when there is no current, the orifice is closed.

To support the cone within the curve-based pressure chamber, a domestic plastic flour jar was used which gives support to the cone, houses the associated solenoid and is optically clear, so that the powder flow can be observed (see figure 3.1.2.6). The Jar was modified with adjustable studding to protrude from four sides and prevent it from tilting on the curved base, and an orifice centring ring was built inside it to align the cone orifice with the powder flow control.

The powder flow control or on/off switch is merely a flexible perspex lever which extends from the solenoid core. On top of this lever there is a needle which is held on by a rubber washer taped to the lever. The needle which extends into the orifice during both the "on" and "off" states has several important functions. It aligns the orifice to the closing rubber washer, its motion initiates flow of the powder and its contact with the powder during discharge, enables better flow of the powder by transmission of incidental vibrations from the solenoid to the exact point of flow. Figure 3.1.2.5 shows the orifice, its adaptor and this lever & needle arrangement.

Two excess pressure safety valves (15 mm and 22 mm) were designed for the lid in case one failed. Figure 3.1.2.7 shows the valve details which are of a simple type working on the same principle as a domestic pressure cooker. They consist of a rod with weights (washers) on the top which can be varied to change the maximum pressure inside the pressure chamber. The critical seal at the top of these valves was obtained by the use of rubber washers and modified parts from domestic "Full-Stop" kits used to stop taps from leaking. The length of each valve and the number of washers to be used was estimated from calculations based on a maximum injection depth of 30 cm and details of the valve cross-sections.

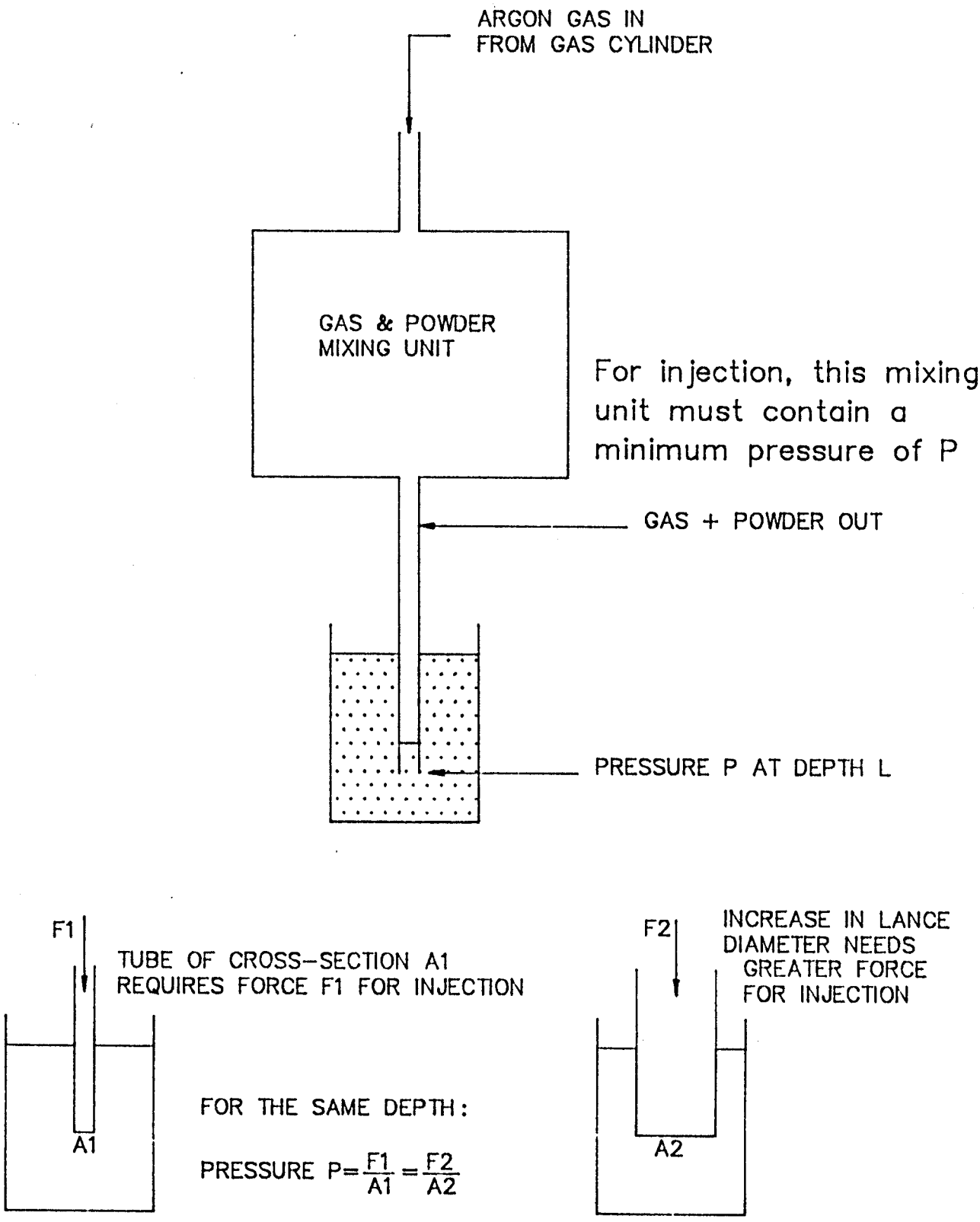

FIGURE 3.1.2.1 : Schematic showing that the pressure inside the powder mixing unit is the same as the static pressure under the melt surface.

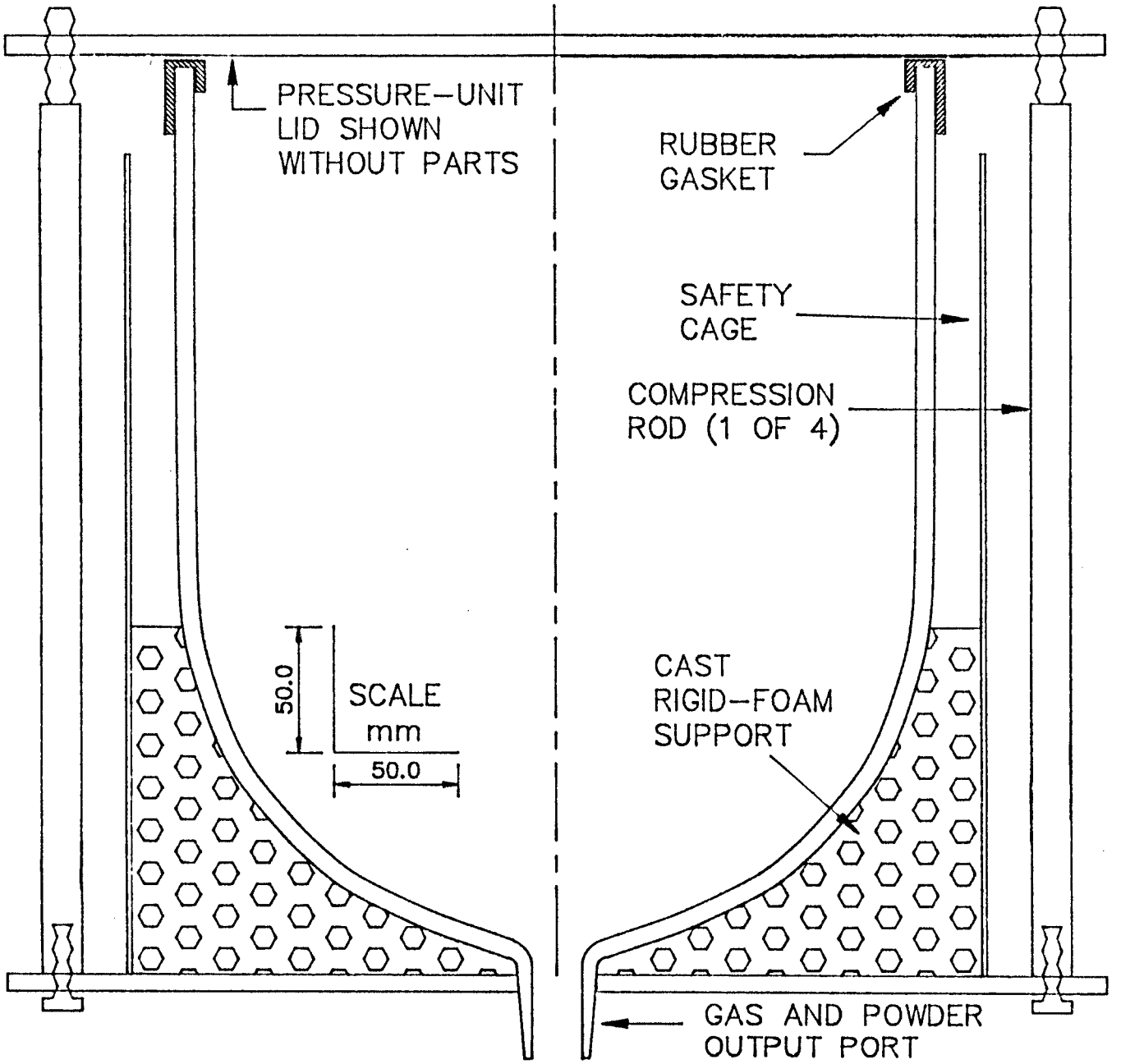

FIGURE 3.1.2.2 : Bell-jar with its supporting structure, compression rods and powder output port.

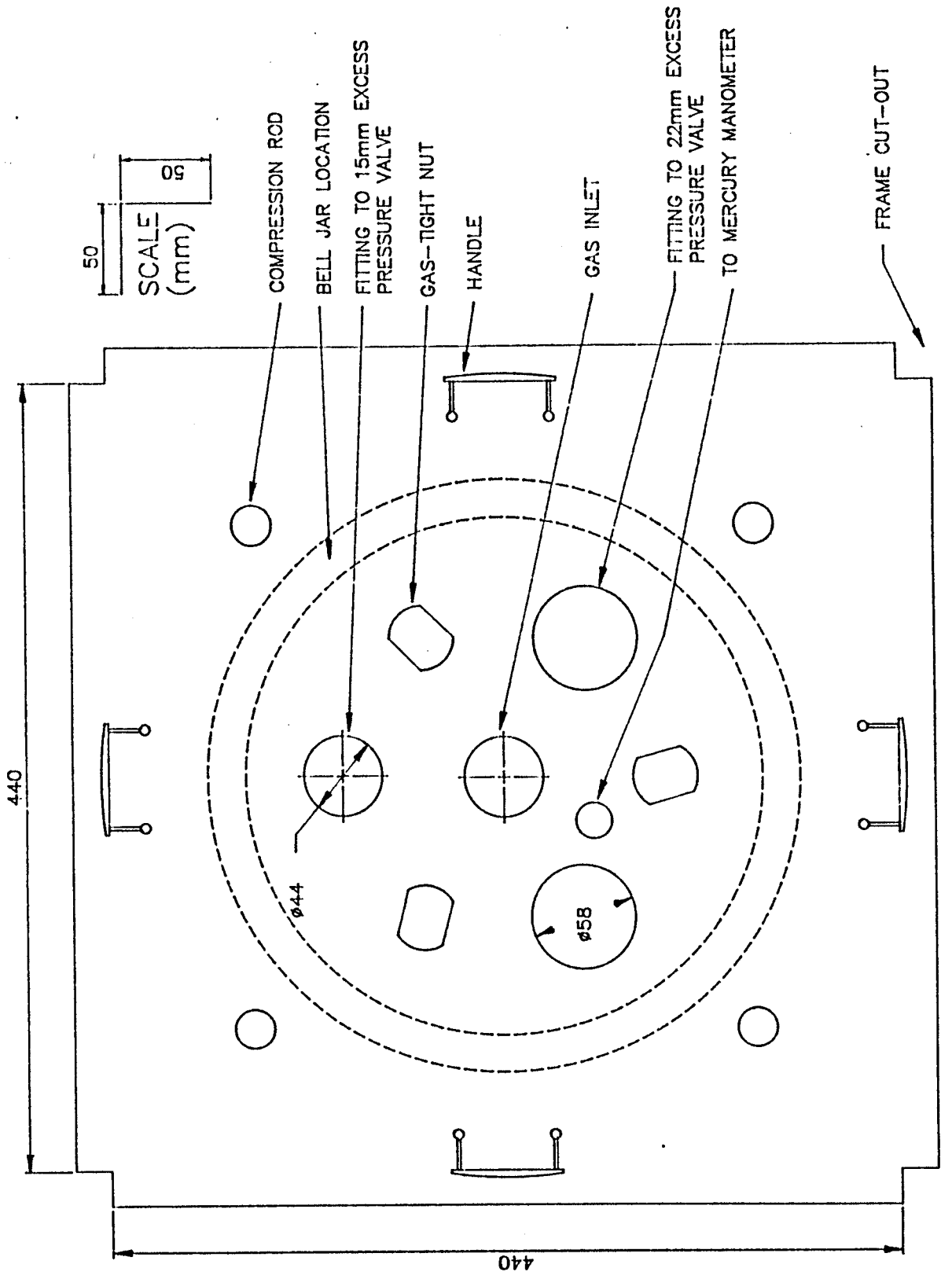

FIGURE 3.1.2.3 : plan of the pressure unit lid which contains ports for gas input, pressure measurement and safety valves.

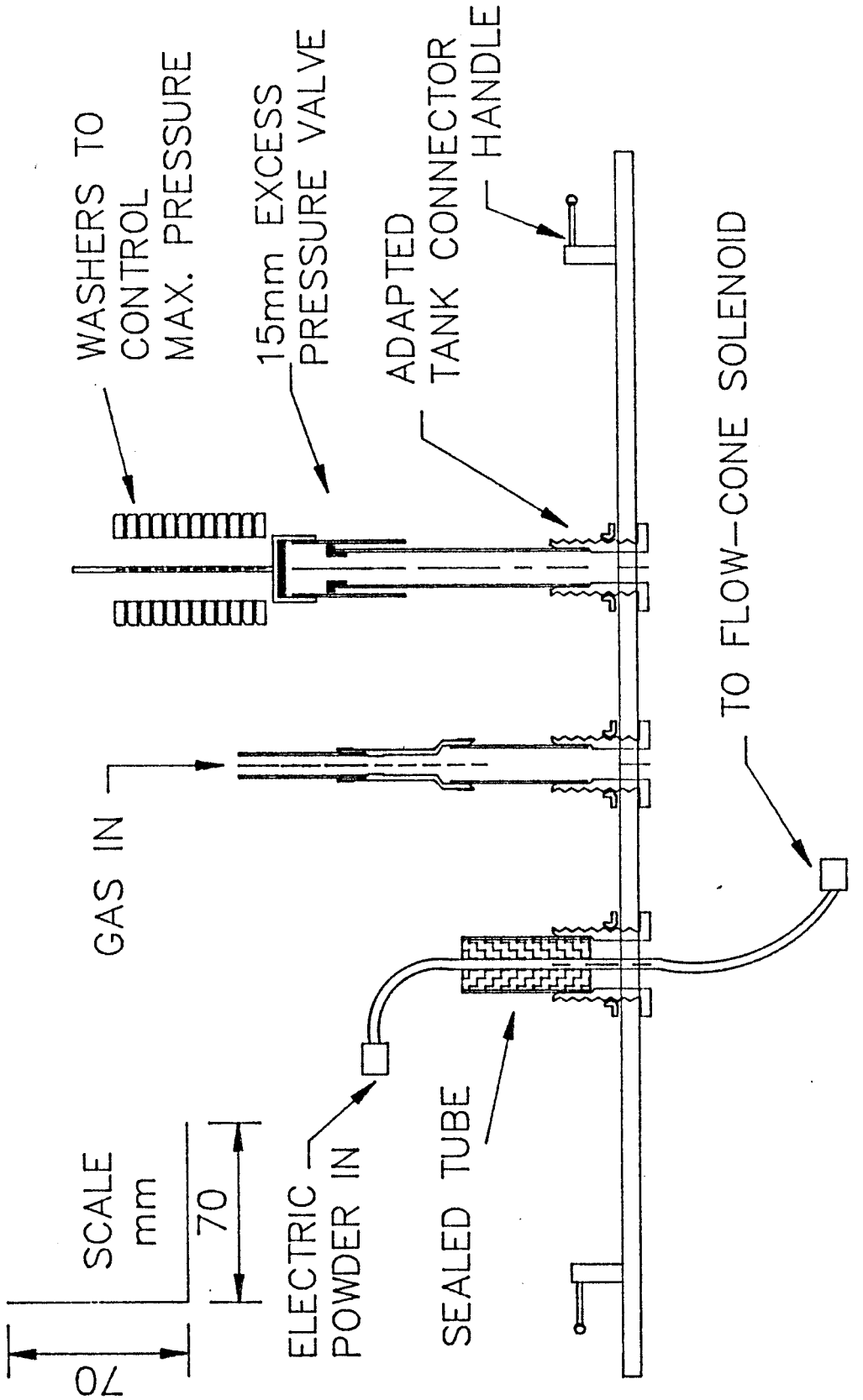

FIGURE 3.1.2.4 : side view of the pressure unit lid that feeds powder under excess pressure for submerged injection.

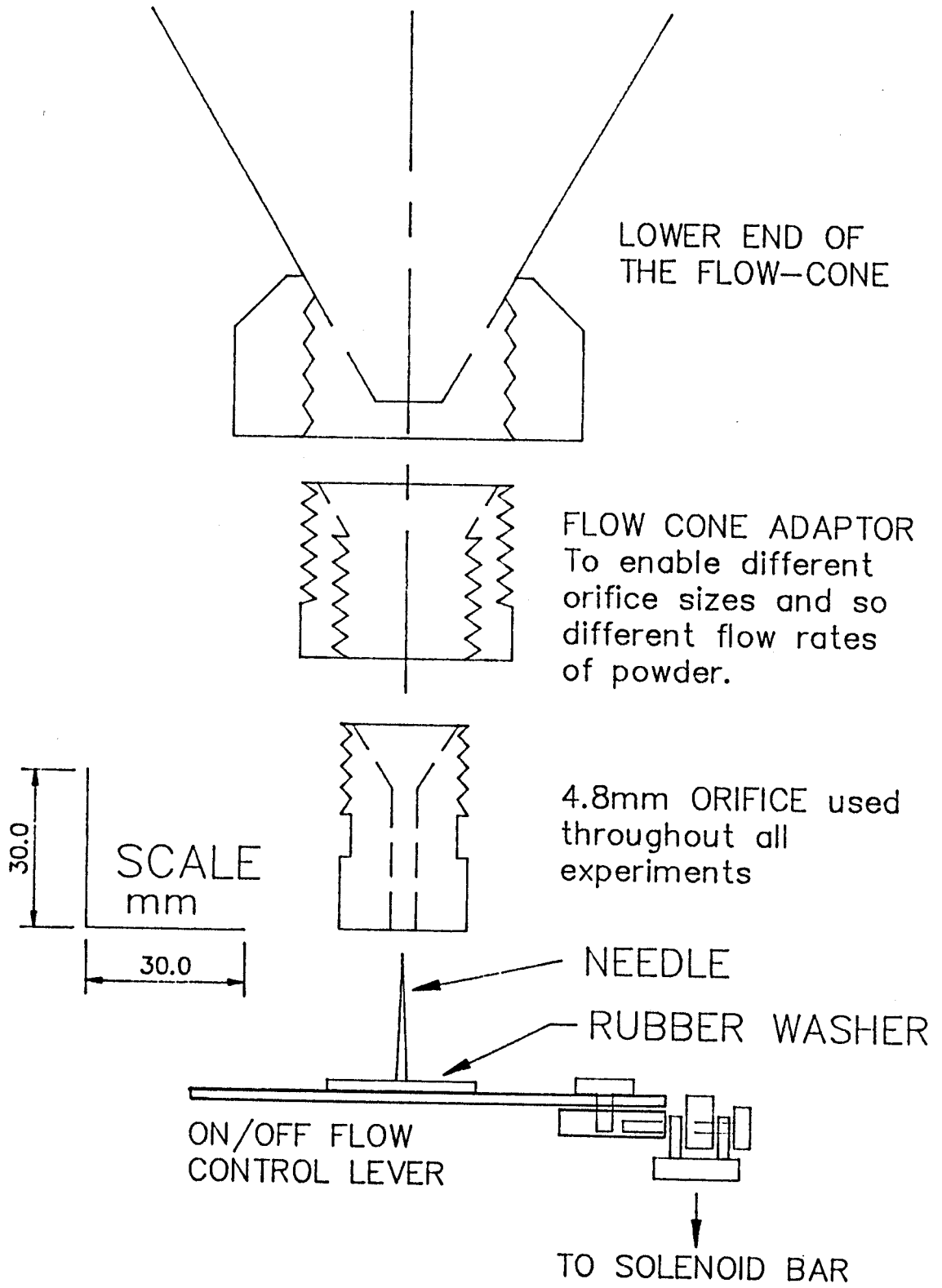

FIGURE 3.1.2.5 : Shows the flow-cone, its small orifice adaptor, the 4.8 mm orifice and the flow control mechanism.

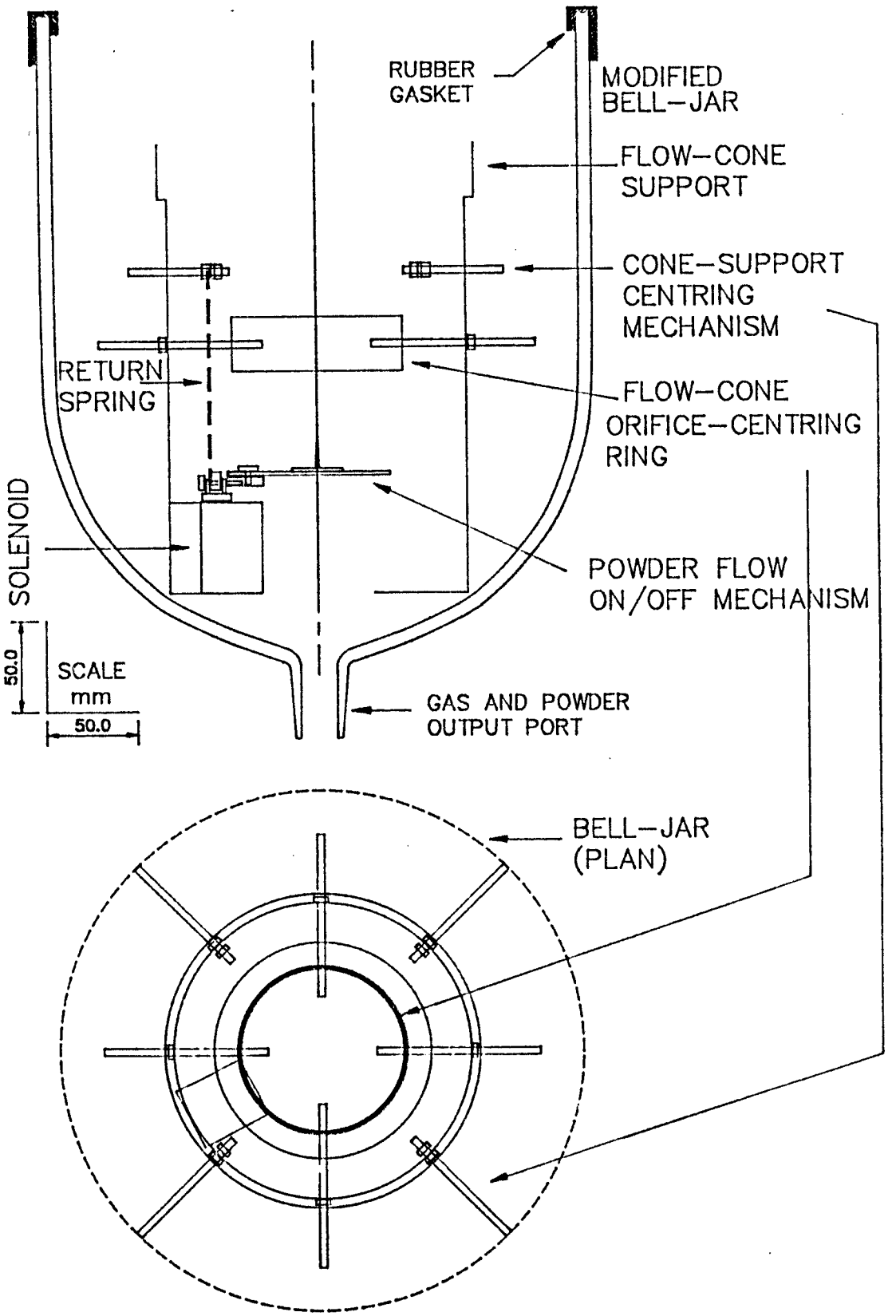

FIGURE 3.1.2.6 : shows the flow-cone support cylinder inside the bell-jar, the orifice centring ring and their adjustable arms.

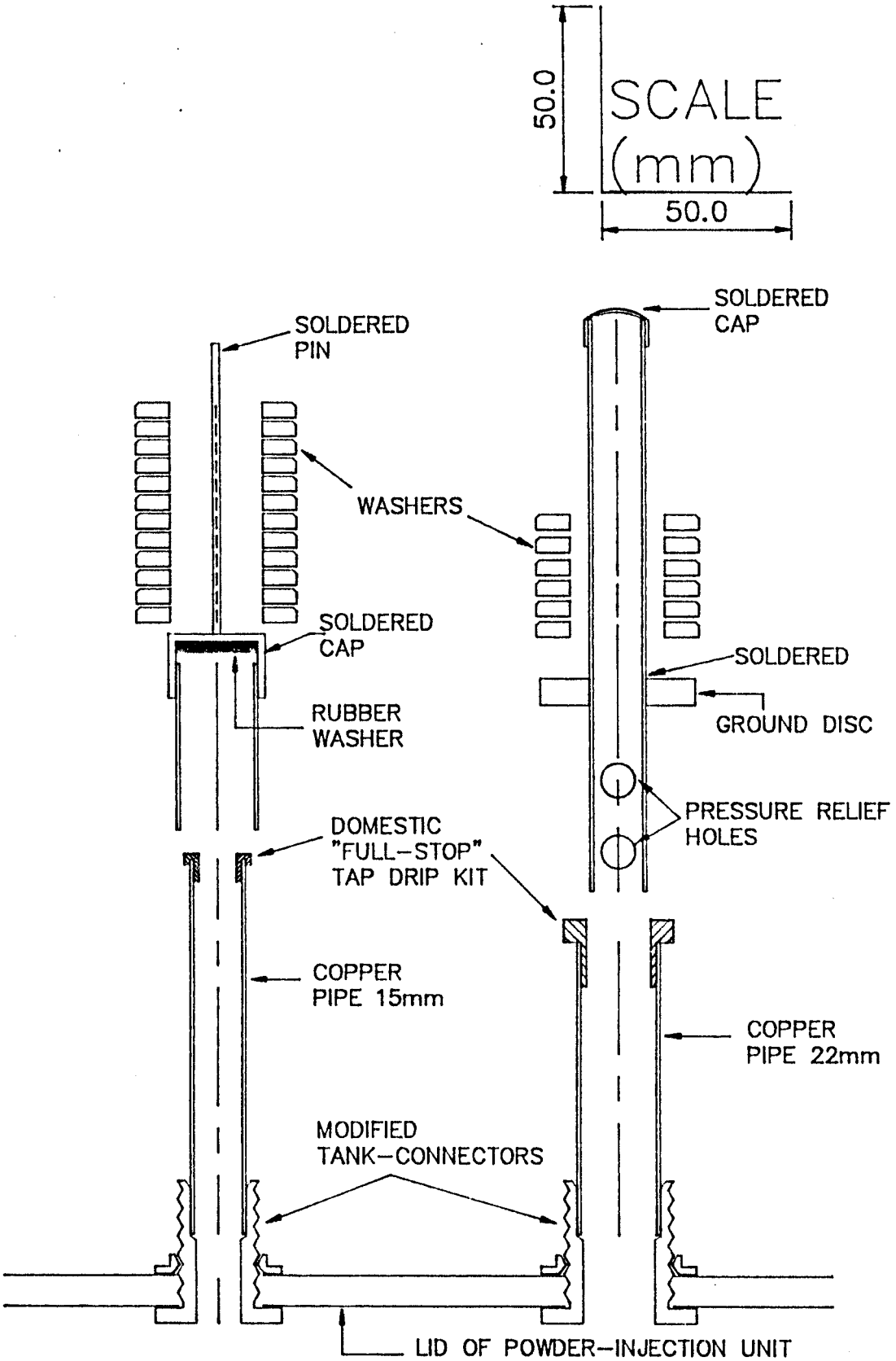

FIGURE 3.1.2.7 : Design of excess pressure valves.

3.1.2.1 >>> Simulation Experiments

A number of simulation experiments were carried out in order to test the powder feeder and to find its working parameters. A head of water 2.8 m high (to simulate about 40 cm depth of molten iron) was prepared by using a roof rain-water pipe bonded by mastic to a 5 litre aspirator bottle with a side outlet. The pipe was filled with water, and sugar was injected into it at various depths using air or argon as the carrier gas. This simulation confirmed the action of the powder feeder under pressure and demonstrated bubble formation and behaviour at various flow rates.

In another simulation experiment hydrogen gas was injected into water to simulate the injection of Argon into molten iron. To measure the flow rate in this simulation, an RS3 MeTeRaTe flow-meter[6] was calibrated for hydrogen gas with a ruby float. This simulation showed that no significant metal loss occurred until a flow rate of 3 l/min was reached.

3.1.3 >> PLUNGE LANCE SELECTION

The plunge lance is just a tube (preferably over 1 m long) of 2-3 cm diameter, at the end of which a powder-containing packet is lodged for plunging into molten iron.

For the plunge experiments, three types of lance were tried with the following results:

An Alumina tube was found to shatter due to the thermal shock, the same was found for Mullite. The melt surface soon became covered with tube debris and further plunging was found to be impractical, since the packets melted before breaking through this surface layer. This method also proved to be expensive.

---

6 From Glass Precision Engineering Ltd., Hemel Hempstead.

Mild steel pipes as used for medium size scaffolding with an ID of 21 mm were found to be a suitable lance for plunging packets. With each plunge a mass of charge froze onto the cool lance and the lance was then held and rotated in the melt until the frozen mass and the end of the lance melted into the crucible. During these experiments, the live lance was handled carefully with a pair of heat-resistant gloves.

3.2 > EXPERIMENTAL ARRANGEMENT

In addition to the simulation and modelling experiments, three main types of experiments were done. These were small scale experiments done in the designed induction furnace, injection experiments and plunge experiments where packets of powder were plunged into the melt. The plunge experiments were similar in set-up to the injection experiments except that a plunge lance was used instead of an injection lance. The general arrangement of the small scale experiments and the injection experiments is described below.

3.2.1 >> SMALL SCALE EXPERIMENTS

The small scale experiments were carried out in the induction furnace described in section 3.1. For these experiments XC or XN type recrystallized alumina crucibles[7] of 30-50 ml capacity were used. The alumina crucible was placed inside another crucible machined out of graphite with a location at its base for the thermocouple rod.

The Silica tube forming the heating chamber was protected from radiant heat by using one alumina tube and one Saffil[8] tube between the graphite susceptor and the silica tube. Figure 3.2.1.1 shows this arrangement

---

7 Obtainable from Morgan Refractories Ltd.

8 Saffil is the trade name of a thermal insulator from Imperial Chemical Industries plc, it contains 95% Alumina & 5% Silica and has a working temperature of 1600 °C.

3.2.2 >> INJECTION EXPERIMENTS

Four sizes of Salemander[9] Super clay-graphite crucibles were used depending on the availability and the most appropriate sizes were found to be E468 and E300. Appendix C shows the composition of these crucibles.

The injection experiments were carried out in a large induction furnace with a coil of ID 245 mm and 330 mm height. A 50 mm thick Saffil disc was cut-out and placed at the base of the coil. The coil was then insulated from heat by a fused Alumina Triangle[10] tube of ID 215, OD 236 and height 340 mm. Alumina powder was packed between the Triangle tube and the heating coil. A similar Saffil disc was cut-out and placed at the base of the Triangle tube with a magnesia brick on top of it that had been cut to size. The magnesia brick was added after it was found that the Saffil disc reached its melting point. Figure 3.2.2.1 shows a typical experimental set-up.

The crucible was placed on top of the magnesia brick which protected the Saffil insulation at the base, and a graphite susceptor of size 122 mm ID, 160 mm OD and 250 mm height was placed around the crucible. The size of the susceptor varied with the crucible size and availability, but in any case Saffil insulation was placed around the susceptor in the form of a cylinder or as strips cut to size (20x40x250 mm) for insulation. The whole assembly was then covered by a sheet of Saffil 50 mm thick and cut to size 300x300 mm with a slot from one side to the centre for viewing, temperature measurement and inserting the injection lance.

---

9 Salemander is a trade name of Morgan Carbon Ltd.

10 Triangle is a trade name of Morgan Refractories Ltd.

As a necessary safety measure, five Triangle M.1.28 [11] insulating bricks were stacked on each of three sides of the furnace chamber to confine molten metal splashes during injection. One side was left blank so that the lid could be removed when required.

The 8 mm ID reinforced PVC tubing which carried the powder from the powder feeder to the lance was protected by a small sheet of thick Saffil against intense radiation from the furnace.

---

[11] M.1.28 is a product of Morgan Refractories Ltd.

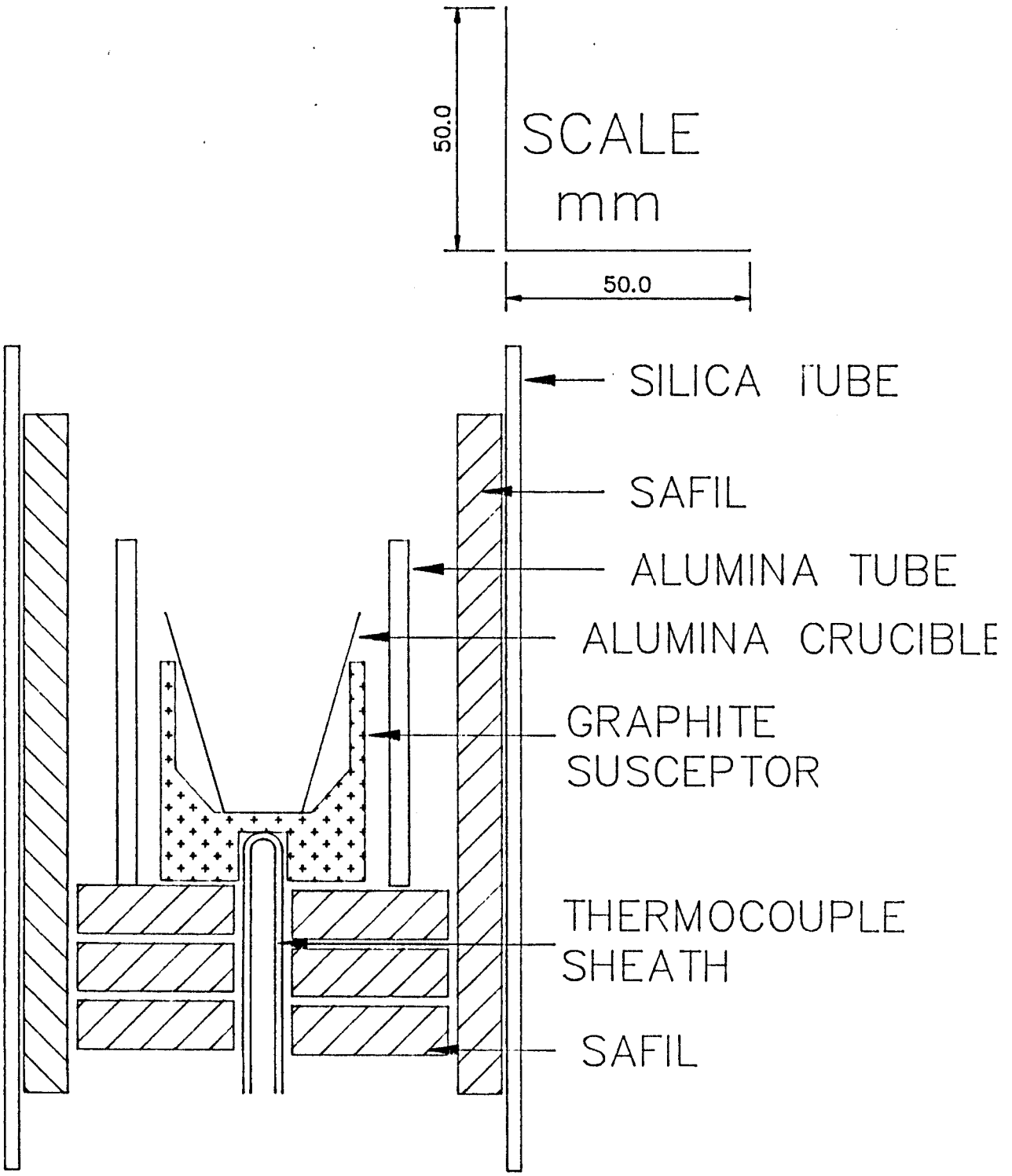

FIGURE 3.2.1.1 : The induction furnace crucible set-up.

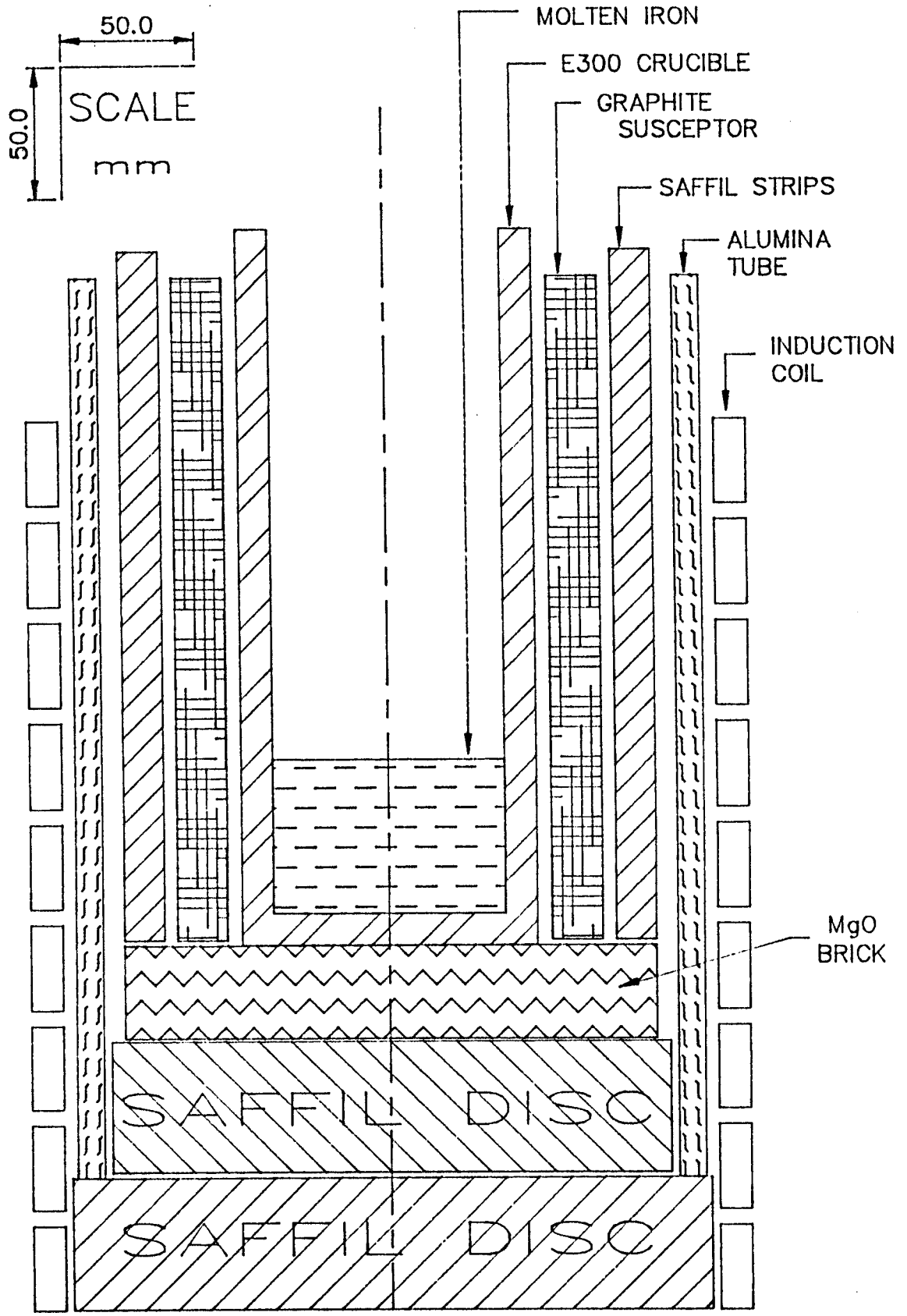

FIGURE 3.2.2.1 : Experimental set-up inside the induction furnace for powder injection.

3.3 > EXPERIMENTAL PREPARATION

This section describes the preparation required before each of the injection and plunge experiments. The preparation for the small scale experiments merely consisted of weighing the components and mixing them.

3.3.1 >> INJECTION EXPERIMENTS

To prepare for an injection experiment the crucible to be used was first cleaned and weighed empty, about 1.5 kg of Electrolyticly produced pure iron was then weighed into it and the crucible was embedded into the induction coil as described in the experimental arrangement section. Most of the Saffil insulation was re-cut and fitted each time due to melting or damage otherwise.

The flow-cone assembly was cleaned, aligned, adjusted and tested each time before loading it with the weighed powder to be injected. All powders to be injected were pre-sieved using a 710 micrometer mesh, then placed in the cone assembly. The cone assembly was then placed into the pressure unit and the electrical connection for the solenoid were made before placing the lid on the powder feeder. The Lance to be used was connected to the outlet tube of the powder feeder and the connector insulated from heat.

To test for pressure, the end of the lance was blocked and Argon was allowed into the pressure chamber at a rate of 10 l/min. The lid nuts were tightened until an internal pressure equivalent to 18 cm of Fe was reached using 12 washers on each of the excess pressure valves. The Argon was then turned off and the apparatus was ready for an injection experiment.

3.3.2 >> PLUNGE EXPERIMENT

To prepare for a plunge experiment, aluminium foil pieces were shaped around a tennis ball to form a cup shape. 50 g of whatever powder was to be used was then weighed, sieved through 710 microns and wrapped into the foil to form a pear shaped powder packet. The aluminium foil pieces were about 152x175 mm in size and 0.05-0.06 mm thick. they weighed on average 3.7 g +/- 0.05 g. Twenty such packets were prepared for each plunge experiment, although not all were used.

The wight of iron used was between 1.5-2 kg and this charge was prepared and melted in the same way as for the injection experiments. The metal lances used for plunging were weighed before the experiment so that the additional weight of iron due to the dissolution of the lances could be estimated.

3.4 > EXPERIMENTAL PROCEDURE

3.4.1 >> INDUCTION FURNACE EXPERIMENTS

These small scale experiments were carried out in order to establish the feasibility of the reactions expected to take place during injection and to determine the working parameters. For example, results from these experiments revealed the reactivity between powders to be injected and the melt containers. They also emphasized the experimental scale problems and were used to determine the reaction products.

All the initial experiments requiring a heating time of more than 90 minutes were carried out in a vertical resistance tube furnace with an internal diameter of about 40 mm. The remainder of these experiments were done in the induction furnace described in section 3.1

The procedure for these experiments was to mix electrolytic iron powder with one of the supplied powders in proportions to give a 3% boron alloy and to place this mixture in the Alumina crucible described above. The mixtures were heated to 1400-1600 °C under an Argon gas flow of 120 ml/min for the resistance furnace and 400-500 ml/min for the induction furnace experiments. The crucibles were then allowed to cool under the same flow of Argon.

The temperature of the reaction crucible was constantly monitored throughout the experiment using a Pt/Pt-13%Rh thermocouple connected to a multimeter or a chart-recorder.

In the case of experiments where a pellet of the reacting powders was made (E4-E5), this was done by the use of a lubricated metal die 12 mm in diameter and 80 mm high. The powders were mixed together first and then pressed under a pressure of about 15 ton-force per square inch (230 MPa) over 1.5 minutes. The resulting pellet was weighed and placed in the reaction crucible.

3.4.1.1 >>> Taking Samples

Samples were taken for analysis after each of the initial series of experiments. This was done after careful examination of the reaction crucible, and where the products were clearly in two or more physical parts these parts were sampled and analyzed separately. These separate samples from the same experiment were labelled S1, S2, S3 and so on.

3.4.2 >> FLOW-CONE EXPERIMENTS

Several flow-cone experiments were carried out using the different powders in order to determine the flow time and specific volume of the powders to be used.

These experiments were carried out using the flow-cone and a fixed container of volume 113.5 ml placed 10 cm below the orifice. After sieving the powders through a 1 mm sieve, a level container-full of powder was timed as it passed through the cone orifice and this was used to calculate the flow rate. Further details of flow-cone experimental procedure are given elsewhere (Meshkot, A., 1985).

The results from these initial experiments were used to predict the size of the crucibles required for high temperature experiments. That is, the specific volume of the powders found from flow-cone experiments were used together with calculations about the boron content of powders to determine what volume of powder would be required to yield a boron content of 3% . This estimate proved to be important in the later design of experiments.

In another set of flow-cone experiments, the flow behaviour of the different powders from the output of the powder feeder were examined. For these experiments, the cone assembly was cleaned and placed centrally into the bell-jar. The flow-cone was then filled with pre-weighed powder. A balance was placed under the powder feeder output so that any powder being gravity fed out of the powder feeder was collected in a beaker on the balance and weighed accumulatively. As in the injection experiments the powder was fed in 1 second bursts and after each discharge the total powder delivered was weighed. The use of the carrier gas was avoided in these flow experiments in order to obtain a more accurate measure of the powder delivery rate. The powders did not flow as well initially without the carrier gas as they would have done with the carrier gas. This was because some powder accumulated on the outlet platform of the bell-jar before a steady state of flow was reached. This is called the plateau effect and is examined in more detail later.

3.4.3 >> INJECTION EXPERIMENTS

The following procedure was used for injection experiments. After the preparation for an injection experiment was complete (see above) the large induction furnace generator, cooling water to the furnace coil and condensers were turned on. The generator field voltage regulator (variac) was set to produce the maximum power output from the generator for the susceptor being used, but in any case not more than 30 kW to avoid the risk of overheating. Capacitors were then selected to match the HF coil to the susceptor, were the correct combination of capacitors indicated a minimum value on the KVAR dial. The reactive KVAR meter indicates the lagging or leading KVAR imposed on the generator.

The temperature of the charge was monitored through a slot in the top insulation where the injection lance tip was also inserted. Above 1000 °C Argon gas alone was injected at 3 l/min through the lance and over the heating charge and around the susceptor in order to reduce oxidation of the metal, susceptor and crucible carbon. During the heating period the lance was also lowered by 1-3 cm at intervals of several minutes in order to reduce thermal shock on injection.

On melting, the Argon flow rate was set, the temperature of the melt was measured with an IR pyrometer and the lance was lowered into the molten iron with the depth of injection being measured indirectly by the internal pressure of the powder feeder. The depth of injection was 4-5 cm.

At this stage of the final experiments when the behaviour of powders was better known, powder was fed from the powder feeder in 1 second bursts with 1-3 second intervals. After each discharge the reinforced clear PVC tubing which carries the powder from the powder feeder was checked for stagnant powder which would indicate that the lance was blocked. This process of feeding bursts of powder was continued until the lance was blocked and this was confirmed by the increase in internal pressure of the powder feeder. This internal pressure would typically reach 14-18 cm of molten iron with some gas still getting through the blockage and bubbling in the melt.

A sample of the melt was then taken using silica sampling tubes of diameters 5x7 mm and a pipette filler. The injection lance was changed and lowered slowly into the melt over 5-7 minutes to avoid thermal shock. The above injection procedure was then repeated until the allocated number of lances were used up.

3.4.4 >> PLUNGE EXPERIMENTS

The following procedure was used for the plunge experiments. After the preparation for a plunge experiment was complete (see above) the iron was melted in the same manner as for the injection experiments using the same furnace. Once the iron was at about 1550 °C, a packet of powder was lodged into the end of a plunge lance made of mild steel tubing. the lance was held by protective gloves and the packet plunged into the melt.

The temperature difference between the lance and the melt caused a mass of melt to solidify into the end of the lance. To overcome this problem and to make the lance ready for the next plunge, it was held and rotated in the melt until the immersed end of the plunge-lance melted and the rest of the lance was removed. The test used here was to see that the lance had both ends open, ready for taking the next packet.

The lance was then quenched in cold water to speed the process and slightly heated again over the melt to evaporate any water droplets which could (and on occasions did) expand violently on plunging. The next packet was then put on and the experiment continued.

3.5 > EXPERIMENTAL DIFFICULTIES

3.5.1 >> WEIGHT ANALYSIS

After initial attempts to carry out weight analysis for the small scale experiments, it was found that the reaction of boron compounds with the alumina crucibles used made this difficult. Aluminium Borate ($9Al_2O_3.2B_2O_3$) was repeatedly identified as the product of this reaction with a melting point of 1100 °C . This relatively low melting-point product resulted in damage to the crucible in almost all small-scale experiments and the subsequent loss of some contents.

In the case of experiment series E4 and E5 where extreme care was taken to obtain reasonable weight analysis figures, the weight loss was found to be an average of 5% by weight of the reactants

3.5.2 >> MELTING IRON

The apparently simple act of melting iron was found to be difficult due to the lack of experience. The main factors which gave rise to these difficulties were as follows:

a) The iron was pure with a melting point of about 1536 °C, so conventional crucibles and insulation aimed for temperatures below 1250 °C could not be used.

b) The iron was to be melted by induction heating, but it was found that the electrolytic iron flakes were not susceptible enough to the induced field to allow melting.

c) Ideally, a container for amorphous metal experiments should contain no carbon because carbon in the final product promotes crystal nucleation and hence reduces the amorphous-crystalline transition temperature. One carbon-free and thermal shock resistant crucible found to be suitable for containing molten iron was an alumina dip-sampling tube[12] made of Triangle 66V Sillimanite (see figure 3.5.1.1 and appendix C for composition). This dip-sampler was used with a graphite susceptor and was fund to be inadequate because the 20 mm wall thickness of the dip-sampler insulated the iron from the heat generated within the susceptor. As a result the dip-sampler also melted by the time the iron had reached its melting point.

d) It was found that clay crucibles impregnated with graphite and made for induction heating, melted the iron after about 45 minutes, but that the rate of increase in temperature was not high enough to enable injection.

e) Coupling between the induction coil size and the size of the clay-graphite crucible was found to be important. Tightly packed insulation around and above the crucible did not help to melt the iron if the coil coupling was not good.

f) It was found necessary to use a graphite tube as a susceptor in addition to a clay-graphite crucible.

3.5.3 >> POWDER INJECTION

The main problem experienced in powder injection was that the boron oxide component of the powder (melting point 437°C) melted in the injection lance forming a viscous liquid and thereby blocking the path for further injection. This problem was resolved by changing the injection lance several times during the experiment.

---

12 A product of Morgan Refractories Ltd.

3.5.4 >> THE PLATEAU PROBLEM

An inherent problem of the powder feeder is that some powder collects at the base of the bell-jar after it has been delivered by the flow-cone

3.6 > EXPERIMENTAL PRECAUTIONS

TEMPERATURE MEASUREMENT During temperature measurements using an infra-red pyrometer, it was found that fumes generated by the crucible and insulation binders resulted in false temperature readings. In order to eliminate this error, the crucible was flushed with Argon before each reading of temperature

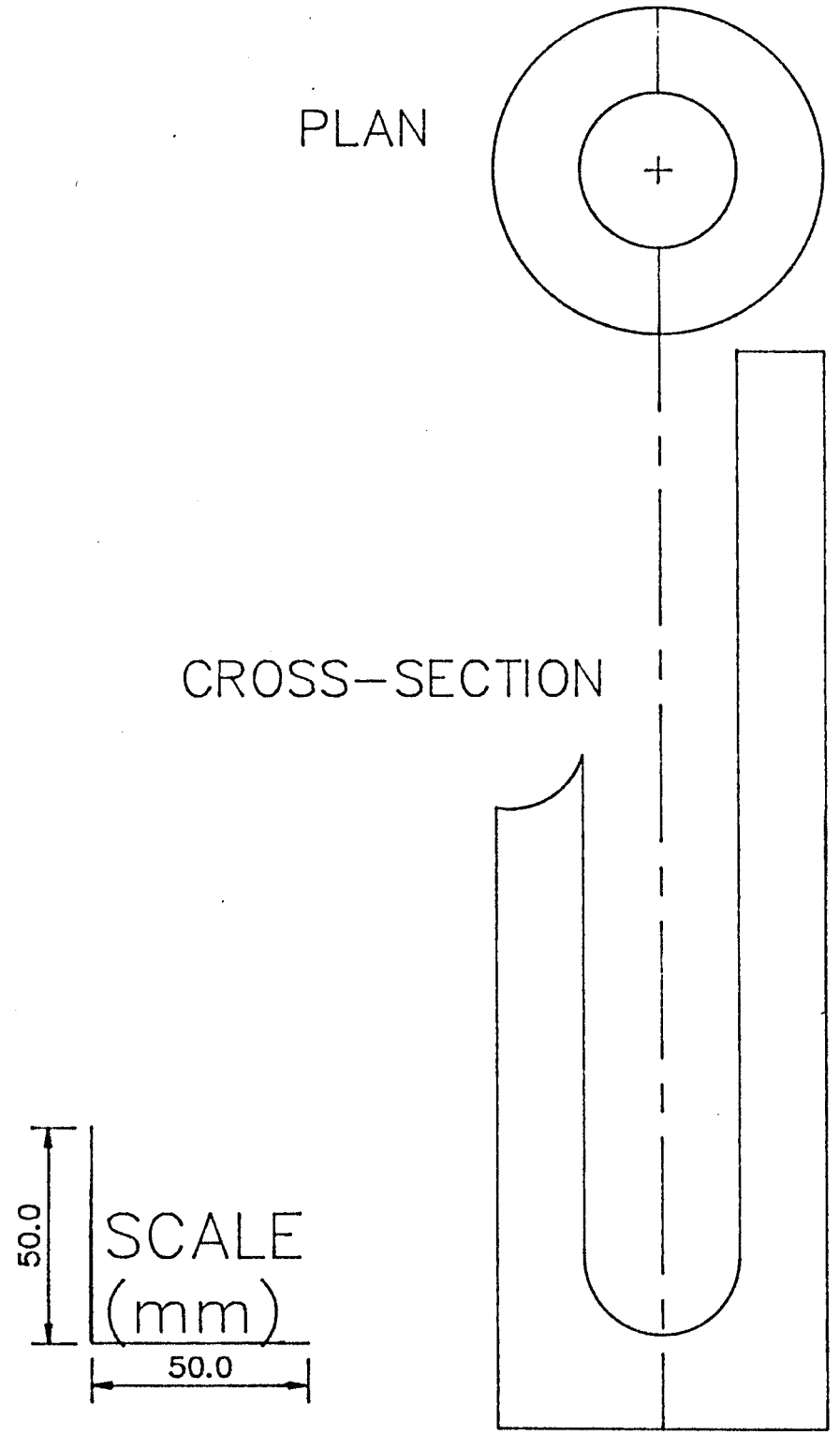

FIGURE 3.5.1.1 : The Dip Sampler with good thermal-shock resistance, normally used to take samples from a molten bath of metal.

4. RESULTS

Experimental results are given in tabular form in four sections below. First there are the initial experiments performed in the resistance or induction furnace described earlier. The results of x-ray analysis are given with the card index number next to the identified compounds and this is followed by flow-cone experimental results. The last two result sections relate to experiments during which powders containing boron oxide were plunged and injected into molten iron respectively.

4.1 > TABLES OF RESULTS

4.1.1 >> INITIAL SMALL-SCALE EXPERIMENTS

The tables that follow contain the result of small-scale preliminary experiments conducted in a resistance tube furnace (for those over 1.5 hours) or the induction furnace that was designed for this purpose. Section 3.1.1 describes the apparatus and section 3.2.1 describes the experimental arrangement.

During these experiments it was found that some reaction products could be physically distinguished with careful observation. From experiment E4.2, two components were retrieved, sample S1- single metallic mass that wetted the crucible and sample S2- a number of small globules not wetting the crucible. Similar globules were observed in experiment E4.3 together with the remainder of the pressed pellet, being a floating slag. Sample S3 from experiment E4.3 was a melted metallic mass with dull surface that wetted the crucible. E4.4 products were found to be similar to E4.3.

From experiment E6.0 a grey porous metallic mass was obtained. Experiment E6.1 contained evidence of gas bubbles at the base of a metallic mass (S1) which was covered by a black glassy slag.

Experiments E6.2 to E6.5 all resulted in a single metallic lump with E6.5 also containing a condensed powder (sample S2) on the outside of the crucible. A few metal globules < 0.5 mm in diameter were also observed.

Experiment E7.1 resulted in white SiC fibres in the crucible lid and a porous grey solid was observed as in E7.3. Experiments E7.4 and E7.5 resulted in a metallic mass with E7.5 containing a grey layer on the metal surface.

In experiment E8.1 and E8.3 metallic globules were found in a non-metallic matrix. For experiment E8.2 a porous solid was found and a white powder inside the lid (S3).

EXPERIMENT NUMBER	REACTANTS	HEATING		HEAT-TREATMENT	
		TIME hrs	TEMP. °C	TIME hrs	TEMP °C
E4.2	saturated $Fe_{(c)}$+10% B_2O_3 + 5% Coal as pressed pellet	16	1410	24	800
E4.3	$FeSi_2$+Si (78% Si) + 10% B_2O_3 pressed pellet	5	1410	24	700
E4.4	$FeSi_2$+Si (78% Si) + 10% B_2O_3 pressed pellet	16	1410	24	700
E4.5	$FeSi_2$+Si (78% Si) + 10% B_2O_3 + 0.5% $CaCl_2$ pressed pellet	5	1410	24	700

TABLE 4.1.1.1 : Initial experiments using iron, silicon and boron oxide. Amounts are by weight percent of the first compound.

EXPERIMENT NUMBER	SAMPLE NUMBER (see sec.3.4.1.1)	α-Fe 06-0696	Fe_3C 23-1113	$Fe_{23}(C,B)_6$ 12-0570	Fe_2B 03-1053	FeB 32-0463	Si 27-1402	$FeSi_2$ 22-1113	$FeSi_2$ 20-0532	B_4Si 13-0210
E4.2	S1	4	5	4						
	S2	2	3	5	5					
E4.3	S2					1	5	4		
	S3						5	4		2
E4.4	S3	3					5	2		
E4.5	S3						5		2	

TABLE 4.1.1.2 : X-ray results from experiment E4 using iron, silicon and boron oxide. Relative intensities are given on a scale of 1 to 5.

EXPERIMENT NUMBER	REACTANTS	HEATING TIME hrs	HEATING TEMP. °C	HEAT-TREATMENT TIME hrs	HEAT-TREATMENT TEMP °C
E6.0	SiC powder mix only	0.5	1600		
E6.1	Fe + 10% SiC powder mix	16	1630	24	1000
E6.2	Fe + modified SiC mix (60:40 ratio of SiC:B_2O_3) to give 4% B	0.5	1600	2	900
E6.3	Fe + SiC mix to give 3% B in product	1	1600	0.5	900
E6.4	Fe + SiC mix to give 3% B in product	0.6	1600	0.5	900
E6.5	Fe + SiC mix to give 3% B in product, heated in vacuum	0.6	1600	0.5	900

TABLE 4.1.1.3 : Initial experiments with the SiC powder mixture.

EXPERIMENT NUMBER	SAMPLE NUMBER (see sec. 3.4.1.1)								
		α-Fe 06-0696		Fe_2B 03-1053		$FeSi_2$ 22-1113		Fe_3Si 11-0616	FeSi 22-0632	SiC cubic 29-1129	SiC hex 29-1130
E6.0								5			
E6.1	S2	5	3	3							
E6.2	S1	3	5								
E6.3	S1		4		4	4					
E6.4			5		2						
E6.5	S1		5		2						
	S2							4	4		

TABLE 4.1.1.4 : X-ray results from experiment E6 using the SiC powder mixture. Relative intensities are given on a scale of 1 to 5.

EXPERIMENT NUMBER	REACTANTS	HEATING TIME hrs	HEATING TEMP. °C	HEAT-TREATMENT TIME hrs	HEAT-TREATMENT TEMP °C
E7.1	FeSi powder mix only	3	1440		
E7.3	FeSi powder mix only	3	1030		
E7.4	Fe + FeSi mix to give 3% B in 20 g of product	0.8	1600	2	900
E7.5	Fe + FeSi mix to give 3% B in 20 g of product	0.5	1600	0.5	900

TABLE 4.1.1.5 : Initial experiments with the FeSi powder mixture.

EXPERIMENT NUMBER	SAMPLE NUMBER	alpha-Fe 06-0696	Si 27-1402	$FeSi_2$ 22-1113	FeSi 22-0632	Fe_2B 03-1053
E7.1			5	5	5	
E7.3			5	2		
E7.4		3				5
E7.5	S1	5				
	S2			5		

TABLE 4.1.1.6 : X-ray results from experiment E7 using the FeSi powder mixture.

EXPERIMENT NUMBER	REACTANTS	HEATING TIME hrs	HEATING TEMP. °C	HEAT-TREATMENT TIME hrs	HEAT-TREATMENT TEMP °C
E8.1	Al powder mix only	3	1440		
E8.3	Al powder mix only	3	1000		
E8.2	Fe + 19% Al powder mix	3	1410		

TABLE 4.1.1.7 : Initial experiments using the Al powder mixture.

EXPERIMENT NUMBER / SAMPLE NUMBER	Al_2O_3 corundum 10-0173	Al_2O_3 delta 04-0877	Al 04-0787	$9Al_2O_3.2B_2O_3$ 09-0248	CaB_6 31-0254	CaF_2 04-0864	$CaO.6Al_2O_3$ 25-0122	$CaCO_3$ 05-0453	α-Fe 06-0696	$Fe_{23}(C,B)_6$ 12-0570
E8.1	5		2		5		3			
E8.2	4								3	5
E8.3 S1	5		4		4	2		1		
S3	5	3		4	1	1				

TABLE 4.1.1.8 : X-ray results from experiment E8 using the Al powder mixture. Relative intensities are given on a scale of 1 to 5.

4.1.2 >> FLOW-CONE EXPERIMENTS

The method for flow-cone experiments are given in section 3.4.2.

POWDER MIX.	MEAN FLOW-TIME (sec.)	MEAN SPECIFIC VOLUME (ml/g)	FLOW RATE g/min
SiC	45.9	0.97	153.16
FeSi	34.7	1.43	137.50
Al	41.7	1.54	106.22

TABLE 4.1.2.1 : Result of flow-cone experiments. The mean is based on three values within 3% of the mean.

4.1.3 >> PLUNGE EXPERIMENTS

4.1.3.1 >>> Plunge of Silicon Carbide Powder Mix

During these experiments, 50 g packets of powder wrapped in aluminium foil were plunged into molten iron using a steel tube. With each plunge, some of the tube was melted into the charge and this is accounted for when calculating the maximum possible percent of boron in the melt. In table 4.1.3.1, the maximum %B as calculated for the melt is compared with the boron levels found by chemical analysis and the calculated maximum %Si of the melt is compared with its analytical values. It is considered that some SiC from the SiC/B_2O_3 powder mixture passes through the system unreacted, and this is referred to as SiC lost during the plunge process. If the remaining powder reacts in accordance with equations [1] and [2] of table 4.1.3.1 then the resulting amount of boron and silicon can be calculated and compared with analytical values. The powder composition for the SiC mix is given in table 4.7.5.1 and further calculation details are presented in appendix E.

4.1.3.2 >>> Plunge of Ferrosilicon Powder Mix

During these experiments, 50 g packets of powder wrapped in aluminium foil were plunged into molten iron using a steel tube. With each plunge, some of the tube was melted into the charge and this is accounted for when calculating the maximum possible percent of boron.

In table 4.1.3.2, the more reliable boron analysis is used to calculate the amount of Si required and calculated values are compared with analytical results. The powder composition for the FeSi mix is given in table 4.7.5.1 and further calculation details are presented in appendix E.

CONSTANTS

POWDER USED = SiC POWDER MIX

INITIAL WEIGHT OF IRON USED = 1800 (g)

MEAN WEIGHT LOSS OF PLUNGER PER PLUNGE = 54 (g)

SiC LOST DURING THE PLUNGE PROCESS = 63.5 %

PLUNGER: Mild Steel, ID 22 mm, OD 27 mm, Length 1300 mm

WEIGHT CONVERSION FACTORS FOR SiC POWDER MIX

TO CONVERT TO :	SiC	B_2O_3	WATER	BORON	Si	CARBON
MULTIPLY BY :	0.644	0.283	0.073	0.088	0.451	0.1928

REACTIONS

$$3\,H_2O + SiC_{(s)} = 3\,H_{2(g)} + (SiO_2) + CO_{(g)} \quad \text{.... [A1]}$$

REL.WT.: 54 40.09 3 60.09 28

$$(B_2O_3) + SiC_{(s)} = 2\,\underline{B} + (SiO_2) + CO_{(g)} \quad \text{.... [A2]}$$

REL.WT.: 69.6 40.09 22 60.09 28

SAMPLE NUMBER	PACKET NUMBER	ACCUM. POWDER WEIGHT (g)	CHEMICAL ANALYSIS % BORON %	CHEMICAL ANALYSIS % SILICON %	CALCULATED % BORON %	CALCULATED % SILICON %
S1	0	0.0	0.01	N/A	0.00	0.00
S2	1	50.0	0.02	N/A	0.05	0.30
S3	2	100.0	0.04	N/A	0.09	0.54
S4	3	150.0	0.10	N/A	0.14	0.78
S5	4	200.0	0.11	N/A	0.17	1.00
S6	5	250.0	N/A	N/A	N/A	N/A
S7	6	300.0	0.21	1.50	0.26	1.45
S8	7	350.0	N/A	N/A	N/A	N/A
S9	8	400.0	0.28	N/A	0.34	1.84
S10	9	450.0	N/A	N/A	N/A	N/A
S11	10	500.0	0.42	N/A	0.40	2.20
S12	11	550.0	N/A	N/A	N/A	N/A
S13	12	600.0	N/A	N/A	N/A	N/A
S14	13	650.0	0.57	1.96	0.49	2.67
S15	14	700.0	0.57	N/A	0.51	N/A

TABLE 4.1.3.1 : Plunge of SiC powder mix into molten iron.

CONSTANTS:

POWDER USED IN PACKETS	=	FeSi POWDER MIX	
NUMBER OF 50 g PACKETS USED	=	19	
INITIAL WEIGHT OF IRON	=	1700	(g)
WEIGHT LOSS OF PLUNGER	=	1996	(g)
MEAN WEIGHT INCREASE PER PLUNGE	=	105	(g)

WEIGHT CONVERSION FACTORS FOR FeSi POWDER MIX

TO CONVERT TO :	Fe	B_2O_3	WATER	CaF_2	BORON	Si
MULTIPLY BY :	0.106	0.319	0.135	0.091	0.099	0.327

REACTIONS:

$$2\ B_2O_{3(s)} + 3\ Si_{(s)} = 4\ \underline{B} + 3\ (SiO_2) \text{ ..... [A3]}$$

REL.WT.: 139.2 84.3 43.2 180.3

$$2\ H_2O + Si_{(s)} = (SiO_2) + 2\ H_{2(g)} \text{ ..... [A4]}$$

REL.WT.: 36 28.1 60.1 4

SAMPLE NUMBER	PACKET NUMBER	ACCUM. POWDER WEIGHT (g)	CHEMICAL ANALYSIS % BORON %	CHEMICAL ANALYSIS % SILICON %	CALCULATED % BORON %	CALCULATED % BORON AT EQUILIBRIUM %	CALCULATED % SILICON %
1	0	0	0.00		0.00		0.00
2	1	50	0.15		0.16		0.30
3	2	100	0.23		0.30		0.57
4.1	3	150	0.41		0.43		0.81
5.1	4	200	0.60		0.52		1.08
6	5	250	0.69		0.60		1.32
7	6	300	0.70		0.69		1.51
8.1	7	350	0.77	1.7	0.77		1.68
9	8	400	0.91		0.84		1.85
10.1	9	450	0.93		0.91		1.99
11.1	10	500	1.01		0.98		2.12
12	11	550	1.05		1.04	1.00	2.32
14	13	650	1.09		1.18	1.11	2.53
16	15	750	1.13		1.33	1.20	2.73
18	17	850	1.28	2.8	1.45	1.29	2.89
20	19	950	N/A				

TABLE 4.1.3.2 : Plunge of FeSi powder mix into molten iron

4.1.4 >> INJECTION EXPERIMENTS

4.1.4.1 >>> Injection of Silicon Carbide Powder Mixture at 10 l/min Argon Flow

The SiC/B_2O_3 powder mixture was injected into molten iron with a carrier gas flow rate of 10 l/min Argon. In table 4.1.4.1, the calculated maximum %B of the melt is compared with the boron levels found by chemical analysis and the calculated maximum %Si of the melt is compared with its analytical values. It is considered that some SiC from the SiC/B_2O_3 powder mixture passes through the system unreacted, and this is referred to as SiC lost during the injection process. If the remaining powder reacts in accordance with equations [1] and [2] of table 4.1.4.1 then the resulting amount of boron and silicon can be calculated and compared with analytical values. The powder composition for the SiC mix is given in table 4.7.5.1 and further calculation details are presented in appendix E.

4.1.4.2 >>> Injection of Silicon Carbide Powder Mixture at 20 l/min Argon Flow

The silicon-carbide/boron-oxide powder mixture was injected into molten iron with a carrier gas flow rate of 20 l/min Argon. In table 4.1.4.2, the maximum %B of the melt is compared with the boron levels found by chemical analysis and the calculated maximum %Si of the melt is compared with its analytical values. The powder composition for the SiC mix is given in table 4.7.5.1 and further calculation details are presented in appendix E.

CONSTANTS

POWDER USED	= SiC POWDER MIX
POWDER FLOW RATE	= 1.412 g/sec.
WEIGHT OF IRON USED	= 1500 (g)
WEIGHT LOSS OF IRON CORRECTED FOR CRUCIBLE	= 596 (g)
SiC LOST DURING THE INJECTION PROCESS	= 50 %
NUMBER OF LANCES USED FOR INJECTION	= 5

WEIGHT CONVERSION FACTORS FOR SiC POWDER MIX

TO CONVERT TO :	SiC	B_2O_3	WATER	BORON	Si	CARBON	BORON
MULTIPLY BY :	0.644	0.283	0.073	0.088	0.451	0.1928	0.088

REACTIONS

$$C + H_2O = CO + H_2 \quad \text{..... [1]}$$

REL.WT. : 12 18 28 2

$$B_2O_3 + 3\,C = 2\,B + 3\,CO \quad \text{..... [2]}$$

REL.WT. : 69.6 36 21.6 84

SAMPLE NUMBER	ACCUM. FLOW TIME (sec)	ACCUM. POWDER WEIGHT (g)	CHEMICAL ANALYSIS % BORON %	CHEMICAL ANALYSIS SOLUBLE % SILICON %	CALCULATED % BORON IN MELT (%)	CALCULATED % SILICON IN MELT (%)
S0	0	0.0	N/A	N/A	0.00	0.00
S1	9	12.7	N/A	N/A	N/A	N/A
S2	18	25.4	0.06	N/A	0.04	0.26
S3	29	40.2	0.05	N/A	0.07	0.41
S4	36	50.8	0.11	N/A	N/A	N/A
S5	44	61.4	0.06	N/A	0.10	0.63
S6	51	72.0	N/A	N/A	N/A	N/A
S7	59	82.6	0.10	N/A	0.14	0.84
S8	65	91.1	0.10	N/A	0.16	0.93
S9	71	99.5	0.12	1.06	0.17	1.02
S10	77	108.0	N/A	N/A	N/A	N/A
S11	83	116.5	0.15	N/A	0.20	1.19
S12	89	125.7	0.22	N/A	0.22	N/A
S13	95	133.4	0.24	N/A	0.23	1.36
S14	122	171.6	0.34	1.60	0.30	1.75

TABLE 4.1.4.1 : Injection of SiC powder mix at 10 l/min.

CONSTANTS

POWDER USED	= SiC POWDER MIX
POWDER FLOW RATE	= 1.412 g/sec.
WEIGHT OF IRON USED	= 2000 (g)
WEIGHT LOSS OF IRON CORRECTED FOR CRUCIBLE	= 1013 (g)
SiC LOST DURING THE INJECTION PROCESS	= 0 %
NUMBER OF LANCES USED FOR INJECTION	= 5

CONVERSION FACTORS FOR SiC POWDER MIX

TO CONVERT TO :	SiC	B_2O_3	WATER	BORON	Si	CARBON	BORON
MULTIPLY BY :	0.644	0.283	0.073	0.088	0.451	0.1928	0.088

REACTIONS

$$C + H_2O = CO + H_2 \quad \text{..... [1]}$$

REL.WT. : 12 18 28 2

$$B_2O_3 + 3\,C = 2\,B + 3\,CO \quad \text{..... [2]}$$

REL.WT. : 69.6 36 21.6 84

SAMPLE NUMBER	ACCUM. FLOW TIME (sec)	ACCUM. POWDER WEIGHT (g)	CHEMICAL ANALYSIS % BORON %	CHEMICAL ANALYSIS SOLUBLE % SILICON %	CALCULATED % BORON IN MELT (%)	CALCULATED % SILICON IN MELT (%)
S0	0	0.0	0.00	N/A	0.00	0.00
S1	6	8.5	0.00	N/A	N/A	N/A
S2	14	19.8	0.04	N/A	0.05	0.39
S3	27	38.1	0.09	0.94	0.09	0.75
S4	41	57.9	0.11	N/A	0.14	1.14
S5	52	73.4	0.22	1.28	0.18	1.45

TABLE 4.1.4.2 : Injection of SiC powder mix at 20 l/min.

4.1.4.3 >>> Injection of Ferrosilicon Powder Mixture at 10 l/min Argon Flow

The ferrosilicon/boron-oxide powder mixture was injected into molten iron with a carrier gas flow rate of 10 l/min Argon. In table 4.1.4.3, the analytical values for %Si by weight of melt (unreacted Si) are used together with the amount of Si reacted with water, to calculate the maximum amount of Si used to reduce B_2O_3, and hence the resulting maximum %B in the melt. This is then compared with the analytical %B levels of the melt. Further calculation details are presented in appendix E.

4.1.4.4 >>> Injection of Aluminium Powder Mixture at 10 l/min Argon Flow

During the injection of aluminium/boron-oxide powder mixture into molten iron at 10 l/min, it is considered that the boron oxide is reduced by the free aluminium. In table 4.1.4.4, the total boron added (expressed as Total %B by weight of melt) and the Maximum %B dissolved into the melt have been calculated for comparison with analytical results. Further details on calculation may be found in appendix E.

CONSTANTS

POWDER USED = FeSi POWDER MIX

POWDER FLOW RATE = 0.96 g/sec.

WEIGHT OF IRON USED = 2000 (g)

WEIGHT LOSS OF IRON CORRECTED FOR CRUCIBLE = 435 (g)

NUMBER OF LANCES USED FOR INJECTION = 5

LANCE TYPE: TSL Aluminus Porcelain of ID 8 mm, OD 12 mm

CONVERSION FACTORS FOR FeSi POWDER MIX

TO CONVERT TO :	Fe	B_2O_3	WATER	CaF_2	BORON	Si
MULTIPLY BY :	0.106	0.319	0.135	0.091	0.099	0.327

REACTIONS $2\ B_2O_3 + 3\ Si = 4\ B + 3\ SiO_2$ ..... [1]

REL.WT. : 139.2 84.3 43.2 180.3

$2\ H_2O + Si = SiO_2 + 2\ H_2$ ..... [2]

REL.WT. : 36 28.1 60.1 4

SAMPLE NUMBER	ACCUM. FLOW TIME (sec)	ACCUM. POWDER WEIGHT (g)	CHEMICAL ANALYSIS % BORON %	CHEMICAL ANALYSIS SOLUBLE % SILICON %	CALCULATED % BORON IN MELT (%)	CALCULATED % SILICON IN MELT (%)
S0	0.0	0.0	0.00	0.00	0.00	0.00
S1	15.0	14.4	0.03	0.12	0.03	0.10
S2	25.0	24.0	0.01	0.17	0.05	0.17
S3	33.0	31.7	N/A	N/A	0.06	0.23
S4	43.0	41.3	0.07	0.30	0.08	0.30
S5	53.0	50.9	0.03	N/A	0.10	0.37
S6	53.0	50.9	0.03	N/A	N/A	N/A

TABLE 4.1.4.3 : Injection of FeSi Powder Mix at 10 l/min.

CONSTANTS

POWDER USED = Al POWDER MIX

POWDER FLOW RATE = 0.884 g/sec.

WEIGHT OF IRON USED = 2000 (g)

WEIGHT LOSS OF IRON CORRECTED FOR CRUCIBLE = 459 (g)

NUMBER OF LANCES USED FOR INJECTION = 5

LANCE TYPE USED: TSL Aluminus Porcelain of ID 8 mm, OD 12 mm

CONVERSION FACTORS FOR Al POWDER MIX

TO CONVERT TO :	Al	B_2O_3	WATER	CaF_2	BORON	OXYGEN
MULTIPLY BY :	0.279	0.422	0.199	0.072	0.131	0.177

REACTIONS

$$2\,Al + 3\,H_2O = Al_2O_3 + H_2 \quad \text{..... [1]}$$

REL.WT. : 54 54 102 2

$$2\,Al + B_2O_3 = Al_2O_3 + 2\,B\ (\text{in Fe}) \quad \text{..... [2]}$$

REL.WT. : 54 69.6 102 21.6

SAMPLE NUMBER	ACCUM. FLOW TIME (sec)	ACCUM. POWDER WEIGHT (g)	ACCUM. ALUMINIUM WEIGHT (g)	CHEMICAL ANALYSIS % BORON %	CALCULATED MAXIMUM % BORON IN MELT (%)
S0	0	0.00	0.00	0.00	0.00
S1	15	13.26	3.70	0.00	0.02
S2	23	20.33	5.67	0.03	0.03
S3	33	29.17	8.14	0.03	0.05
S4	41	36.24	10.11	0.01	0.06
S5	49	43.32	12.09	0.06	0.07

TABLE 4.1.4.4 : Injection of Al powder mix at 10 l/min.

5. DISCUSSION OF RESULTS

5.1 > INTRODUCTION

5.1.1 >> THE ROLE OF VOLATILE BORON MONOXIDE IN FERROBORON PRODUCTION

It is now generally accepted that in the transfer of silicon from slag to metal, the production of silicon, ferrosilicon and silicon carbide, silicon monoxide plays an important part. The equivalent boron systems are very similar involving a very acid oxide, a carbide, B_4C and a volatile oxide. Although ferroboron production on a commercial scale has taken place for decades, it is worthwhile to consider the possible importance of boron monoxide vapour on the thermodynamics and mechanism of the process.

Applying the phase rule, for a system of three components; boron, oxygen and carbon, the sum P + F = 5. For any arbitrary temperature and pressure, three phases e.g. two condensed phases and a gas can exist at equilibrium. The condensed phases are B_2O_3, C, B_4C and B whereas the gas is made up of a mixture of CO and BO. For these phases, a number of monovariant equilibria are possible such as:

$$B_2O_{3(l)} + C_{(S)} = 2\ BO_{(g)} + CO_{(g)} \qquad [1]$$

$$5\ B_2O_{3(l)} + B_4C_{(S)} = 14\ BO_{(g)} + CO_{(g)} \qquad [2]$$

$$B_2O_{3(l)} + B_{(S)} = 3\ BO_{(g)} \qquad [3]$$

$$5\ B_{(S)} + CO_{(g)} = B_4C_{(S)} + BO_{(g)} \qquad [4]$$

$$B_4C_{(S)} + 4\ CO_{(g)} = 5\ C_{(S)} + 4\ BO_{(g)} \qquad [5].$$

If at a given temperature, the partial pressure of one gaseous component is established, the partial pressure of the second component is fixed for each of the above phase combinations or the gas composition is fixed.

The following thermodynamic data has been used to estimate the above equilibria:

$B_2O_3\ (l) = 2\ B_{(S)} + {}^3/_2\ O_2\ (g)$	$\Delta G^\circ =$	$293{,}700 - 50.20\ T$
$BO_{(g)} = B_{(S)} + \frac{1}{2}\ O_2\ (g)$	$\Delta G^\circ =$	$909 + 21.22\ T$
$B_4C_{(S)} = 4\ B_{(S)} + C_{(S)}$	$\Delta G^\circ =$	$9{,}920 + 1.33\ T$
$CO_{(g)} = C_{(S)} + \frac{1}{2}\ O_2\ (g)$	$\Delta G^\circ =$	$27{,}340 + 20.50\ T$

The following free energy values for the above equilibrium of interest in ferroboron production are:

$$\Delta G^\circ_{[1]} = 264{,}542 - 113.14\ T$$
$$\Delta G^\circ_{[2]} = 1437{,}445 - 569.91\ T$$
$$\Delta G^\circ_{[3]} = 290{,}937 - 113.86\ T$$
$$\Delta G^\circ_{[4]} = 116{,}511 + 0.61\ T$$
$$\Delta G^\circ_{[5]} = 115{,}644 - 4.21\ T$$

For a total working pressure of one bar [$p_{CO} = p_{BO}$] the variation of the partial pressure of BO is shown in Graph 5.1.1.1 as a function of temperature for each of the above monovariant equilibria. It can be seen that the set of curves intersect at the points X (1585°C) and Y (1815°C) corresponding to the non-variant phase combinations $B_2O_3 + B_4C + C$ and $B_2O_3 + B_4C + B$ respectively. In this diagram, the full drawn curves denote stable phase equilibria and the broken curves to metastable phase combinations. Thus at point 2, which corresponds to the metastable equilibria between $B_2O_3 + B + C$, the system is unstable (but not by much) and would react to form B_4C. It can also be observed that at points X and Y the boron monoxide partial pressure are approximately 10^{-3} bar and 10^{-2} bar respectively indicating that the gas contains ≈ 0.1% and ≈ 1% BO respectively. All the curves relate to boron being present as pure phase.

The mechanism for the production of boron can be considered in a shaft furnace at atmospheric pressure. The reaction mixture of boric acid and carbon will descend in an atmosphere of BO and CO with the temperature increasing as it descends. At temperatures above 1585°C, carbon can react with BO by a reversion of reaction [5] to produce B_4C. A direct reaction between B_2O_3 and carbon is also possible as in reaction [1] above. The mixture of B_4C and B_2O_3 will descend to the hottest part of the furnace. At temperatures above 1815°C, they react by a combination of reaction [2] and the reverse of reactions [3] and [4] to give boron, $CO_{(g)}$ and $BO_{(g)}$.

The stoichiometry of the process can now be considered. By considering B_4C formation by the reversion of reaction [5] and by reaction of carbon with B_2O_3 (reaction [1]), the following stoichiometry is arrived at:

$$200\ BO + 250\ C = 50\ B_4C + 200\ CO$$

$$>1585^\circ C \qquad 100\ B_2O_3 + 350\ C = 50\ B_4C + 300\ CO$$

$$>1815^\circ C \qquad 17\ B_2O_3 + 50\ B_4C = 233\ B + BO + 50\ CO$$

The stoichiometry given for the high temperature reaction is derived from the fact that the equilibrium mixture at point Y contains about 2% BO. According to this scheme, the process is remarkably efficient with a 99.5% recovery of carbon and only 0.5% loss of boron as boron monoxide. Indeed the efficiency of the process is likely to be even more favourable because boron monoxide is expected to condense at lower temperatures. It is expected that the addition of iron should facilitate the process. Iron will lower the activity of boron and as a result reduce the pressure of boron monoxide at point Y. Graph 5.1.1.2 and 5.1.1.3 represent the variation of boron monoxide pressures with temperature under conditions of ferroboron production with boron activities of 0.5 and 0.1 respectively.

The first factor to note is that under these conditions, the phase field associated with B_4C disappears due to the instability of this phase. It is necessary to include a further reaction involving boron and carbon i.e:

$$BO + C = B + CO \qquad \Delta G^{\circ}_{[6]} = -26431 + 0.72\ T$$

It is also observed that the temperature of ferroboron formation decreases to 1580°C and 1485°C for a_B=0.5 and 0.1 respectively. In addition, the critical boron monoxide pressure is reduced significantly suggesting an increase in productivity.

Overall, the thermodynamics indicate a very efficient process. One factor which may effect the process is the association of liquid boric oxide with carbon and iron as well as the gas flow. Certainly, interfacial tension and viscosity factors could play an important role in this context.

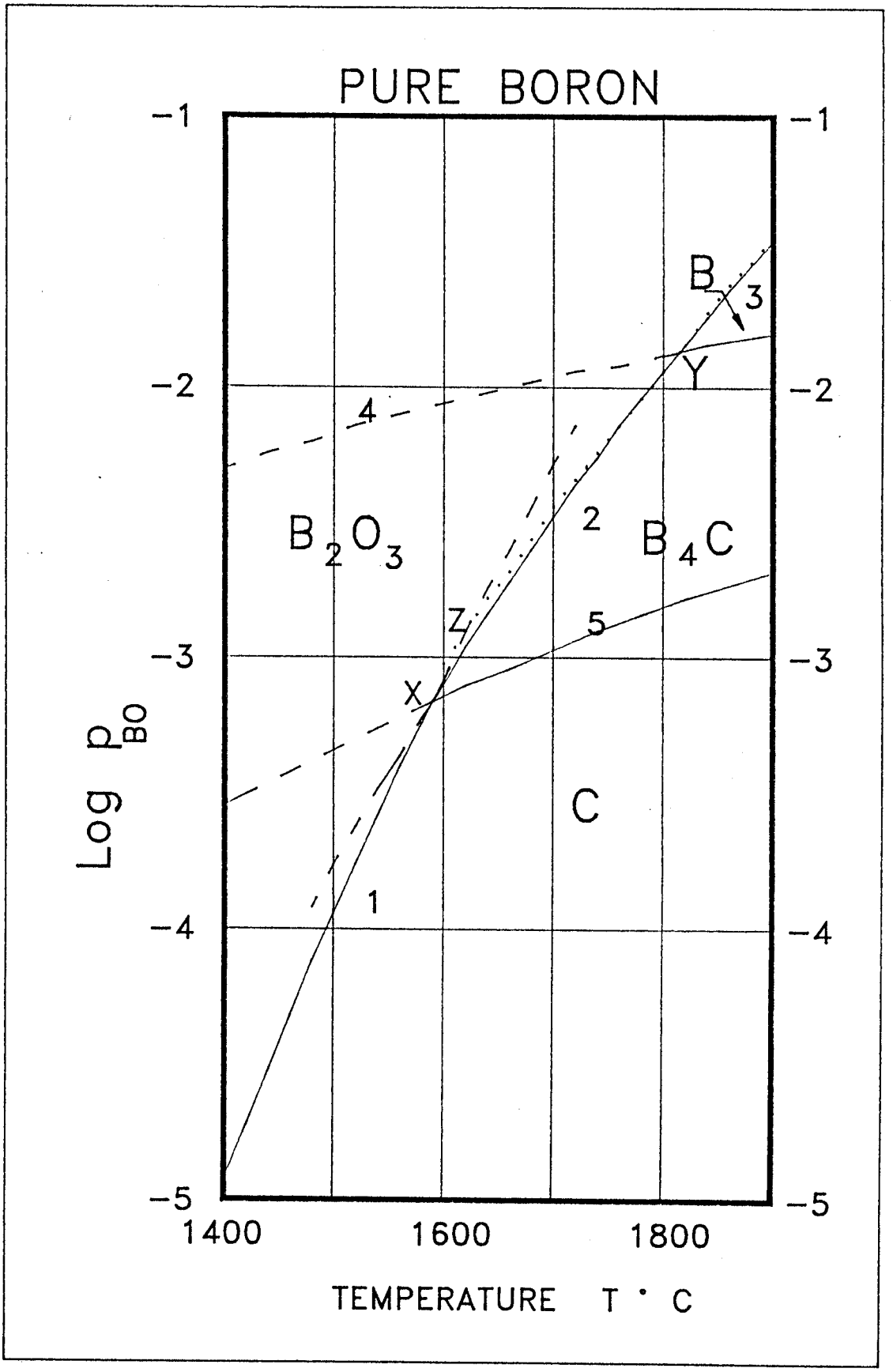

GRAPH 5.1.1.1 : The variation in partial pressure of BO with temperature for various monovariant equilibria.

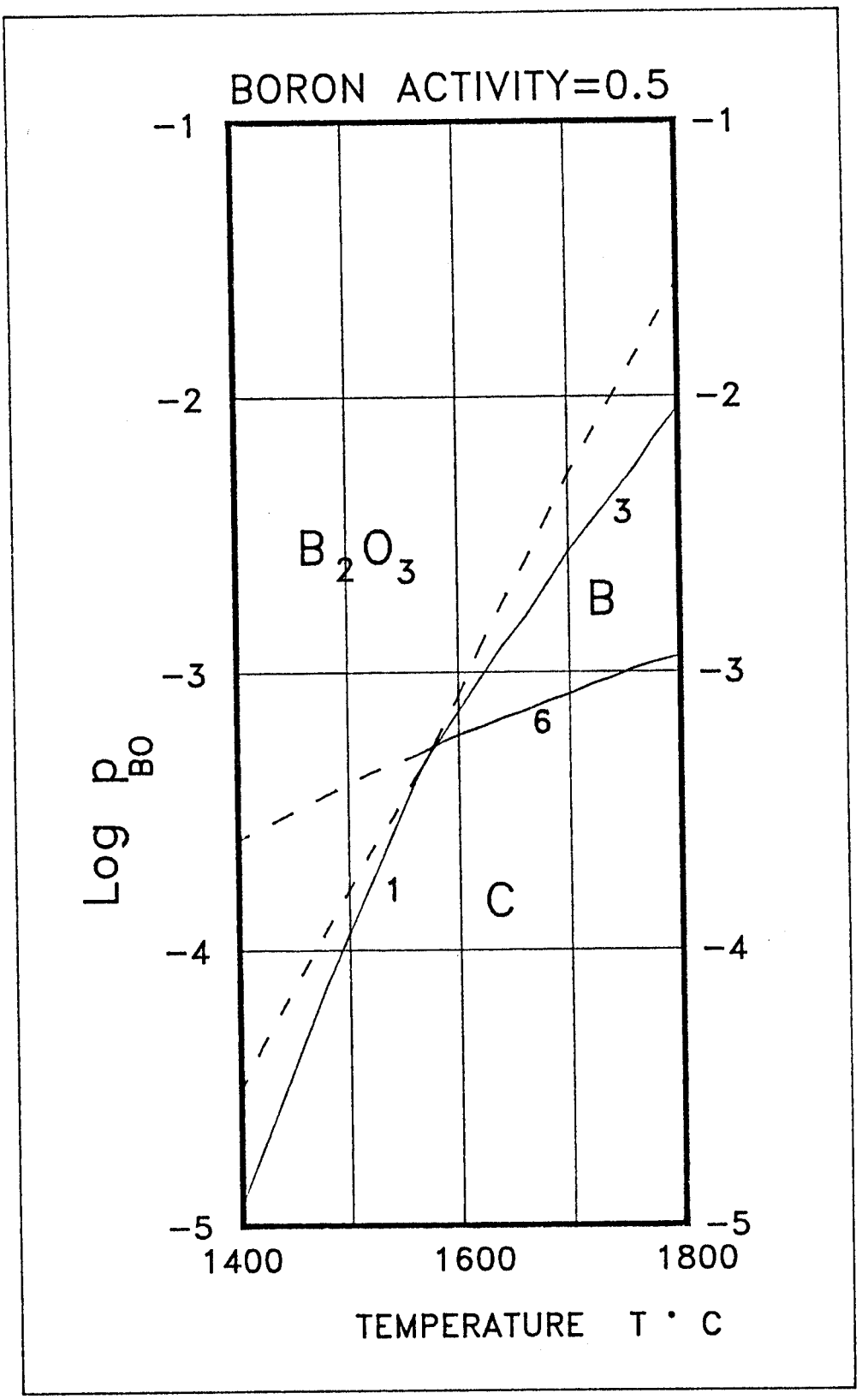

GRAPH 5.1.1.2 : The variation in partial pressure of BO with temperature under conditions of ferroboron production with boron activity = 0.5 .

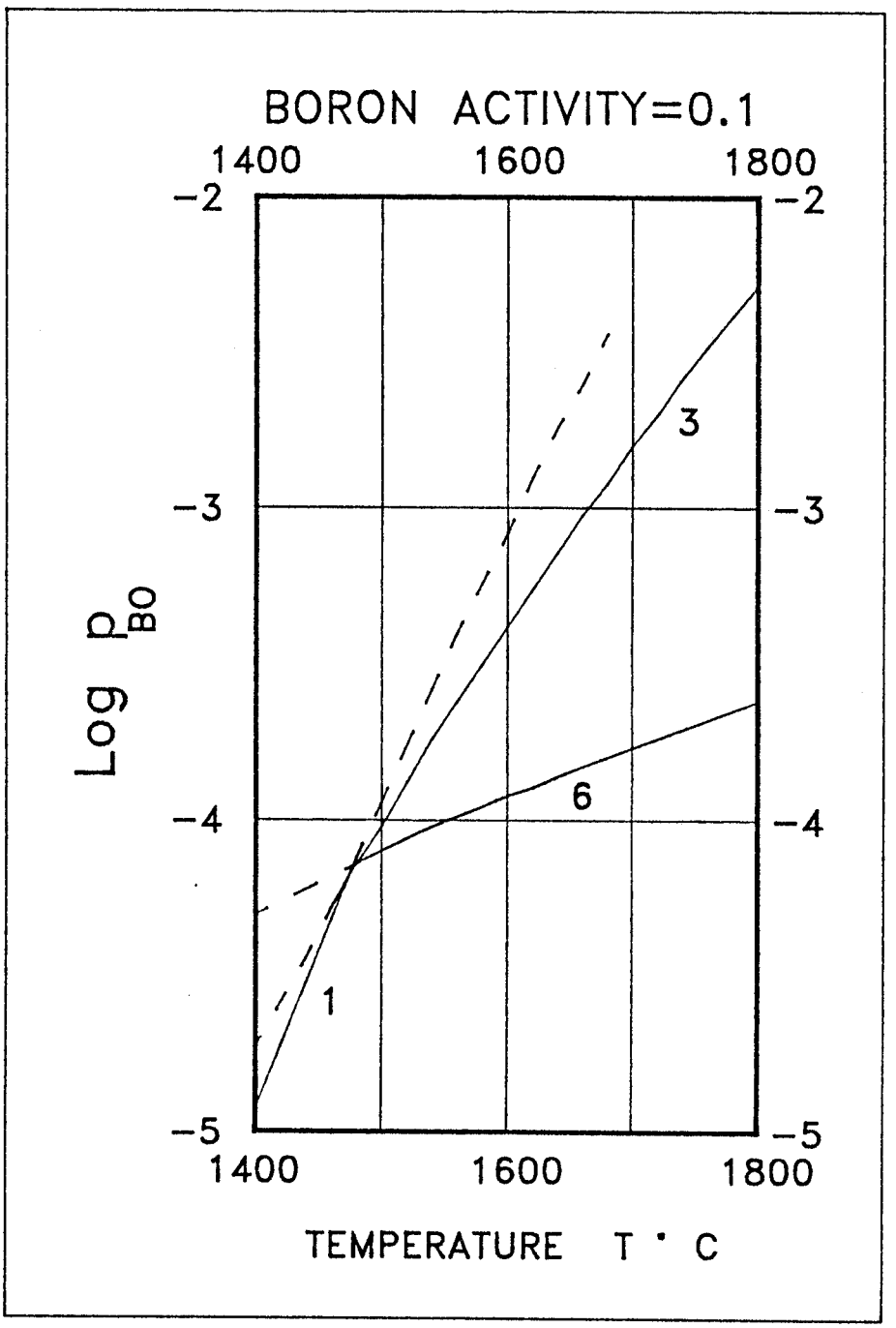

GRAPH 5.1.1.3 : The variation in partial pressure of BO with temperature under conditions of ferroboron production with boron activity = 0.1 .

5.1.2 >> BUBBLES IN MOLTEN IRON

The motion of bubbles in a liquid depends on the liquid density (ρ), viscosity (η), surface tension (σ) and bubble velocity (u) as expressed by the Reynolds number (N_{re}), Eotvos number (N_{eo}) and Morton number (N_m) defined below (Turkdogan, E.T., 1980).

$$N_{re} = ul/v \qquad 5.1.2.1$$

$$N_{eo} = gl^2(\rho-\rho^\circ)/\sigma \qquad 5.1.2.2$$

$$N_m = g\eta^4/\rho\sigma^3 \qquad 5.1.2.3$$

Where: l = characteristic length
ρ° = density of dispersed phase
ρ = density of continuous phase
g = acceleration due to gravity
u = velocity
η = viscosity
v = kinematic viscosity
and σ = surface tension.

The shape of bubbles can be spherical, ellipsoidal or spherical cap, and for all shapes, the size is defined as the diameter of the equivalent sphere.

Figure 5.1.2.1 has been derived from data on the velocity of rise and shape of bubbles for liquids with Morton numbers between 10^{-14}–10^{8}.

For Reynolds numbers less than 2 and for all N_{eo}, a spherical bubble is obtained (see figure 5.1.2.1), the terminal velocity of which is governed by Stoke's law and Hadamard-Rybczynski equation. Stoke's law applies to bubbles that behave like rigid spheres and gives the terminal velocity as:

$$u_t = gd^2\Delta\rho/18\eta$$

where: d = bubble diameter
$\Delta\rho$ = difference between the liquid and gas densities
η = viscosity of the liquid

For large bubbles with mobile surfaces, there is a transfer of momentum across the bubble interface and gas circulation within the bubble. For these large bubbles the Hadamard-Rybczynski equation predicts u_t to be 50% more than that obtained by Stoke's law.

Reynolds numbers >100 and Eotvos number more than about 40 result in spherical cap bubbles. The straight lines in figure 5.1.2.1 are in accordance with the terminal velocity (u_t) derived by Davies and Taylor (1950). They found that the equation for potential flow around a sphere in the region near the forward stagnation point could be combined with the Bernouilli's equation to give the terminal velocity for a spherical cap u_t as:

$$u_t = 0.72\ (g.d)^{0.5}$$

Experimental values of u_t for the rise of spherical cap bubbles in water and mercury (Davenport, Richardson and Bradshaw 1967) agree with this equation for bubbles with an equivalent diameter of 1-1.5 cm. Larger bubbles give rise to lower u_t values than predicted, and this discrepancy is attributed to container wall effects.

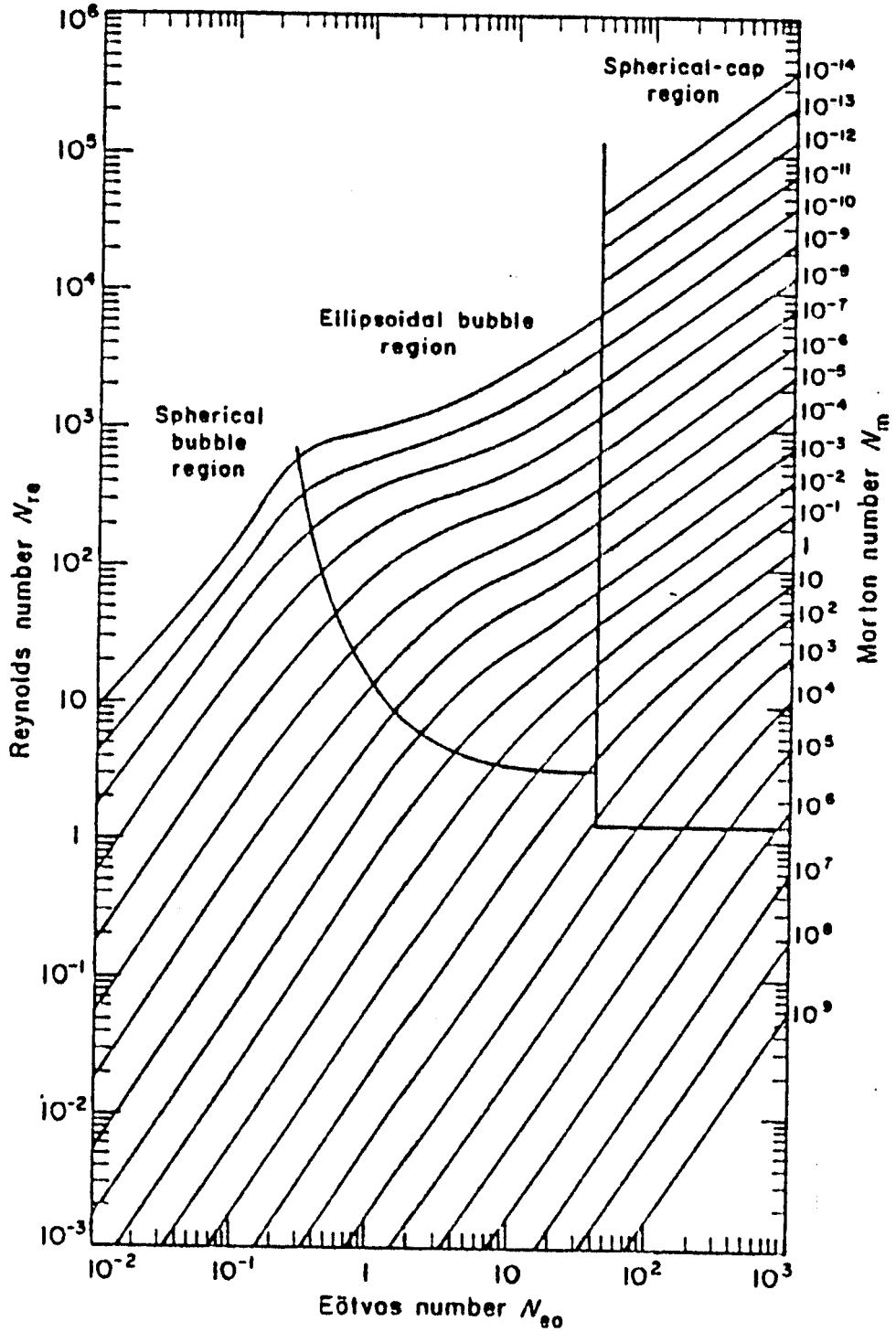

FIGURE 5.1.2.1 : Correlation between Reynolds number and Eotvos number for single bubbles in a Newtonian liquid (Grace 1973)

5.1.3 >> DISPERSION OF METAL IN SLAG BY GAS BUBBLES

There are three mechanisms for the dispersion of metals in slags. Spontaneous emulsification of the metal at the interface, diffusion of the metal and precipitation away from the interface (stranding) and mechanical transfer by gas bubbles. In this section the transfer of metal to slag by gas bubbles is discussed.

The phenomenon of metal dispersion in slag by the use of gas bubbles is well known and used in pneumatic metal refining processes. Kozakevitch and Leroy (1954) examined the extent of metal dispersion in slags and showed that 20-40% metallic iron from 0.1-5 mm were entrapped in the slag during decarburization in the Bessemer process. Foaming slags entrain more metal and when the foam collapses, larger metal droplets are formed.

Davenport et al (1967) showed using pictures, how one liquid is transported to another when bubbles cross the interface between the two liquids (see figure 5.1.3.1).

Poggi et al (1969) showed that an increase in the viscosity of the top liquid, or an increase in the gas flow rate, increased the amount of metal that was dispersed in the upper liquid. Minto and Davenport (1972) proposed a generalization based on the minimum interfacial energy, which illustrates three types of behaviour when bubbles cross the interface between two liquids:

a) The bubble carries an intact film of metal to the slag layer when the film coefficient

$$\Gamma = (\sigma_{g/s} - \sigma_{g/m} - \sigma_{m/s}) \text{ is } > 0 \qquad 5.1.3.1$$

where σ is the surface energy between gas/slag, gas/metal and metal/slag.

b) The metal film breaks, but some metal droplets become attached to bubbles and they are floated up when the floatation coefficient

$$\Delta = (\sigma_{g/s} - \sigma_{g/m} + \sigma_{m/s}) \text{ is } > 0 \qquad 5.1.3.2$$

Floating is by attachment to a bubble (see figure 5.1.3.2).

c) The metal film breaks, but the droplets are dispersed instead of being floated when $\Delta < 0$ (see figure 5.1.3.2).

Conochie & Robertson (1980) extended this idea and considered the contact angle between the gas and two liquids, ignoring the difference in density between them. (see figure 5.1.3.3 (a))

The forces at point A in the direction x and y are given by:

x: $\sigma_{g/s} = \sigma_{g/m} \cos\theta + \sigma_{m/s} \cos\phi$

y: $\sigma_{g/m} \sin\theta = \sigma_{m/s} \sin\phi$

σ is now made dimensionless by the definitions:

$$X = \sigma_{m/s} / \Sigma\sigma$$

$$Y = \sigma_{g/m} / \Sigma\sigma$$

and $Z = \sigma_{g/s} / \Sigma\sigma$

where $\Sigma\sigma = \sigma_{g/m} + \sigma_{g/s} + \sigma_{m/s}$

Note that the values of X, Y and Z are bounded by :

$$-1 \leq \cos\theta \leq 1$$

and $-1 \leq \cos\phi \leq 1$

This gives four limiting combinations of θ and ϕ as follows:

a) $\theta = 0°$, $\phi = 0°$

The metal is spread as a thin film between the gas and the slag, for which $X + Y + Z = 0.5$

b) $\theta = 0^\circ$, $\phi = 180^\circ$

The metal is only in contact with the slag. That is, the metal is dispersed in the slag, for which $Y = 0.5$

c) $\theta = 180^\circ$, $\phi = 0^\circ$

The metal is only in contact with the gas, for which $X = 0.5$

d) $\theta = \phi$

The metal is spaced between the gas and slag for which $X = Y$.

Figure 5.1.3.3 (b) shows a ternary interfacial energy diagram with each of the above four boundary conditions plotted on it. This figure shows that for each of $X > 0.5$, $Y > 0.5$ and $Z > 0.5$, one of the surface energy values (σ) is > (the sum of the other two). Hence a 3-phase contact is not energetically favoured, as indicated also by the film coefficient Γ in equation 5.1.3.1 . The criterion for the floatation coefficient Δ defined by equation 5.1.3.2 is given by $Y < 0.5$.

Conochie & Robertson (1980) provided a unique distinction between the four modes of floatation of metal in slag (or a phase m in a phase s) by gas bubbles.

In practice, the Three criteria established by Minto and Davenport (1972) are found to be sufficient to describe the overall physical phenomenon when gas bubbles cross the interface between Two liquids.

Application of these predictions by E.T. Turkdogan (1983) to the experimental data of Minto and Davenport for interfacial energies in Cu melt/slag systems shows that a decrease in the slag basicity and an increase in the melt grade (increased copper sulphide content) results in floatation region conditions.

For gas-slag-metal systems, only the following conditions are most likely to occur:

Floatation

$\sigma_{g/s} < \sigma_{g/m} + \sigma_{m/s}$ i.e. $Z < 0.5$

$\sigma_{m/s} < \sigma_{g/m} + \sigma_{g/s}$ i.e. $X < 0.5$

$\sigma_{g/m} < \sigma_{g/s} + \sigma_{m/s}$ i.e. $Y < 0.5$

Dispersion

$\sigma_{g/m} > \sigma_{g/s} + \sigma_{m/s}$ i.e. $Y > 0.5$

However, this will not be the same for foam slags with much larger gas/liquid volume ratios. Note also, that the above considerations only apply to gas bubbling up from one liquid and through another on top of it. The motion and residence time of the floated or dispersed particles of phase m in phase s also depend on other factors, such as the density difference, viscosity and the rate of bubbling.

Urquhart and Davenport (1970) performed room temperature and high temperature experiments simulating oxygen top blowing conditions in the blown oxygen steel-making process. The room temperature experiments were done in a 1:50 scale model of the steel-making furnace, and a 1:40 scale model was used for the high temperature experiments.

The Oxygen jet velocities were based on a modified Froude number as follows: $\rho_g V_j^2 / (\rho_l d g)$

Where: V_j = exit velocity of the gas

d = lance internal diameter

ρ_g = gas density

ρ_l = liquid density

g = 9.81

The rate of dispersion of the lower liquid in the upper one was measured together with the rate of reaction with the blowing gas.

Some results of Urquhart and Davenport have been reproduced in figure 5.1.3.4 which shows that at a steady state, about 30 vol% of the lower liquid is dispersed in the upper one with iron droplets in the range 0.1 to 3 mm in diameter, which is similar to the oxygen blown process.

Metal droplets in the slag were decarbonised at a faster rate than the underlying bulk metal as expected.

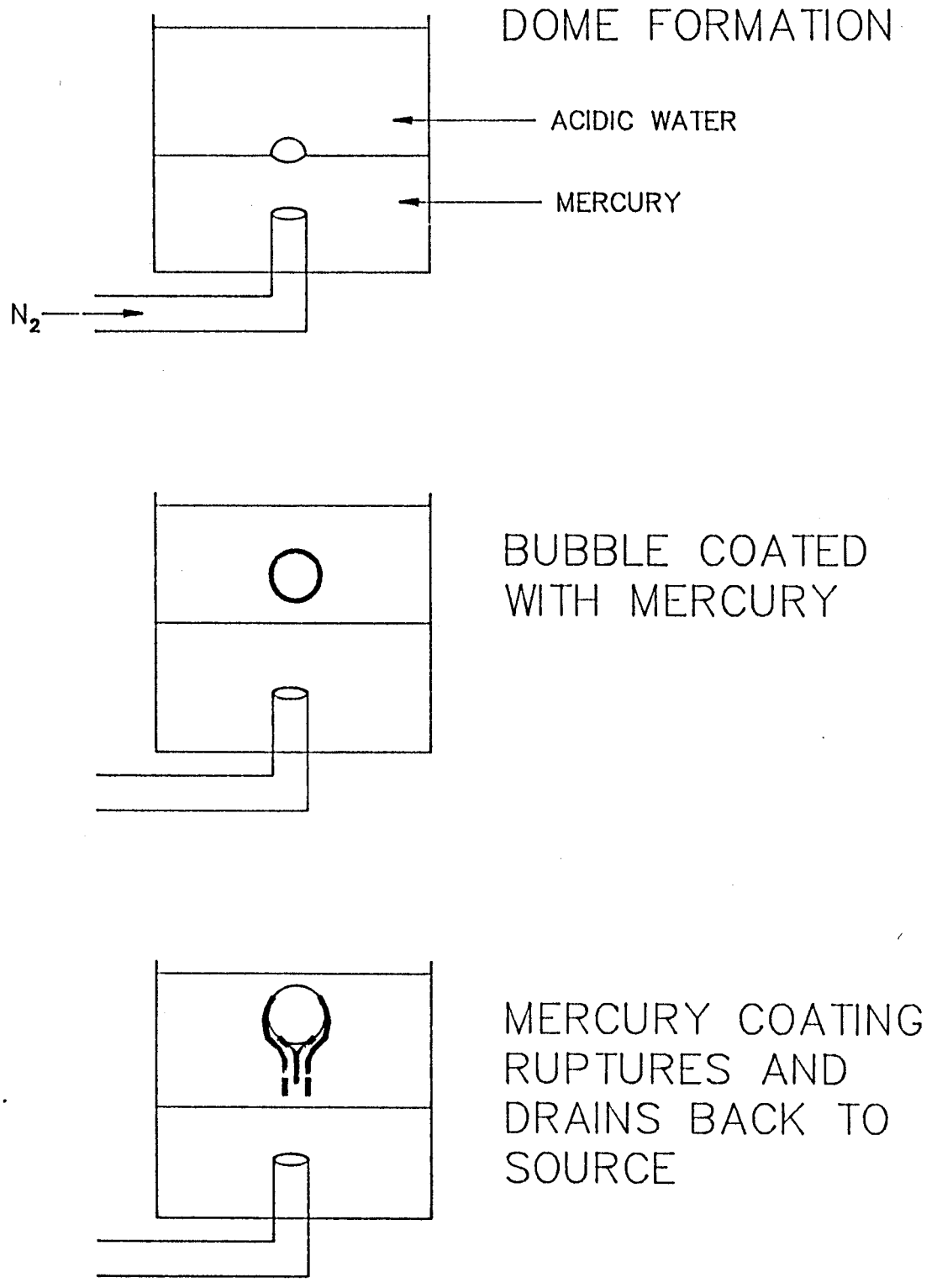

FIGURE 5.1.3.1 : Transportation of one liquid to another when bubbles cross the interface between the two liquids.

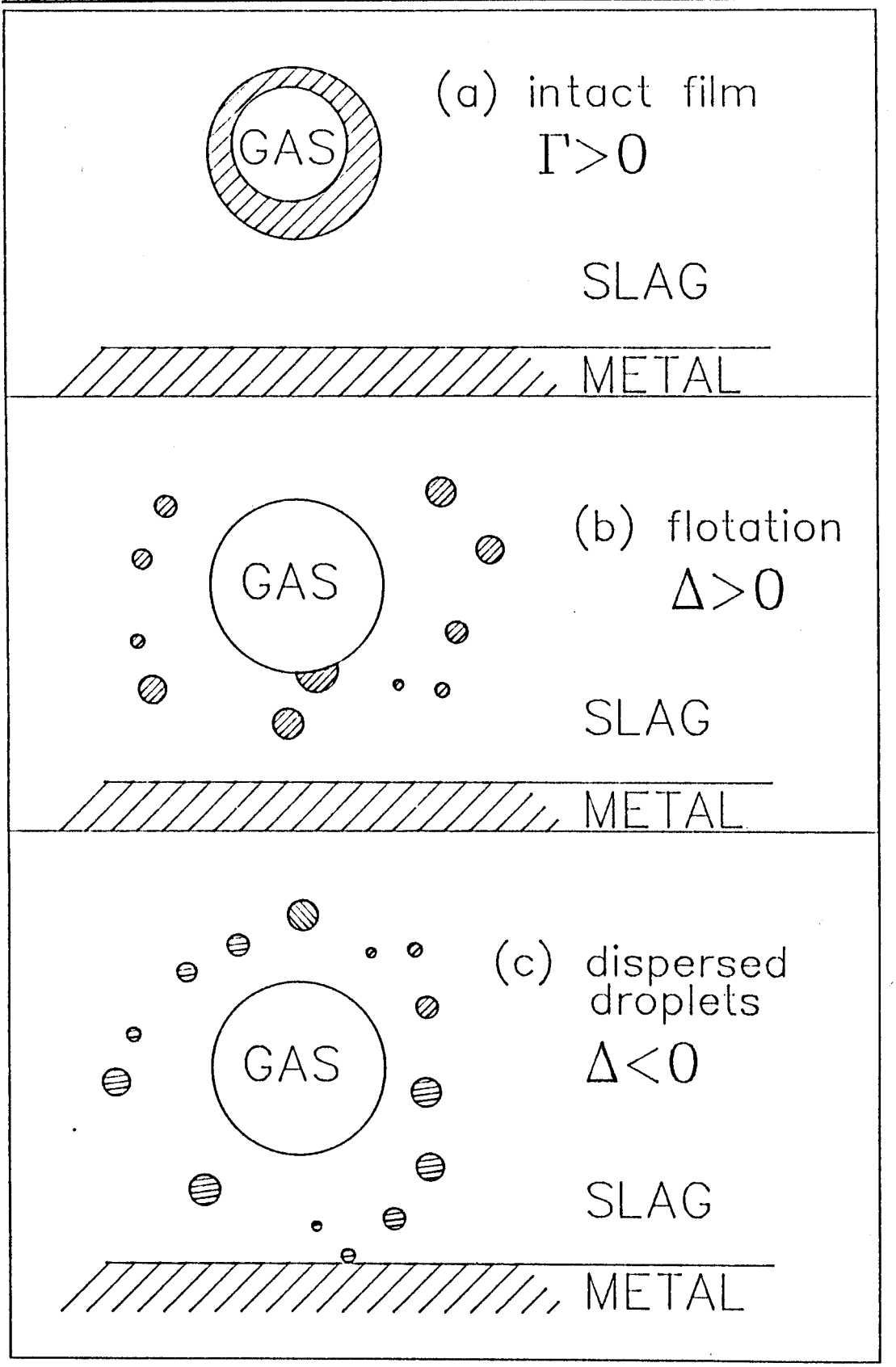

FIGURE 5.1.3.2 : Three types of behaviour when bubbles cross the interface between two liquids.

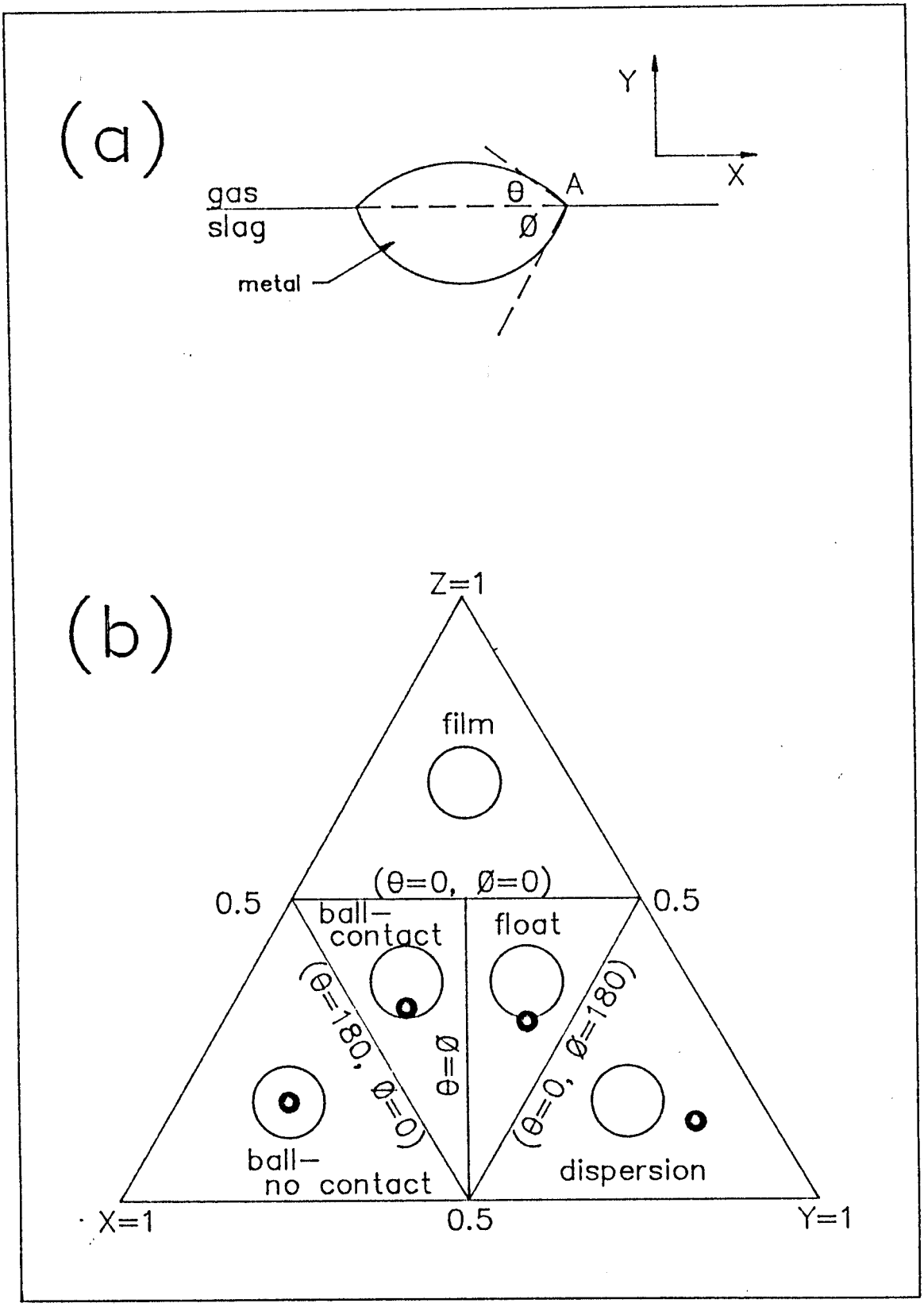

FIGURE 5.1.3.3 : (a) The contact angles θ and Φ between a gas bubble and two liquids. (b) Ternary interfacial energy diagram with each of the four boundary conditions.

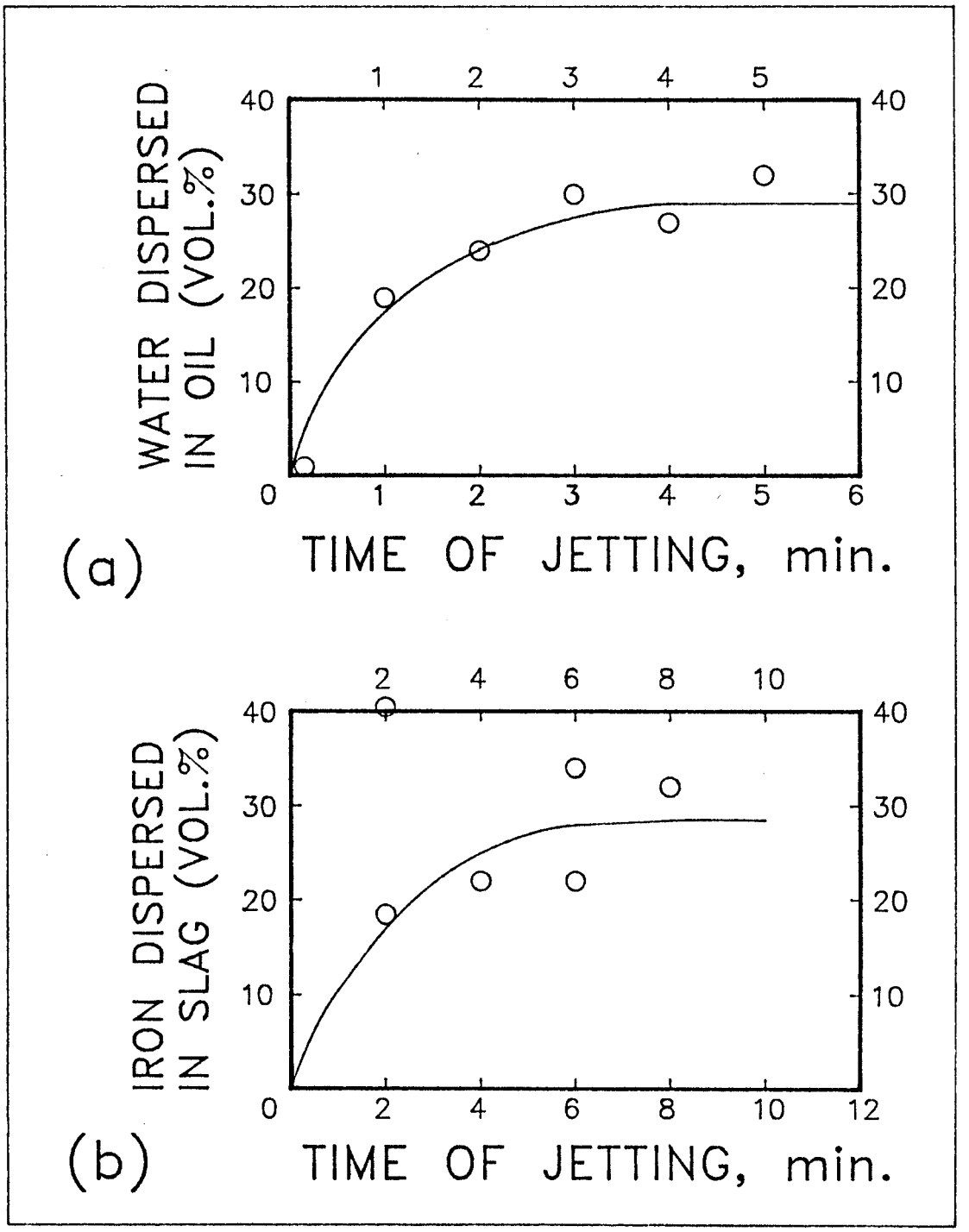

FIGURE 5.1.3.4 : Extent of dispersion of water in oil and liquid iron in slag: (a) water-oil system for Froude number = 340; (b) liquid iron (carbon)-slag system at 1350°C for Froude number = 30. After Urquhart and Davenport (1970)

5.2 > THERMODYNAMIC CONSIDERATIONS FOR BORON REDUCTION

This investigation has dealt with the reduction of boron compounds, B_2O_3 and H_3BO_3, with silicon carbide, ferrosilicon and aluminium. The reducing reactions of interest are:

$$2(B_2O_3) + 3\,\underline{Si} = 4\,\underline{B} + 3(SiO_2) \quad \ldots\ldots\ldots \quad 5.2.1$$

$$(B_2O_3) + 3\,C = 2\,\underline{B} + 3\,CO_{(g)} \quad \ldots\ldots\ldots \quad 5.2.2$$

$$(B_2O_3) + 2\,Al = 2\,\underline{B} + (Al_2O_3) \quad \ldots\ldots\ldots \quad 5.2.3$$

$$(B_2O_3) + 3\,H_{2(g)} = 2\,\underline{B} + 3\,H_2O_{(g)} \quad \ldots\ldots \quad 5.2.4$$

where slag components are shown in brackets and melt components are underlined. It should be noted that equilibria involving boric acid have been ignored because boric acid easily dissociates at low temperatures to give boric oxide and water. Because of the presence of reducing agents silicon and aluminium, it is assumed that the water produced will be quickly reduced to hydrogen as indicated by the following reactions:

$$2\,H_2O_{(g)} + \underline{Si} = 2\,H_{2(g)} + (SiO_2) \quad \ldots\ldots \quad 5.2.5$$

$$3\,H_2O_{(g)} + 2\,Al = 3\,H_{2(g)} + (Al_2O_3) \quad \ldots \quad 5.2.6$$

Each of these reactions can be calculated in terms of the available thermodynamic data. In all cases, the elements boron silicon and aluminium are given a standard state of 1 wt.% due to the small final quantities in solution in iron.

The thermochemical data for equation 5.2.1 can be computed from the following equations:

$2\ B_2O_{3(l)} = 4\ B_{(S)} + 3\ O_2\ (g)$ $\quad \Delta G^\circ = -587{,}400 - 100.4\ T$

$4\ B_{(S)} = 4\ \underline{B}\ (1\%)$ $\quad \Delta G^\circ = -62{,}400 - 20.6\ T$

$3\ \underline{Si}\ (1\%) = 3\ Si_{(l)}$ $\quad \Delta G^\circ = 92{,}290 + 12.4\ T$

$3\ Si_{(l)} + 3\ O_2\ (g) = 3\ Si_2O_2\ (S)$ $\quad \Delta G^\circ = -649{,}500 + 125.9\ T$

$2B_2O_{3(l)} + 3\ Si(1\%) = 4\ B(1\%) + 3\ SiO_{2(l)}$ $\quad \Delta G^\circ = -30{,}210 + 17.3\ T$

The equilibrium reaction gives $\Delta G^\circ = -\ RT\ \ln(K)$

Where: $K = (a^3_{(SiO_2)}\ .\ \%B^4)\ /\ (a^2_{(B_2O_3)}.\ \%Si^3)$

At 1500°C, K = 0.69

For reaction 5.2.2 the following is obtained:

$B_2O_3\ (l) = 2\ B_{(S)} + {}^3/_2\ O_2\ (g)$ $\quad \Delta G^\circ = 293{,}700 - 50.2\ T$

$3\ C\ (S) + {}^3/_2\ O_2\ (g) = 3\ CO\ (g)$ $\quad \Delta G^\circ = -82{,}020 - 61.5\ T$

$2\ B\ (S) = 2\ B\ (1\%)$ $\quad \Delta G^\circ = -31{,}200 - 10.3\ T$

$B_2O_{3(l)} + 3\ C_{(S)} = 2\ B(1\%) + 3\ CO_{(g)}$ $\quad \Delta G^\circ = 180{,}480 + 122.0\ T$

The equilibrium reaction gives $\Delta G^\circ = -\ RT\ \ln(K)$

Where: $K = (p^3(CO)\ .\ \%B^2)\ /\ (a_{(B_2O_3)}\ .\ a^3_{(C)})$

At 1550°C, $K = 1.06 \times 10^5$

For 1% carbon dissolved in iron,

$3\ C\ (1\%) = 3\ C\ (S)$ $\quad \Delta G^\circ = -16{,}200 + 30.3\ T$

and the equilibrium reaction gives $\Delta G^\circ = 164{,}280 - 91.7\ T$, $\quad K = 2.22$

.

For reaction 5.2.3 thus:

$B_2O_{3(l)} = 2\ B_{(S)} + {}^3/_2\ O_2\ (g)$	$\Delta G^\circ = 293{,}700 - 50.2\ T$
$2\ B\ _{(S)} = 2\ \underline{B}\ (1\%)$	$\Delta G^\circ = -31{,}200 - 10.3\ T$
$2\ \underline{Al}\ (1\%) = 2\ Al\ _{(l)}$	$\Delta G^\circ = 30{,}200 + 13.3\ T$
$2\ Al\ _{(l)} + {}^3/_2\ O_2\ (g) = Al_2O_3\ (S)$	$\Delta G^\circ = -403{,}260 + 78.1\ T$
$B_2O_{3(l)} + 2\ Al\ (1\%) = 2\ B\ (1\%) + Al_2O_3\ (S)$	$\Delta G^\circ = -110{,}560 + 30.9\ T$

The equilibrium reaction gives $\Delta G^\circ = -\ RT\ \ln(K)$

Where $K = (a(Al_2O_3)\ .\ \%B^2)\ /\ (a(B_2O_3)\ .\ \%\ Al^2)$

At 1500°C, $K = 3.18 \times 10^6$

For reaction 5.2.4 the following is obtained:

$B_2O_{3(l)} = 2\ B_{(S)} + {}^3/_2\ O_2\ (g)$	$\Delta G^\circ = 293{,}700 - 50.2\ T$
$3\ H_2\ (g) + {}^3/_2\ O_2\ (g) = 3\ H_2O\ (g)$	$\Delta G^\circ = -177{,}450 + 40.1\ T$
$2\ B\ _{(S)} = 2\ B\ (1\%)$	$\Delta G^\circ = -31{,}200 - 10.3\ T$
$B_2O_{3(l)} + 3\ H_2\ (g) = 2\ B\ (1\%) + 3\ H_2O\ (g)$	$\Delta G^\circ = 85{,}050 - 20.4\ T$

The equilibrium reaction gives $\Delta G^\circ = -\ RT\ \ln(K)$

Where: $K = (p^3(H_2O)\ .\ \%B^2)\ /\ (a(B_2O_3)\ .\ p^3(H_2))$

At 1550°C, $K = 1.8 \times 10^{-6}$

5.3 > DISCUSSION OF SILICON-CARBIDE/BORIC-OXIDE POWDER MIXTURE EXPERIMENTS

5.3.1 >> MASS BALANCE CONSIDERATIONS

The silicon-carbide/boric-oxide mixture was produced from these materials in the ratio 65% silicon carbide and 35% boric oxide. Experience showed that boric oxide is very hygroscopic and quickly hydrates to produce hydrated oxides. A chemical analysis of the powder gave SiC = 64.4 wt%; B_2O_3 = 28.3 wt% and H_2O = 7.3 wt%.

During the plunge and injection experiments it was expected that water would be liberated very quickly. The rapid evolution of water from the mixture was proved by heating the powder at 1000°C in a thermogravometric apparatus where the loss in weight due to water evaporation occurred in less than two minutes. Due account of the presence of water in the mixture must be taken in any mass balance calculations for these experiments. It is assumes that the water present reacts with the silicon carbide as follows:

$$3\ H_2O_{(g)} + SiC_{(S)} = 3\ H_{2\ (g)} + (SiO_2) + CO_{(g)}$$

Relative weights: 54 40 6 60 28

It is considered that the overall reaction may take place in stages, that is, the reaction of water with molten iron to give oxygen dissolved in iron and hydrogen :

$$3\ H_2O_{(g)} \longrightarrow 3\ H_{2\ (g)} + 3\ \underline{O}$$

followed by the reaction with silicon carbide thus:

$$3\ \underline{O} + SiC_{(S)} = (SiO_2) + CO_{(g)}$$

In addition, it is considered that silicon carbide reacts with molten boric oxide to produce boron dissolved in the iron and silica according to the following reaction:

$$(B_2O_3) + SiC_{(S)} = 2\ \underline{B} + (SiO_2) + CO_{(g)}$$

5.3.2 >> PLUNGE EXPERIMENTS

Initial calculations based on the above considerations gave very poor agreement with the experimental values giving silicon and boron levels in the metal, which were approximately three times the observed values. Such poor agreement for the mass balance is obviously unacceptable especially since it is considered that experimental error even in difficult experiments such as these is much less than a factor of three. It was decided that these errors could only be accounted for if a proportion of the silicon carbide passed through the system unreacted. On this basis, fair agreement for the mass balance was achieved by assuming 36.5% of the silicon carbide reacted in the system whilst 63.5% passed out into the top slag unreacted. The experimental and calculated boron and silicon contents of the metal with various plunge additions of 50 g packets of mixture are presented in Graph 5.3.2.1 .

The mass balance calculations gave a slag analysis at the top of the metal of 59% B_2O_3 and 41% SiO_2 .

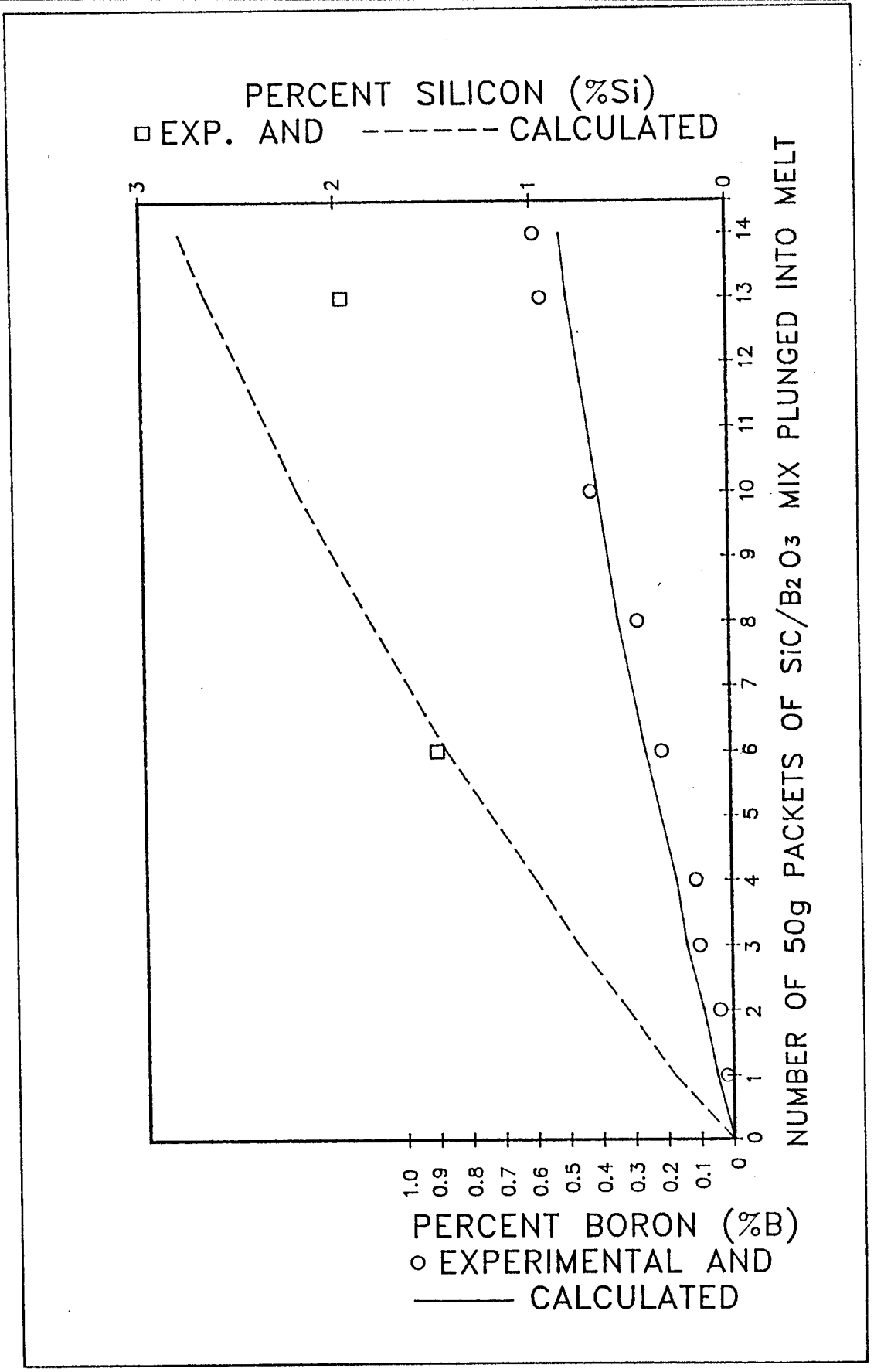

GRAPH 5.3.2.1 : Plunge of 50 g packets of SiC/B_2O_3 powder mixture into molten iron. Experimental and calculated values for %B and %Si in the melt.

5.3.3 >> INJECTION OF SiC/B_2O_3 POWDER WITH 10 L/MIN ARGON GAS

Once again, very poor agreement was obtained for mass balance calculations if all the silicon carbide was assumed to react. For these experiments the error involved was a factor of two. On the assumption that 50% of the silicon carbide passed through without reacting, fair agreement was again obtained with the boron and silicon analysis as shown in Graph 5.3.3.1 . The slag analysis obtained from these mass balance calculations is 56% B_2O_3 and 44% SiO_2 indicating improved boron reduction efficiency for the injection experiment compared with the plunge method.

5.3.4 >> INJECTION OF SiC/B_2O_3 POWDER WITH 20 L/MIN ARGON GAS

Contrary to the previous experiments, reasonable mass balance calculations were obtained when injection flow rate of 20 l/min of argon carrier gas was used. A further surprise was that the experimental values for increase in silicon content with time agreed well with the total silicon injected (see Graph 5.3.4.1) . The fact that dissolution of silicon carbide was complete under these conditions must be related to the increased mass transfer accompanying the increased gas injection rate. However, the good agreement with the silicon contents indicates that boron oxide reduction was achieved solely by the carbon. This mechanism seems most unlikely especially as silicon is a more potent reducing agent than carbon and because the other silicon carbide experiments are explicable only in terms of some silicon reaction. The mechanism which is more acceptable is that silicon is produced by the reactions:

$$3\ H_2O_{(g)} + SiC_{(S)} = 3\ H_2\ _{(g)} + (SiO_2) + CO_{(g)}$$

$$(B_2O_3) + SiC_{(S)} = 2\ \underline{B} + (SiO_2) + CO_{(g)}$$

The silica thus produced is subsequently reduced by carbon according to the reaction:

$$(SiO_2) + 2\ \underline{C} = \underline{Si} + 2\ CO_{(g)}$$

Further considerations of this mechanism will be made when the kinetics of the reactions are considered.

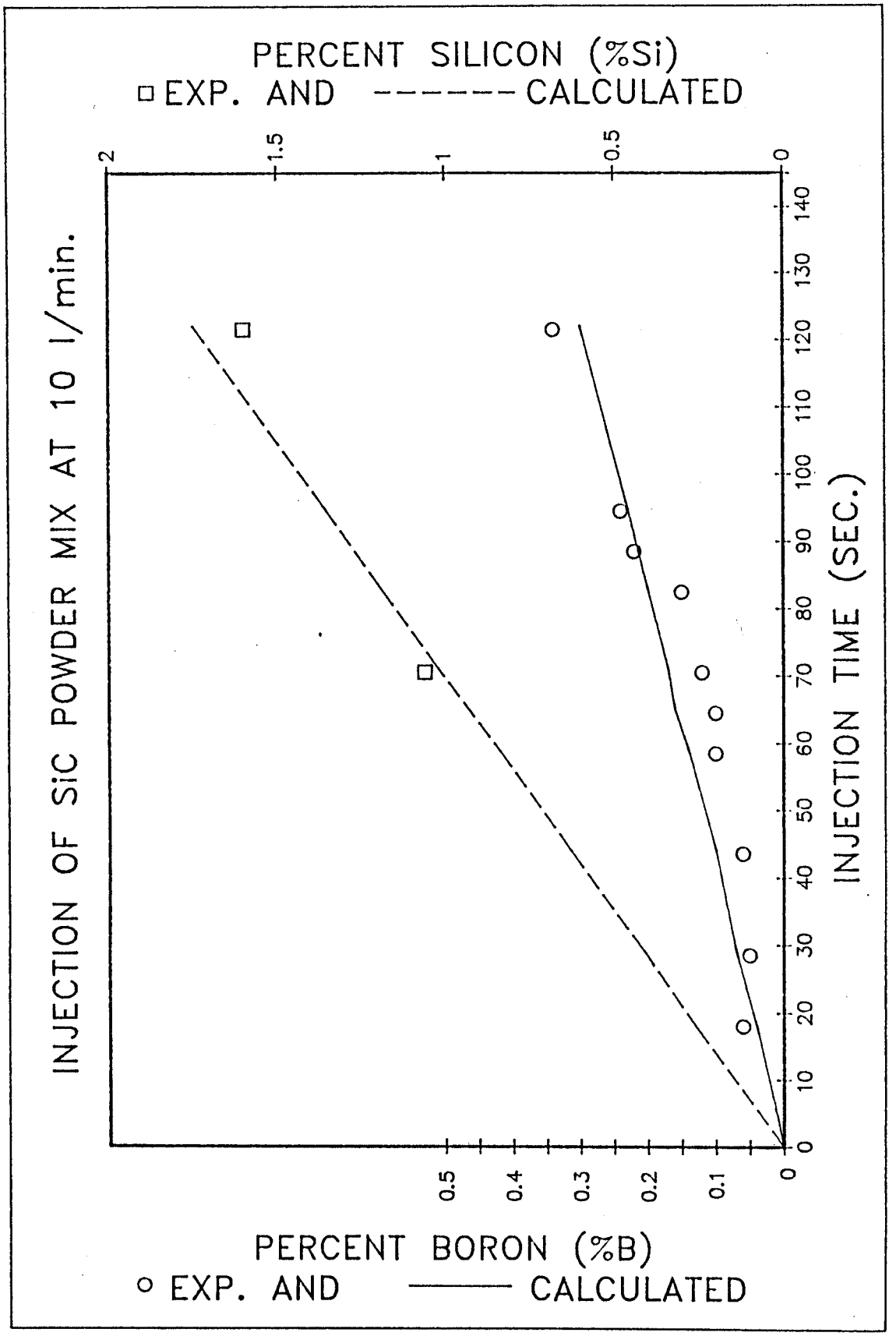

GRAPH 5.3.3.1 : Injection of SiC/B_2O_3 powder mixture into molten iron at 10 l/min. Experimental and calculated values of %B and %Si in the melt are compared against injection time.

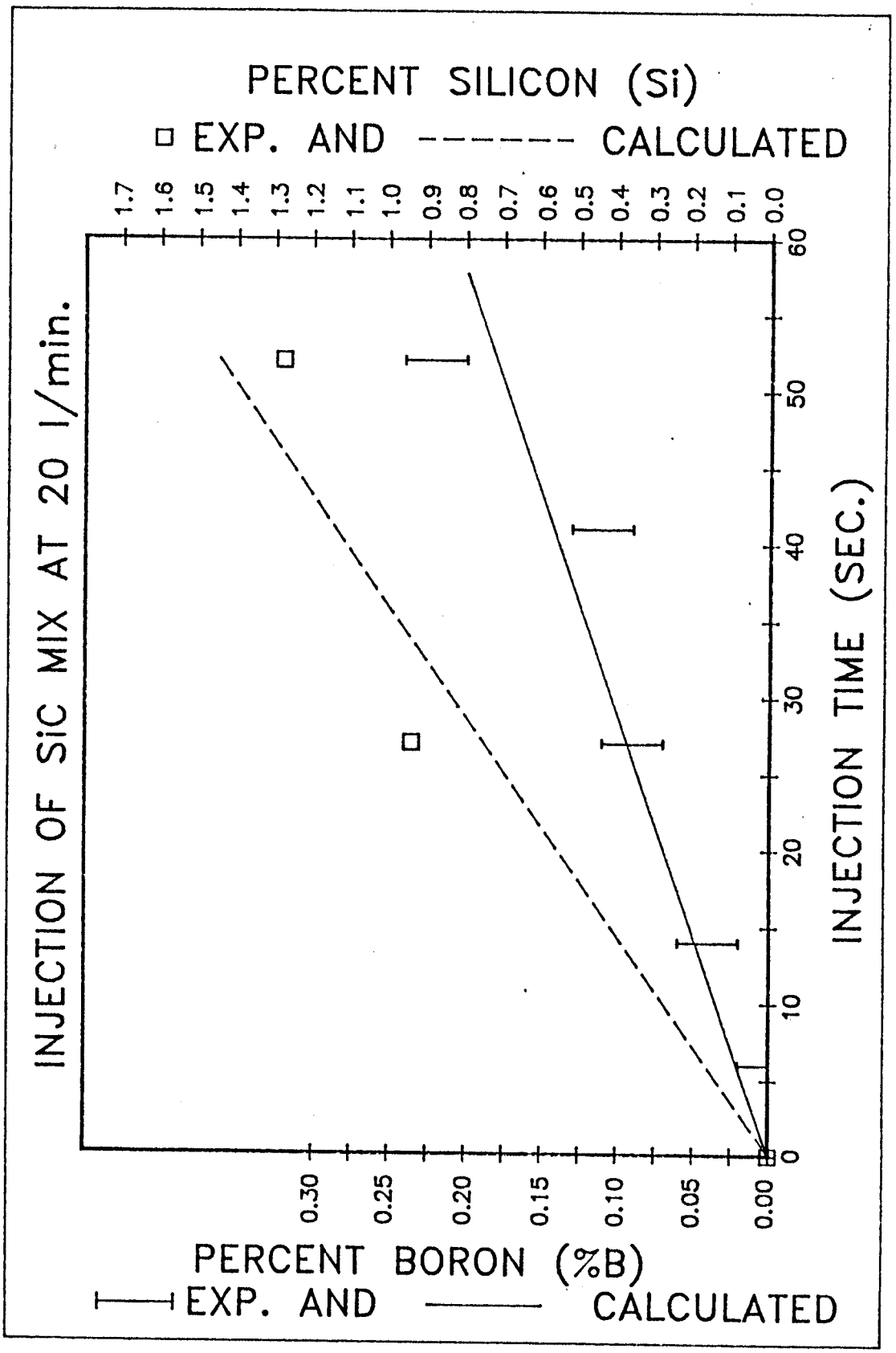

GRAPH 5.3.4.1 : Injection of SiC/B_2O_3 powder mixture into molten iron at 20 l/min. Experimental and calculated values of %B and %Si in the melt are compared against injection time.

5.3.5 >> KINETICS OF SILICON-CARBIDE / BORIC-OXIDE REACTION IN IRON

In gas-liquid, solid-liquid and liquid-liquid systems, forced or natural convection currents have a pronounced effect on the transport of reactants and products to and from the reaction interface. From the mass balance calculations, only a portion of the silicon carbide reacts and dissolves in the iron for the experiments involving plunging and powder injection with an argon flow rate of 10 l/min. Under these conditions it seems probable that the dissolution of silicon carbide in iron may be the rate controlling process. This hypothesis seems appropriate when it is realised that for experiments with $SiC-B_2O_3$ powders the extent of boron reaction is related directly to the silicon content of the iron.

For the dissolution of silicon carbide in iron, the total number of moles of silicon dissolved in a unit time, $n_{Si} = J_{Si}.A$ where A is the interfacial area between the silicon carbide and the liquid iron, and

$$J_{si} = k_{Si} [(C_{Si})_{eqm} - C_{Si}]$$

where J_{si} is the rate of transfer of silicon per unit area per unit time and C_{Si} is the bulk molar concentration of Si per unit volume and k_{Si} is the mass transfer coefficient.

Therefore: $n_{Si} = A.k_{Si} [(C_{Si})_{eqm} - C_{Si}]$

If V is the volume of liquid iron, the rate of increase in concentration of silicon C_{Si} with time (t) is given by:

$$- \frac{dC_{Si}}{dt} = \frac{n_{Si}}{V}$$

Inserting in the above equation,

$$- \frac{dC_{Si}}{dt} = \frac{A}{V}. k_{Si} [(C_{Si})_{eqm} - C_{Si}]$$

Since the same concentration term is present on both sides of the equation, any units can be used for C_{Si} and weight percent will be used here.

By arranging and integrating this equation, the following is obtained:

$$- \ln [(\%Si)_{eqm} - \%Si] = - \frac{k.A}{V}. t + I$$

Where I is an integration constant which can be evaluated from the original composition of the iron.

In order to test the equilibrium silicon content, $(C_{Si})_{eqm}$ must be evaluated. The available data for the effect of silicon on the solubility of carbon is presented in Graph 5.3.5.1 for 1550°C. On the assumption that silicon carbide dissolves as the compound, 1.2% carbon will be equivalent to 2.8% silicon in solution. From this mass balance and the solubility data, a value for $(C_{Si})_{eqm}$ of 7.3 wt% can be obtained.

The experimental result for the argon injection rate of 10 l/min are plotted in accordance with this mass transport relationship in Graph 5.3.5.2 . The value of k.A/V obtained is 2.3×10^{-3}/sec.

It is interesting to compare this experimental rate parameter with a theoretical prediction. The model proposed by Engh (1972) is considered to be applicable to the transitory reaction under the present experimental conditions, i.e fine powder injection. In this model, the injected powder was assumed not to penetrate into the melt but rather to cover the whole surface of the gas bubbles. The model gives the total interfacial area available for reaction as:

$$A = 3.v_g.\Omega.H \;/\; r.v_b$$

where v_g is the injection gas flow rate, Ω is the shape factor of the gas bubble (ratio of the surface area of a bubble to the surface area of a sphere of equivalent volume), H is the lance immersion depth, r is the bubble radius and v_b is the upward velocity. The radius r for this expression is given by:

$$r = 12.\sigma \;/\; \rho.f.v_b^2$$

where σ is the surface tension of the metal, f is the friction factor for rise of the gas bubble and ρ is the metal density, and v_b is given by:

$$v_b = (4.\sigma.g/f.\rho)^{1/4}$$

where g is acceleration due to gravity.

Engh et al also estimated the mass transfer coefficient in the metal phase as: $k = (8.D.v_b / \pi.r)^{\frac{1}{2}}$
where D is the diffusivity of silicon in molten iron.

These equations yield the following relationships in terms of end-point variables: $r = 6\ (\sigma/\rho.f.g)^{\frac{1}{2}}$

$$k = 0.77\ D^{1/2}\ (\rho.f.g^3/\sigma)^{1/8}$$

$$A.k = 0.27\ D^{1/2}\ (\rho.f/\sigma)^{7/8}\ g^{3/8}\ v_g.\Omega.H$$

This model has been applied to the present case using $v_g = 1.75 \times 10^3$ ml/sec at 1623°K, H = 4.5 cm, σ = 1800 dynes/cm, ρ = 7 g/cm^3, D = 5×10^{-5} cm^2/sec, Ω=1.5, f = 0.5 and a value of A.k/V of 5.5×10^{-3} sec^{-1} was obtained.

The value estimated from Engh's theory is 2.4 times larger than that deduced from the experimental results. This is not a bad agreement, taking into account the uncertainties of both the theory and the present experiment. When applying the theory, the injection depth was taken as 4.5 cm which is the submerged depth of the injection lance. The effective depth of the bubble ascent may be slightly larger due to jet penetration into the melt.

One possible explanation of the large value obtained from the theory is as follows. In the model it is assumed that the film covers the whole surface of the gas bubble. However it is known that bubbles of equivalent diameter 2r>2 cm rise through molten metal as spherical caps. Conochie and Robertson (1980) using the open top bubble technique, found that slag existed only on the base of spherical cap bubbles. If this correction is applied, the reaction area is reduced by $^1/_3$ or $^1/_2$, thus giving much better agreement with the present experiment. In addition, the flux used in this work contained only $^2/_3$ silicon carbide. In view of the large uncertainties, the agreement between experiment and theory is as good as can be expected in support of the hypothesis that silicon carbide dissolution in the liquid iron is the probable rate controlling process.

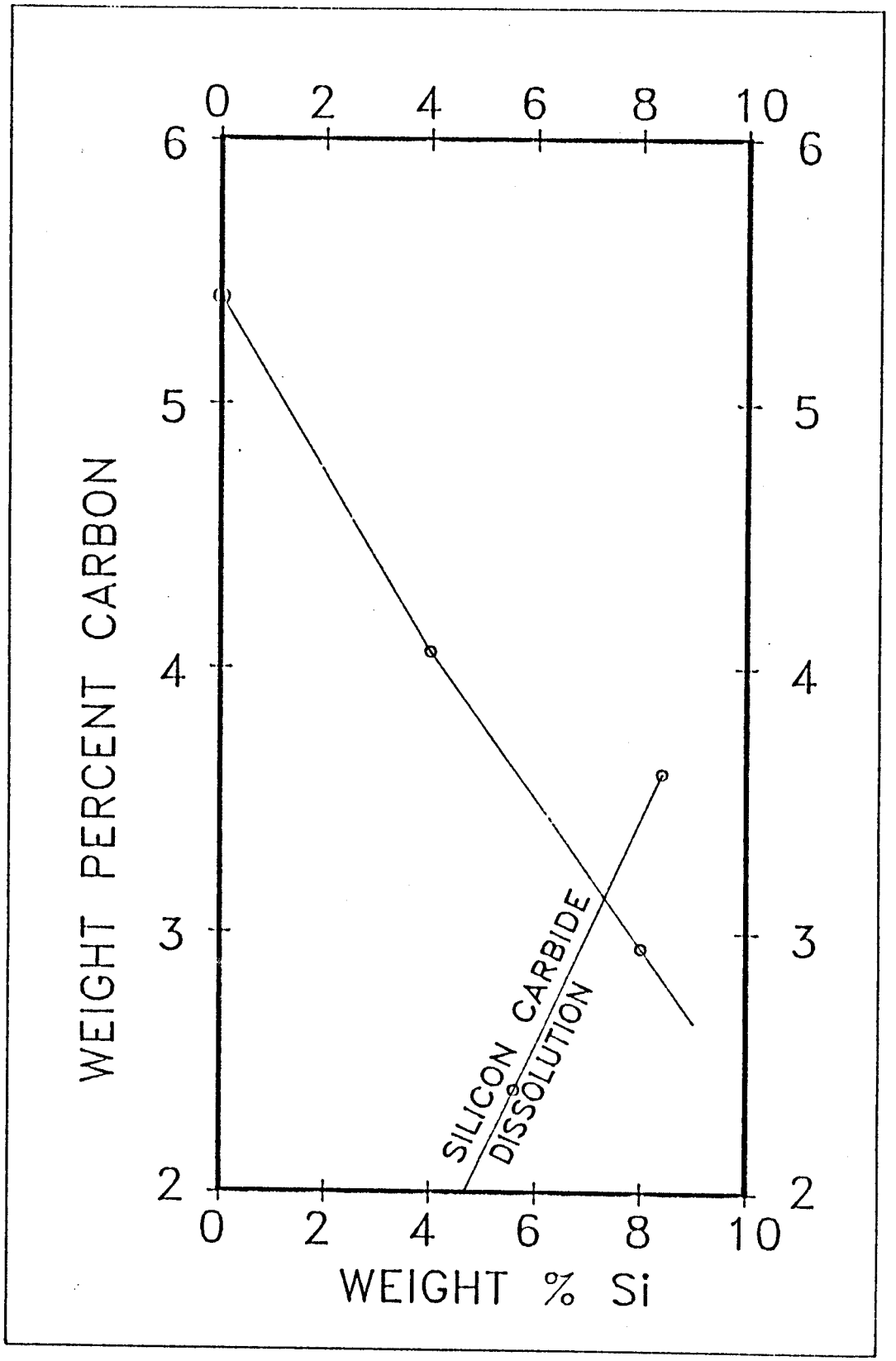

GRAPH 5.3.5.1 : Effect of silicon on the solubility of carbon in molten iron. Chipman et al (1952).

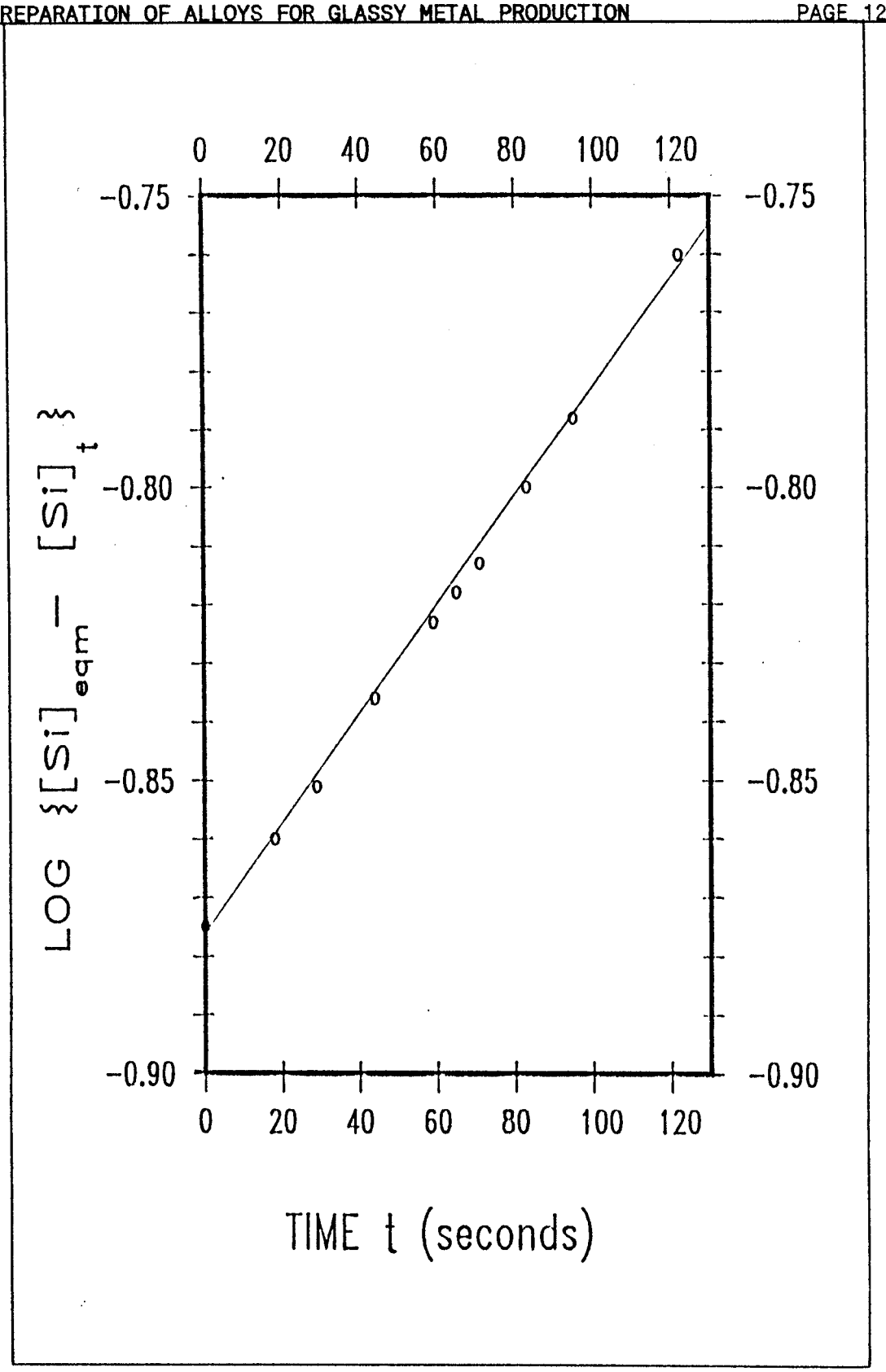

GRAPH 5.3.5.2 : The variation of silicon concentration with time in molten iron when considering the mass transfer coefficient. Comparison of calculated and experimental results for the experiment where SiC/B_2O_3 powder mixture was injected at 10 l/min.

5.4 > DISCUSSION OF FERROSILICON/BORIC-OXIDE POWDER EXPERIMENTS

As with the silicon carbide - boric acid mixture, the ferrosilicon - boric oxide powder proved to be very hygroscopic and quickly absorbed water to produce hydrated boric oxide. A chemical analysis of the mixture gave:

FeSi Mix	32.7%	Si
	10.6%	Fe
	31.9%	B_2O_3
	13.5%	H_2O
	9.1%	CaF_2
	2.2%	unknown

Once again it was expected that water would be liberated rapidly upon heating and this was proved correct by heating the powder to 1000°C where a rapid weight loss occurred. It is assumed that the water present reacts with the silicon as follows:

$$2\ H_2O_{(g)} + \underline{Si} = 2\ H_{2(g)} + 3\ (SiO_2)$$

In addition, it is also considered that silicon also reacts with molten boric oxide to produce boron dissolved in iron and silica according to the reaction:

$$2\ (B_2O_3) + 3\ \underline{Si} = 4\ \underline{B} + 3\ ((SiO_2)$$

5.4.1 >> FERROSILICON / BORIC-OXIDE POWDER PLUNGE EXPERIMENTS

For short reaction times, mass balance considerations gave fairly good agreement with the boron content of the metal on the basis that reaction proceeded in the mixture to produce a mixture containing 40% Si and 23.5% B. The slag produced by this reaction was 29% B_2O_3, 68% SiO_2 and 13% CaF_2. The experimental and calculated boron and silicon contents of the metal with various plunge additions of 50 g packets are presented in figure 5.4.1.1. In view of the experimental as well as analytical problems, the agreement is probably as good as can be expected. It is noted that for larger quantities of powder addition, the values of boron fell below the calculated values to a significant level.

It was decided to test these data by equilibrium considerations. Thus a graph of log %B verses log %Si was plotted and is shown in figure 5.4.1.2. It can be seen that the values for the higher levels of boron and silicon lie on a straight line with a slope of 3/4 as expected for partial equilibrium according to the reaction:

$$2\ (B_2O_3) + 3\ \underline{Si} = 4\ \underline{B} + 3\ (SiO_2)$$

These results indicate that boron absorption by the iron is limited by the silicon content for boron levels above ≈1%. For comparison the results for the silicon carbide experiment are included on this graph to show that ferrosilicon is a more efficient boron reducing agent than silicon carbide.

5.4.2 >> INJECTION OF FERROSILICON / BORIC-OXIDE POWDER WITH 10 l/min ARGON GAS

These results (shown on graph 5.4.2.1) are also consistent with the mass balance calculations but surprisingly the quantity of boron reduced was less than observed for the plunge experiments for the same weight of powder. The results are consistent with the production of a slag containing 58% SiO_2, 28.5% B_2O_3 and 13.5% CaF_2, and with the metal produced containing 50% Si and 13.6% B.

5.4.3 >> KINETICS OF FERROSILICON/BORIC-OXIDE REACTION IN IRON

Comparison of the efficiency of reaction of the ferrosilicon mixture in comparison with the silicon carbide mixture indicates that more boron is reduced per gram of silicon absorbed by the iron. Once again, it is expected that increasing the stirring by bubbling argon would produce increased reduction rates. It was most surprising to find that the argon stirred experiments gave lower rates than the plunge experiments. For gas injection into liquids, we are not concerned with single bubbles but rather a swarm of bubbles. A model has been proposed by Engh et al (1972) which is considered to be appropriate in the present case. Engh inter relates the bubble radius (r) and its upward velocity (v)

as $v = (4.\sigma.g/f.\rho)^{1/4}$

and $r = 12.\sigma/\rho.f.v^2$

It should be noted that both individual bubble radius and upward velocity are independent of gas volume. For mass transfer in the metal phase,

$$A.k = 0.27\ D^{1/2}\ (\rho.f/\sigma)^{7/8}\ g^{3/8}\ v.\Omega.H$$

Thus for mass transfer control the rate of boron absorption by the iron bath would be proportional to the volume of gas and the depth of melt.

Analysis of the experimental results showed that the rate of absorption of boron was dependant only on the melt depth and not on gas volume (see graph 5.4.3.1). The inference that must be drawn is that absorption of boron is only related to the retention time in the system. In view of this conclusion, it seems reasonable to assume that reduction of boron only occurs in the bubble as it ascends through the metal bath. This hypothesis is particularly satisfying as the design of these powders was carried out to achieve reaction between the ferrosilicon and boric-oxide before dissolution in the iron reduced the silicon activity very significantly. The present results seem to support this concept and indicate that similar mixtures can well be used for a wide variety of reduction reactions in molten iron baths. The use of cheap oxides and ferrosilicon must be of economic advantage for alloy additions of rare metals compared to the addition of expensive alloying elements.

5.5 > DISCUSSION OF ALUMINIUM/BORIC-OXIDE POWDER EXPERIMENTS

The experiments with aluminium-boric oxide mixture gave results which indicate that all the aluminium reacted during the course of the experiment (see graph 5.5.1). Once again, it is considered that the reduction reactions take place in the bubbles prior to the dissolution in the metal bath as anticipated in their design. The mass balances and lower residual aluminium contents determined by chemical analysis certainly support this view. It should be noted that aluminium like silicon exhibits a very low activity coefficient in iron and it seems most unlikely that these rapid reduction reactions would be feasible with such dilute aluminium solutions which would exist if rapid dissolution occurred. As with ferrosilicon powders, the use of aluminium-metal oxide mixtures for the production of expensive alloys in ferrous and nickel process metallurgy is worthy of much greater consideration.

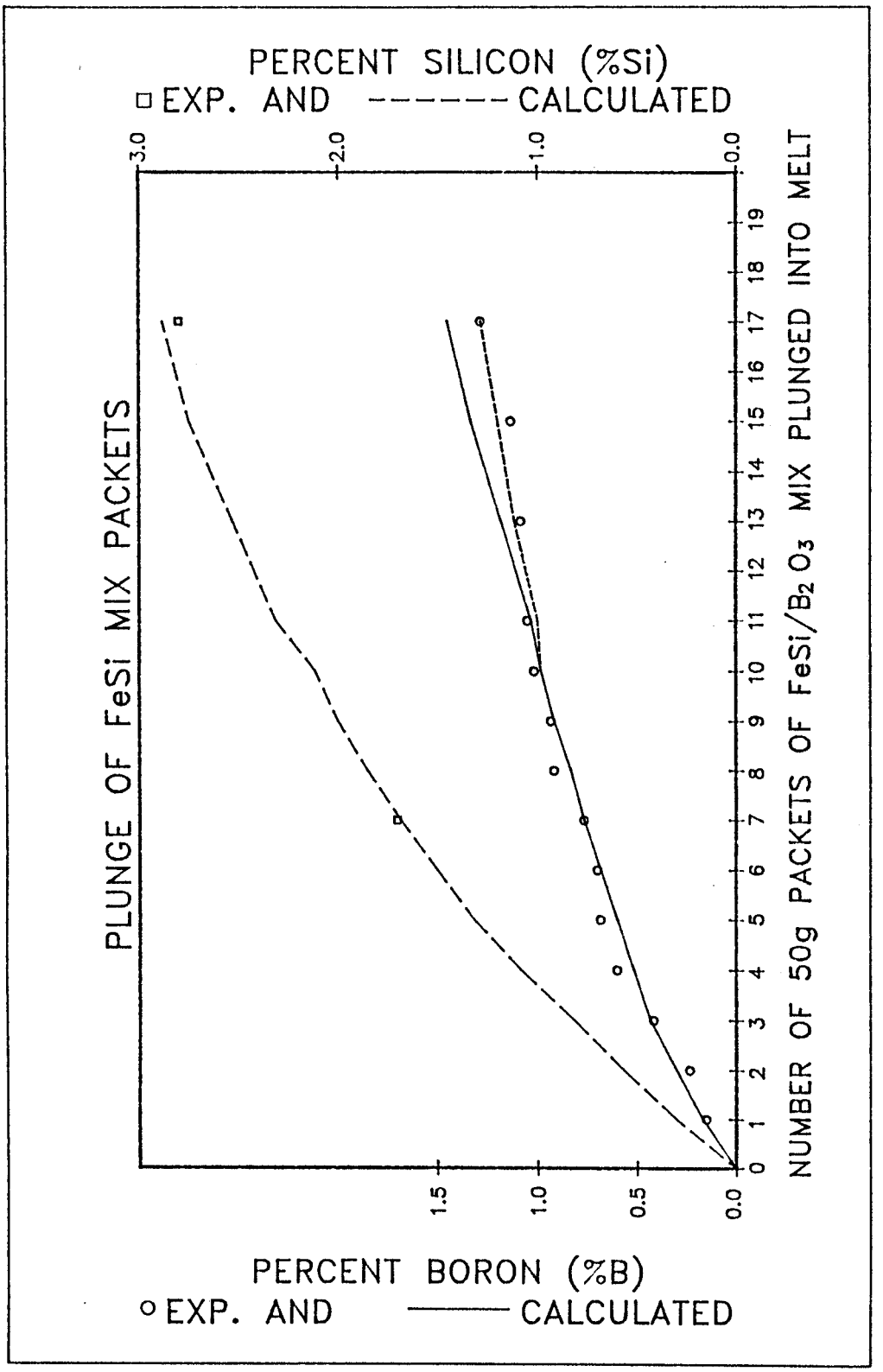

GRAPH 5.4.1.1 : Plunge of 50 g packets of FeSi/B_2O_3 powder mixture into molten iron. Experimental and calculated values for %B and %Si in the melt.

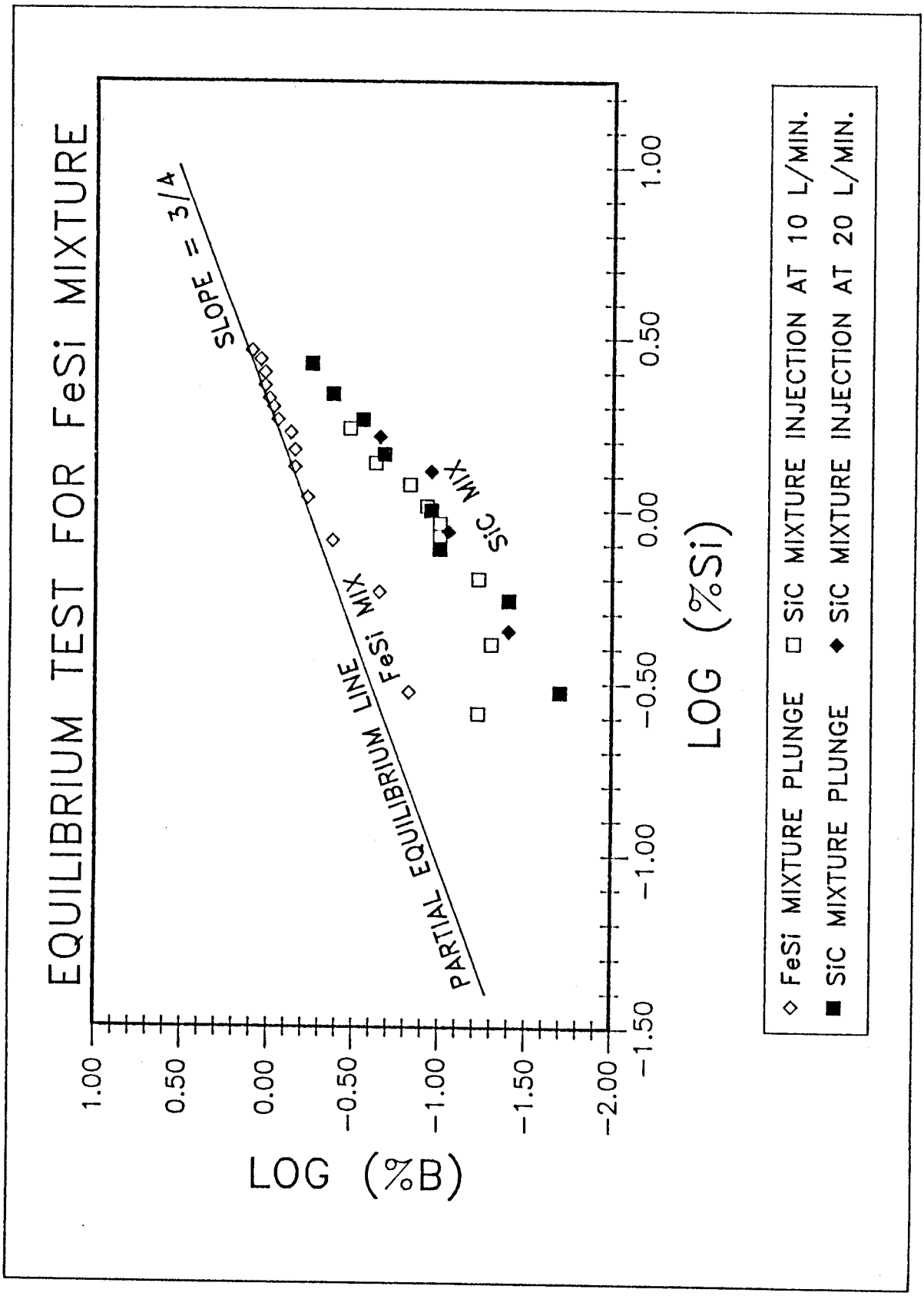

GRAPH 5.4.1.2 : Graph of log %B verses log %Si for FeSi mix injection at 10 l/min. argon, showing that boron absorption by the iron is limited by the silicon content for boron levels above ≈1%.

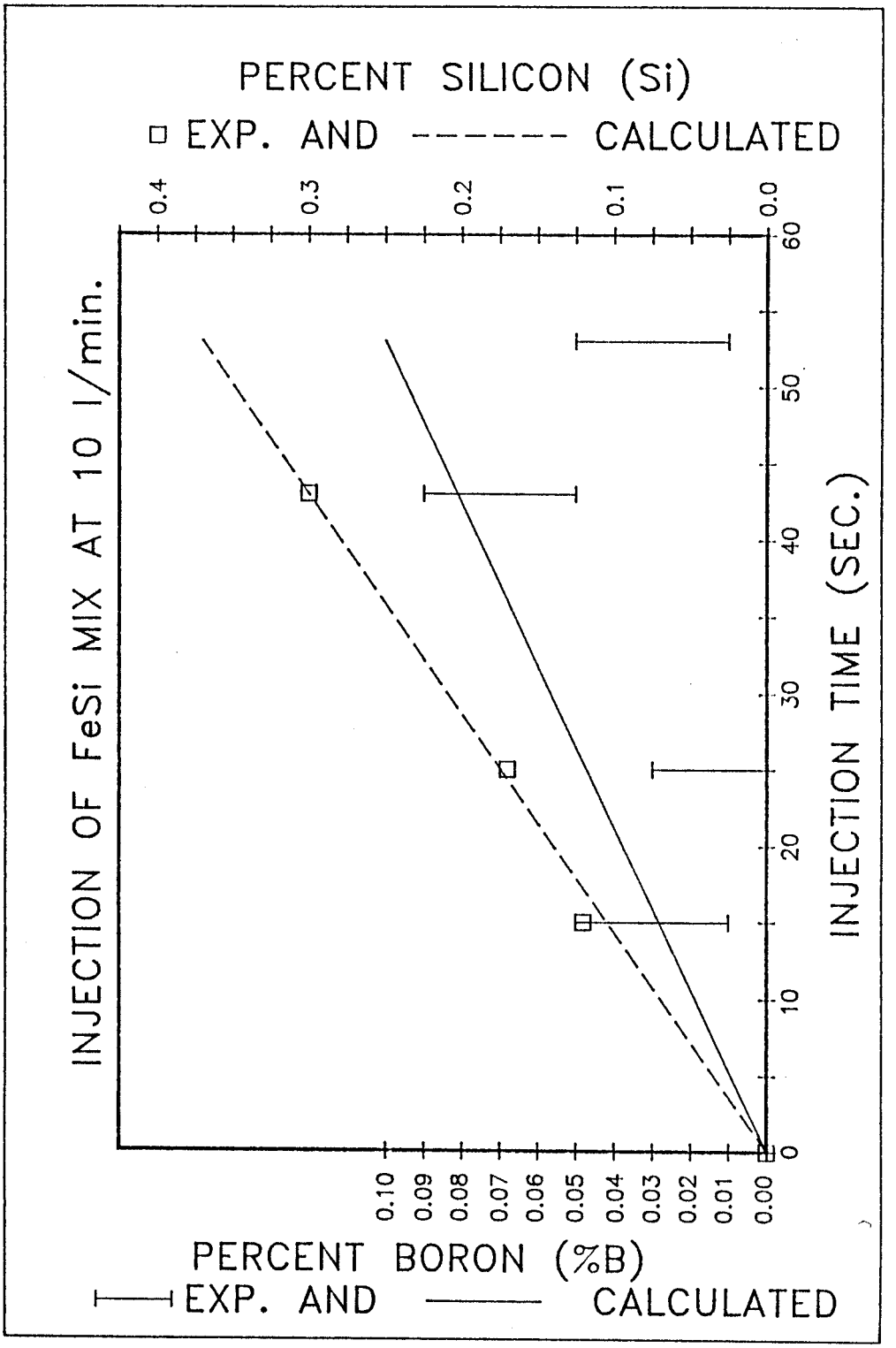

GRAPH 5.4.2.1 : Experimental and calculated values for %B and %Si in the melt for FeSi mixture injected at 10 l/min argon.

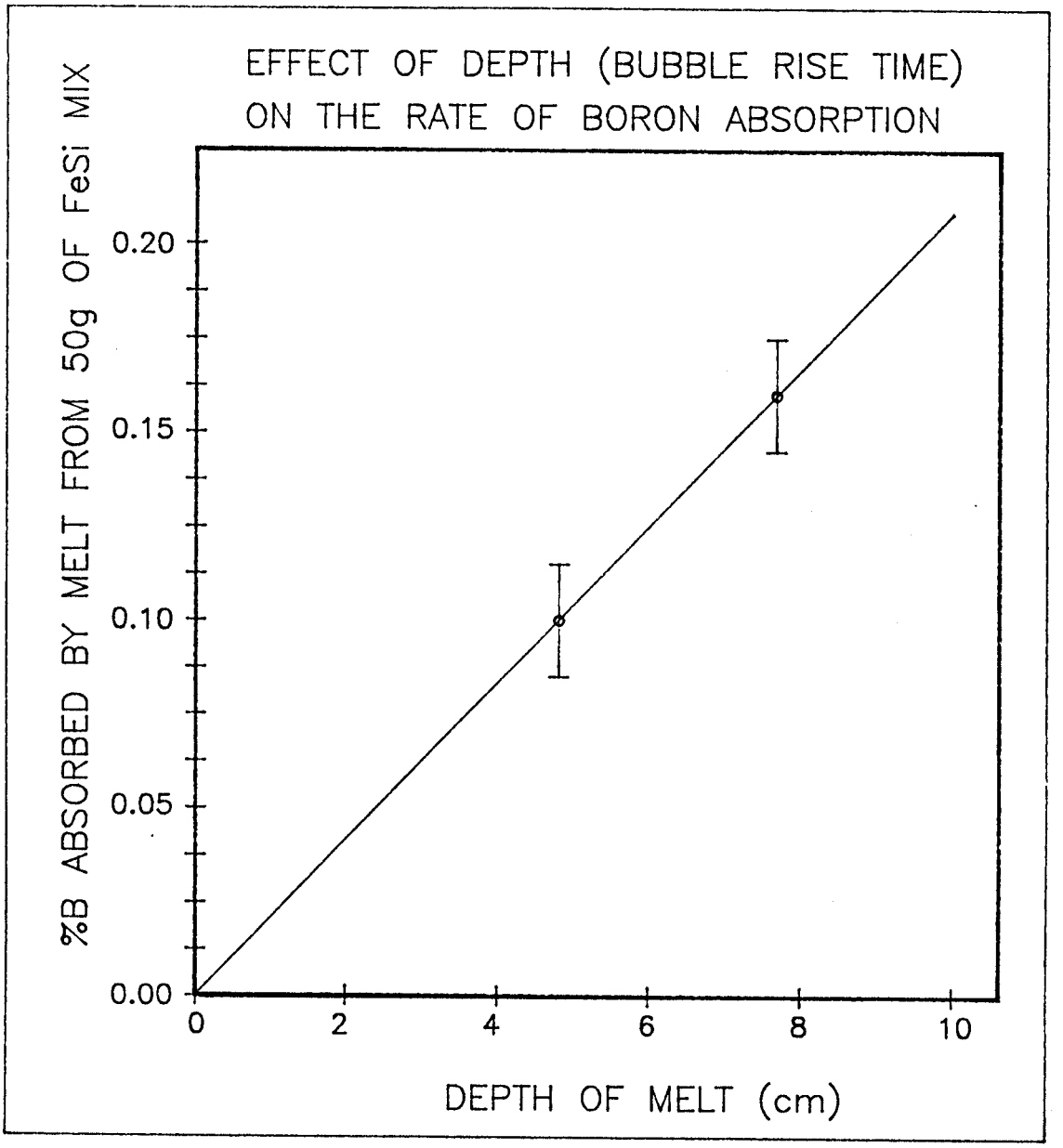

GRAPH 5.4.3.1 : Variation of boron absorption rate with depth of melt for FeSi mixture injected at 10 l/min argon and plunged.

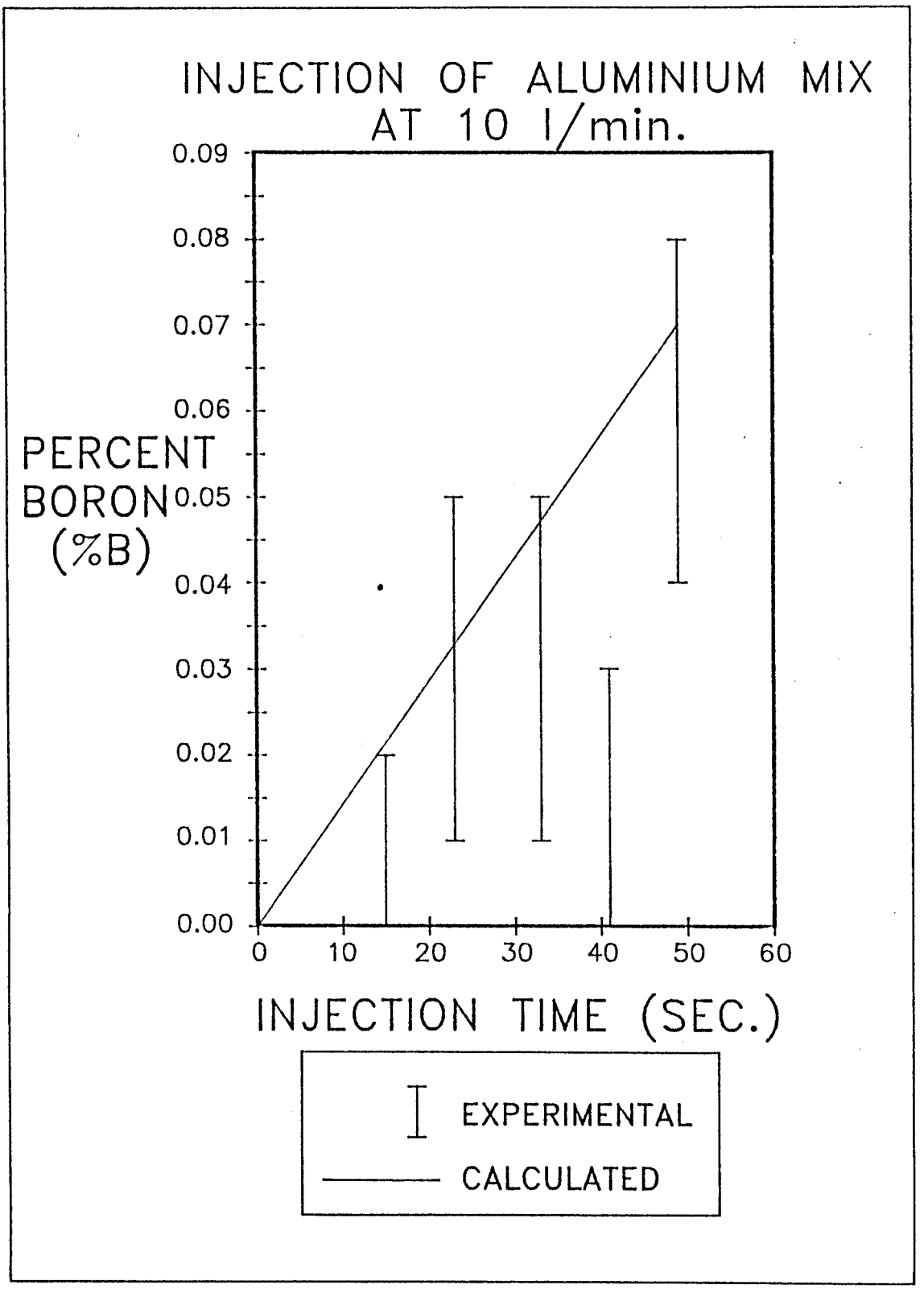

GRAPH 5.5.1 : Experimental and calculated values for %B in the melt for aluminium / boron-oxide mixture injected at 10 l/min argon.

6. CONCLUSION

It is feasible to reduce boron oxide to boron by submerged powder injection or plunge of powder packets into molten iron where the powders contain the oxide and a reducing agent such as SiC, Si or Al. The resulting boron will dissolve in the iron.

1. For powders containing 64% SiC and 28% B_2O_3, injection of powders is a more efficient process than plunging powder packets because the increased stirring assists mass transfer. Injection with 20 l/min carrier gas flow is more efficient that with 10 l/min . For these experiments it is considered that the reduction reactions take place during bubble ascent. It is probable that the slag lies at the bottom of a spherical cap bubble and evidence suggests that the rate determining factor in SiC-B_2O_3 powder reactions is the dissolution of SiC in liquid iron.

2. For powders containing 33% Si and 32% B_2O_3, boron reduction is more efficient than for the SiC powder mixture. The rate of absorption of boron is dependant only on the melt depth and not on gas volume because boron absorption takes place during the bubble rise-time. For boron levels above about 1%, the quantity of boron dissolved into the iron is limited by the silicon content of the powder.

3. For powders containing 28% Al and 42% B_2O_3, all the aluminium is found to react to reduce boron oxide before its activity is reduced by dissolution into the iron.

APPENDIX A : USER INSTRUCTIONS FOR THE SMALL SCALE INDUCTION FURNACE

Instructions for use of the designed induction furnace.

The following is the detailed general procedure followed for the small scale experiments done in the induction furnace.

TO SWITCH THE FURNACE ON

1. Align furnace trolley with the generator
2. Connect HF coil to generator
3. Place susceptor/specimen crucible on the thermocouple rod and insert thermal insulation cylinders
4. Close Pyrex hood and all ports
5. Connect manometer tube to heating chamber and remove manometer/air dust stop
6. Connect gas input tube to cylinder and set cylinder pressure for flush flow
7. Connect power supply to generator, vacuum pump and recorder
8. Connect and turn on cooling water for the heating chamber flanges and for the HF generator
9. Connect cooling water outputs
10. Evacuate heating chamber and check for water and gas leaks
11. Evacuate gas line and flush chamber with input gas until atmospheric pressure is reached
12. Connect gas output port to exhaust
13. Switch on and set chart recorder for temperature monitoring
14. Switch on HF.

TO SWITCH OFF AND DISCONNECT THE FURNACE FROM THE HF GENERATOR

1. Switch off HF control
2. Wait at least 40 minutes, then disconnect gas input and output and seal the ports
3. Disconnect gas from cylinder and remove the regulator
4. Switch off chart recorder
5. Wait at least 90 minutes, then turn off HF main power and cooling water supplies.
6. Disconnect cooling water to the furnace flanges and power to the furnace trolley
7. Disconnect HF coil from the generator and remove trolley.

APPENDIX B : VARIATION OF PRESSURE WITH DEPTH OF INJECTION

The following table shows how the static pressure under a liquid (molten iron) increases with depth. This pressure depends on depth and the density of the liquid, and it must be overcome before submerged injection can take place. The pressure is presented in various pressure units.

CONSTANTS

DENSITY OF Fe at 1550 °C	=	7010	kg/m^3
g	=	9.81	m/s^2
1 Atmos	=	0.1013	MPa
1 kg/cm^2	=	0.0981	MPa

Excess pressure (Pa) = DENSITY of Fe x g x DEPTH (m)

Excess Pressure (atmos) = excess pressure (MPa) / 0.1013

Excess Pressure (kg/cm^2) = excess pressure (MPa) / 0.0981

Excess Pressure (mm Hg) = excess pressure (atmos) x 760

Excess Pressure (cm water) = excess pressure (cm Fe) x 7.01

DEPTH OF INJECTION (cm Fe)	Excess Pressure (MPa)	Excess Pressure (atmos)	Excess Pressure (kg/cm^2)	Excess Pressure (mm Hg)	Excess Pressure (cm Water)
0	0.000000	0.000000	0.0000	0.00	0.00
1	0.000688	0.006789	0.0070	5.16	7.01
2	0.001375	0.013577	0.0140	10.32	14.02
3	0.002063	0.020366	0.0210	15.48	21.03
4	0.002751	0.027154	0.0280	20.64	28.04
5	0.003438	0.033943	0.0351	25.80	35.05
6	0.004126	0.040731	0.0421	30.96	42.06
7	0.004814	0.047520	0.0491	36.12	49.07
8	0.005501	0.054308	0.0561	41.27	56.08
9	0.006189	0.061097	0.0631	46.43	63.09
10	0.006877	0.067886	0.0701	51.59	70.10
11	0.007564	0.074674	0.0771	56.75	77.11
12	0.008252	0.081463	0.0841	61.91	84.12
13	0.008940	0.088251	0.0911	67.07	91.13
14	0.009628	0.095040	0.0981	72.23	98.14
15	0.010315	0.101828	0.1052	77.39	105.15
16	0.011003	0.108617	0.1122	82.55	112.16
17	0.011691	0.115405	0.1192	87.71	119.17
18	0.012378	0.122194	0.1262	92.87	126.18
19	0.013066	0.128983	0.1332	98.03	133.19
20	0.013754	0.135771	0.1402	103.19	140.20
25	0.017192	0.169714	0.1753	128.98	175.25
30	0.020630	0.203657	0.2103	154.78	210.30
35	0.024069	0.237600	0.2454	180.58	245.35
40	0.027507	0.271542	0.2804	206.37	280.40
50	0.034384	0.339428	0.3505	257.97	350.50

APPENDIX C : CRUCIBLE COMPOSITIONS

The following is the composition of the crucibles used for the injection experiments. This data was provided by the manufacturer.

TRIANGLE 66V SILLIMANITE (SPECIAL SHEATH/DIP-SAMPLER)

	(%)
Al_2O_3	65.5
SiO_2	30.6
Fe_2O_3	0.95
TiO_2	1.08
CaO/MgO	0.27
Na_2O/K_2O	1.22

Salemander Super Clay-Graphite Crucibles

	(%)
SiO_2	35
C	35
SiC	12
Al_2O_3	13
Fe_2O_3	4

PUROX RECRYSTALLIZED ALUMINA

	(%)
Al_2O_3	99.7
SiO_2	0.05
Fe_2O_3	0.1
Na_2O_3	0.1
K_2O	0.05

APPENDIX D : DEPTH OF MELT

Direct measurement of the melt depth was found to be difficult because initially the metal was in flake form, and on melting: in the case of plunge experiments the volume increased with each plunge as the plunger melted, and for injection experiments the volume decreased as splashing occurred.

In the table below, dimensions of the crucible for each experiment has been used to calculate the melt depth (±0.25 cm) from the mass of metal used. The initial and final figures relate to the initial and final mass of iron. The final depth is less accurate because the crucible itself had lost some mass and it was not possible to distinguish between this loss and the loss of metal. The final mass of melt also includes any metal adhering to the walls of the crucible and thus not contributing to the melt depth.

	CRUCIBLE USED	METAL WEIGHT		MELT VOLUME		DEPTH OF METAL	
		INITIAL (g)	FINAL (g)	INITIAL (ml)	FINAL (ml)	INITIAL (cm)	FINAL (cm)
SiC MIX							
PLUNGE	A3	1800	2556	256	364	8	10.5
INJ 10 l/min	E468	1500	804	213	114	6.1	3.2
INJ 20 l/min	E300	2000	987	285	140	4.8	2.4
FeSi MIX							
PLUNGE	A3	1700	3205	242	456	7.7	> 11
INJ 10 l/min	E300	2000	1565	285	223	4.8	3.8
Al MIX							
INJ 10 l/min	E300	2000	1541	285	219	4.8	3.7

The depth of injection was measured directly by monitoring the pressure within the powder feeder. A manometer marked with pressure in units of $cmFe_{(liq,\ 1550°C)}$ was used to monitor the pressure. For each injection lance, the initial pressure reading was the most reliable. That is, when the lance was bubbling before any powder flow.

The procedure was to allow powder flow in 1 or 2 second bursts, after which the lance would be restricted and the powder feeder internal pressure would increase. Often the restriction partially melted and injection could continue until the lance broke.

The back-pressure generated in the powder feeder by only the flow of gas through the lance has been ignored. Air was used to measure the apparatus back-pressure when not injecting, and this was found to be 2 mmHg at 10 l/min and 3 mmHg at 20 l/min

Based on the initial powder feeder pressure, the depth of injection was as follows:

INJECTION EXPERIMENT	LANCE NUMBER	PRESSURE (cmFe) ±0.25 cm
SiC mix at 10 l/min	all	5±0.5 cm
SiC mix 20 l/min	1	7
	2	7
	3	4.5
	4	8
	5	5
FeSi mix 10 l/min	1	4
	2	5
	3	4
	4	4
	5	4.5
Al mix 10 l/min	1	4
	2	5
	3	5
	4	5
	5	5

APPENDIX E : CALCULATION DETAILS

In this appendix details of mass balance calculations are given for plunge and injection experiments using various powders. The detailed version of tables presented in the results section appear in this appendix for a selection of samples.

E.1 > SILICON-CARBIDE/BORON-OXIDE POWDER MIXTURE

The SiC powder mixture was supplied with the following composition:

SiC Mix 64.4% SiC
28.3% B_2O_3
7.3% H_2O.

From the powder composition, the following conversion factors were calculated for convenience:

WEIGHT CONVERSION FACTORS FOR SiC POWDER MIX

TO CONVERT TO :	SiC	B_2O_3	WATER	BORON	Si	CARBON
MULTIPLY BY :	0.644	0.283	0.073	0.088	0.451	0.1928

The following reactions are considered to be dominant during the plunge and injection experiments involving the SiC mix.

REACTIONS

$$3\,H_2O + SiC_{(s)} = 3\,H_{2(g)} + (SiO_2) + CO_{(g)} \quad \ldots\ [A1]$$

REL.WT.:	54	40.09	3	60.09	28

$$(B_2O_3) + SiC_{(s)} = 2\,\underline{B} + (SiO_2) + CO_{(g)} \quad \ldots\ [A2]$$

REL.WT.:	69.6	40.09	22	60.09	28

E.1.1 >> SiC MIX PLUNGE EXPERIMENTS

CONSTANTS

POWDER USED	= SiC POWDER MIX
INITIAL WEIGHT OF IRON USED	= 1800 (g)
MEAN WEIGHT LOSS OF PLUNGER PER PLUNGE	= 54 (g)
SiC LOST DURING THE PLUNGE PROCESS	= 63.5 %

PLUNGER: Mild Steel, ID 22 mm, OD 27 mm, Length 1300 mm

In the results section, the boron and silicon content of the melt has been calculated based on experimental results from chemical analysis. Part of the SiC content of the added powder is considered to be used in reaction [A1] above with the water contained in the powder, some is used in reaction [A2] above to reduce boron oxide, some has dissolved in the melt and some is lost to the slag.

The amount of SiC used in reactions [A1] and [A2] above can be calculated from the amount of water in the powder and the %B found by analysis respectively. The amount of SiC dissolved in the melt can be calculated from the %Si found by analysis for the samples where this data is available. Thus knowing the percentage of SiC in the added powder, the loss of SiC to the slag can be estimated.

Having estimated the loss of SiC from the powder mix and the amount dissolved in the melt, these ratios can be applied to other samples where no analytical data is available for the %Si in the melt. Hence the %B in the melt can be calculated from the SiC used in reaction [A1], the ratio of SiC lost, the ratio of SiC dissolved in the melt and the remaining SiC for reaction [A2]. Note that the melt weight increased slightly with each plunge.

Finally, the calculated %B and calculated %Si in the melt can be balanced to better fit the experimental data. In the following table calculation details for the first few samples of the plunge experiment are given.

SAMPLE NUMBER - EXPERIMENTAL		S4	S5	S6	S7
SAMPLE NUMBER - ANALYSIS		4	5	-	6
PLUNGE OF SiC POWDER MIX					
PACKET NUMBER		3	4	5	6
ACCUM. WEIGHT OF POWDER	(g)	150	200	250	300
MELT CONTENT - BY CHEMICAL ANALYSIS					
% BORON FOUND BY ANALYSIS	%	0.10	0.11	n/a	0.21
SOLUBLE % Si - BY ANALYSIS	%	n/a	n/a	n/a	1.50
SiC ADDED LESS THAT LOST	(g)	35.26	47.01	58.77	70.52
TOTAL WATER ADDED	(g)	10.95	14.60	18.25	21.90
SiC USED IN [A1]	(g)	14.75	19.67	24.58	29.50
B_2O_3 ADDED	(g)	42.45	56.60	70.75	84.90
CALCULATED %BORON IN Fe	%	0.14	0.17	n/a	0.26
CALCULATED %SILICON IN Fe	%	0.78	1.00	n/a	1.45

E.1.2 >> SiC MIX INJECTION EXPERIMENTS AT 10 L/MIN ARGON

CONSTANTS	
POWDER USED	= SiC POWDER MIX
POWDER FLOW RATE	= 1.412 g/sec.
WEIGHT OF IRON USED	= 1500 (g)
WEIGHT LOSS OF IRON CORRECTED FOR CRUCIBLE	= 596 (g)
SiC LOST DURING THE INJECTION PROCESS	= 50 %
NUMBER OF LANCES USED FOR INJECTION	= 5

Calculations for the injection experiments at carrier gas flow rate of 10 l/min was very similar to that of the plunge experiment. That is, the two silicon analysis points were used to determine the %Si dissolved in the melt and hence the mass of SiC that was lost. This ratio was then applied to other points for which the %Si was not known.

As an example, consider 71 seconds of powder flow by injection at a rate of 1.412 g/sec . This gives 99.5 g of powder (SiC + B_2O_3). At this point the chemical analysis shows that there is 0.12% (1.8 g) of boron and 1.06% (15.9 g) silicon in the iron melt of 1500 g. Using the conversion factors, it is found that 64.08 g of SiC was added, 7.26 g of water and 28.16 g of B_2O_3.

For dissolution of 15.9 g Si in Fe, 22.7 g SiC is required and to obtain 1.8 g B in Fe, 3.4 g SiC is required according to the relative weights of reaction [A2], and to react with all the water, 5.39 g SiC is required.

Therefore the amount of SiC lost is the total added (64.08 g) less that used in reaction [A1] (5.39 g), less that used in reaction [A2] (3.4 g), less that dissolved (22.7 g), which leaves 32.6 g or 50% loss.

Calculation details for a few samples from the SiC MIX injection experiment at 10 l/min are given below.

SAMPLE NUMBER - EXPERIMENTAL		S6	S7	S8	S9
SAMPLE NUMBER - ANALYSIS		-	17	18	19
INJECTION OF SiC POWDER					
ACCUM. FLOW TIME	(sec)	51	59	65	71
ACCUM. WEIGHT OF POWDER	(g)	72.0	82.6	91.1	99.5
MELT CONTENT - BY CHEMICAL ANALYSIS					
% BORON FOUND BY ANALYSIS	%	n/a	0.10	0.10	0.12
SOLUBLE % Si - BY ANALYSIS	%	n/a	n/a	n/a	1.06
SiC ADDED LESS THAT LOST	(g)	23.19	26.60	29.33	32.05
TOTAL WATER ADDED	(g)	5.26	6.03	6.65	7.27
SiC USED IN [A1]	(g)	7.08	8.12	8.96	9.79
B_2O_3 ADDED	(g)	20.38	23.38	25.77	28.17
CALCULATED %BORON IN Fe	%	n/a	0.14	0.16	0.17
CALCULATED %SILICON IN Fe	%	n/a	8.84	0.93	1.02

E.1.3 >> SiC MIX INJECTION EXPERIMENTS AT 20 L/MIN ARGON

CONSTANTS

POWDER USED	= SiC POWDER MIX
POWDER FLOW RATE	= 1.412 g/sec.
WEIGHT OF IRON USED	= 2000 (g)
WEIGHT LOSS OF IRON CORRECTED FOR CRUCIBLE	= 1013 (g)
SiC LOST DURING THE INJECTION PROCESS	= 0 %
NUMBER OF LANCES USED FOR INJECTION	= 5

Calculation details for the injection experiment at a carrier gas flow rate of 20 l/min was very similar to that of 10 l/min with the difference that all the added SiC was found to have reacted.

Calculation details for a few samples from the SiC MIX injection experiment at 20 l/min are given below.

SAMPLE NUMBER - EXPERIMENTAL		S1	S2	S3	S4
SAMPLE NUMBER - ANALYSIS		25	26	27	28
INJECTION OF SiC POWDER					
ACCUM. FLOW TIME		6	14	27	41
ACCUM. WEIGHT OF POWDER		8.5	19.8	38.1	57.9
MELT CONTENT - BY CHEMICAL ANALYSIS					
% BORON FOUND BY ANALYSIS	%	0.00	0.04	0.09	0.11
SOLUBLE % Si - BY ANALYSIS	%	N/A	N/A	0.94	N/A
SiC ADDED LESS THAT LOST	(g)	5.46	12.73	24.55	37.28
WATER ADDED	(g)	0.62	1.44	2.78	4.23
SiC USED IN [A1]	(g)	0.46	1.07	2.07	3.14
WEIGHT OF BORON FROM %B	(g)	N/A	1.00	1.80	2.80
SiC USED IN [A2]	(g)	N/A	0.54	0.97	1.51
SiC REMAINING	(g)	N/A	11.12	21.52	32.64
Silicon IN REMAINING SiC	(g)	N/A	7.78	15.06	22.85
B_2O_3 ADDED	(g)	2.40	5.59	10.79	16.38
CALCULATED %B IN Fe	%	N/A	0.05	0.09	0.14
CALCULATED %Si IN Fe	%	N/A	0.39	0.75	1.14

E.2 > FERROSILICON/BORON-OXIDE POWDER MIXTURE

The FeSi powder mixture was supplied with the following composition:

FeSi Mix	32.7% Si
	10.6% Fe
	31.9% B_2O_3
	13.5% H_2O
	9.1% CaF_2
	2.2% unknown

From the powder composition, the following conversion factors were calculated for convenience:

WEIGHT CONVERSION FACTORS FOR FeSi POWDER MIX

TO CONVERT TO :	Fe	B_2O_3	WATER	CaF_2	BORON	Si
MULTIPLY BY :	0.106	0.319	0.135	0.091	0.099	0.327

The following reactions are considered to be dominant during the plunge and injection experiments involving the FeSi mix.

REACTIONS:

$$2\ B_2O_{3(s)} + 3\ Si_{(s)} = 4\ \underline{B} + 3\ (SiO_2) \ldots\ldots\ [A3]$$

REL.WT.: 139.2 84.3 43.2 180.3

$$2\ H_2O + Si_{(s)} = (SiO_2) + 2\ H_{2(g)} \ldots\ldots\ [A4]$$

REL.WT.: 36 28.1 60.1 4

E.2.1 >> FeSi MIX PLUNGE EXPERIMENTS

CONSTANTS: POWDER USED IN PACKETS	=	FeSi POWDER MIX	
NUMBER OF 50 g PACKETS USED	=	19	
INITIAL WEIGHT OF IRON	=	1700	(g)
WEIGHT LOSS OF PLUNGER	=	1996	(g)
MEAN WEIGHT INCREASE PER PLUNGE	=	105	(g)

In the case of FeSi MIX plunge experiments the boron analysis were more reliable and they were used to calculate the %Si expected in the melt. The amount of silicon required for reactions [A3] and [A4] were calculated from the %B found by analysis and the amount of water added respectively. The expected %Si of the melt was calculated from the silicon remaining after reactions [A3] and [A4]. The "total %B by weight of melt" quoted is merely the total boron added expressed as a percentage. In the following table, calculation details for a few samples from the FeSi MIX plunge experiment are given.

SAMPLE NUMBER - EXPERIMENTAL		5.1	6	7	8.1
SAMPLE NUMBER - ANALYSIS		44	46	47	48
PLUNGE OF FeSi POWDER MIX					
NUMBER OF 50 g PACKETS		4	5	6	7
ACCUM. WEIGHT OF POWDER	(g)	200	250	300	350
ACCUM. WEIGHT OF MELT	(g)	2120	2225	2330	2435
MELT CONTENT - BY CHEMICAL ANALYSIS					
% BORON FOUND BY ANALYSIS	%	0.60	0.69	0.70	0.77
BEST-FIT LINE ON %B FOUND	%	0.52	0.60	0.69	0.77
BORON WEIGHT-FROM BEST-FIT LINE	(g)	11.02	13.35	16.08	18.75
SOLUBLE %Si - BY ANALYSIS	%				1.7
SILICON USED AND SiO_2 FORMED IN REACTIONS (1) & (2) ABOVE					
SILICON ADDED	(g)	65.40	81.75	98.10	114.45
SILICON REQUIRED IN [A3]	(g)	21.51	26.05	31.37	36.59
SiO_2 PRODUCED IN [A3]	(g)	46.01	55.72	67.10	78.25
TOTAL WATER ADDED	(g)	27.00	33.75	40.50	47.25
SILICON REACTING IN [A4]	(g)	21.08	26.34	31.61	36.88
SiO_2 PRODUCED IN [A4]	(g)	45.08	56.34	67.61	78.88
SILICON LEFT AFTER [A3] & [A4]	(g)	22.81	29.36	35.12	40.98
CALCULATED % Si IN IRON MELT	(%)	1.08	1.32	1.51	1.68
B_2O_3 USED					
B_2O_3 ADDED	(g)	63.80	79.75	95.70	111.65
B_2O_3 USED IN [A3]	(g)	35.52	43.02	51.80	60.42
B_2O_3 LEFT FROM [A3]	(g)	28.28	36.73	43.90	51.23
SLAG COMPOSITION					
CaF_2 ADDED	(g)	18.20	22.75	27.30	31.85
TOTAL WEIGHT OF SLAG	(g)	137.56	171.54	205.91	240.22
% B_2O_3 REMAINING FROM [A3]	%	20.56	21.41	21.32	21.33
% SiO_2 PRODUCED IN [A3] & [A4]	%	66.21	65.32	65.42	65.41
% CaF_2 ADDED	%	13.23	13.26	13.26	13.26
TOTAL %Si BY WEIGHT OF MELT	%	3.08	3.67	4.21	4.70
TOTAL %B BY WEIGHT OF MELT	%	0.93	1.11	1.27	1.42
% B FOUND BY ANALYSIS (IN SLAG)	%	6.28	N/A	N/A	N/A

E.2.2 >> FeSi MIX INJECTION EXPERIMENTS AT 10 L/MIN ARGON

CONSTANTS

POWDER USED = FeSi POWDER MIX

POWDER FLOW RATE = 0.96 g/sec.

WEIGHT OF IRON USED = 2000 (g)

WEIGHT LOSS OF IRON CORRECTED FOR CRUCIBLE = 435 (g)

NUMBER OF LANCES USED FOR INJECTION = 5

LANCE TYPE: TSL Aluminus Porcelain of ID 8 mm, OD 12 mm

For the injection of FeSi MIX at 10 l/min it was found that at such low concentrations of boron, the silicon analysis results (unreacted silicon) were more reliable. Hence the silicon analysis were used together with the amount of silicon used to react with all the water to calculate the amount of silicon required to calculate the maximum %B in the melt according to reaction [A3].

In the following table calculation details are given for a few samples from the FeSi MIX injection experiments as illustration.

SAMPLE NUMBER - EXPERIMENTAL		S1	S2	S3	S4
SAMPLE NUMBER - ANALYSIS		30	31	32	33
INJECTION OF FeSi POWDER					
ACCUM. FLOW TIME	(sec)	15.0	25.0	33.0	43.0
ACCUM. WEIGHT OF POWDER	(g)	14.4	24.0	31.7	41.3
MELT CONTENT - BY CHEMICAL ANALYSIS					
% B FOUND BY ANALYSIS	%	0.03	0.01	N/A	0.07
SOLUBLE % Si-BY ANALYSIS	%	0.12	0.17	N/A	0.30
BEST-FIT ON % Si-BY ANALYSIS	%	0.10	0.17	0.23	0.30
WEIGHT OF Si-FROM BEST-FIT	(g)	2.1	3.5	4.6	6.0
SILICON USED AND SiO_2 FORMED IN REACTIONS [A3] & [A4]					
TOTAL SILICON ADDED	(g)	4.71	7.85	10.36	13.50
WATER ADDED	(g)	1.94	3.24	4.28	5.57
SILICON USED IN [A4]	(g)	1.52	2.53	3.34	4.35
SiO_2 FORMED IN [A4]	(g)	3.25	5.41	7.14	9.30
SILICON USED IN [A3]	(g)	1.11	1.84	2.42	3.15
SiO_2 FORMED IN [A3]	(g)	2.38	3.93	5.18	6.73
BORON, B_2O_3 AND SLAG COMPOSITION					
B_2O_3 ADDED	(g)	4.59	7.66	10.11	13.17
B_2O_3 USED IN [A3]	(g)	1.84	3.04	4.00	5.20
BORON FORMED IN [A3]	(g)	0.57	0.94	1.24	1.61
MAX. %B FROM BEST-FIT %Si	(%)	0.03	0.05	0.06	0.08
B_2O_3 LEFT FROM [A3]	(g)	2.76	4.62	6.11	7.97
CaF_2 ADDED	(g)	1.31	2.18	2.88	3.76
TOTAL WEIGHT OF SLAG	(g)	9.69	16.15	21.31	27.76
%B_2O_3 REMAINING FROM [A3]	%	28.46	28.61	28.66	28.70
% SiO_2 PRODUCED IN [A3]&[A4]	%	58.02	57.86	57.81	57.77
% CaF_2 ADDED	%	13.52	13.53	13.53	13.53
TOTAL %B BY Wt. OF Fe	%	0.07	0.12	0.16	0.20
TOTAL %Si BY Wt. OF Fe	%	0.24	0.39	0.52	0.67

E.3 > ALUMINIUM/BORON-OXIDE POWDER MIXTURE

The aluminium powder mixture was supplied with the following composition:

Al Mix	42.2%	B_2O_3
	27.9%	Al
	19.9%	H_2O
	7.2%	CaF_2
	2.8%	unknown

From the powder composition, the following conversion factors were calculated for convenience:

WEIGHT CONVERSION FACTORS FOR Al POWDER MIX

TO CONVERT TO :	Al	B_2O_3	WATER	CaF_2	BORON	OXYGEN
MULTIPLY BY :	0.279	0.422	0.199	0.072	0.131	0.177

The following reactions are considered to be dominant during the injection experiments involving the aluminium powder mix.

REACTIONS

$$2\,Al + 3\,H_2O = Al_2O_3 + 3\,H_2 \quad \text{..... [A5]}$$

REL.WT. : 54 54 102 6

$$2\,Al + B_2O_3 = Al_2O_3 + 2\,B\ (\text{in Fe}) \quad \text{..... [A6]}$$

REL.WT. : 54 69.6 102 21.6

E.3.1 >> Al MIX INJECTION EXPERIMENTS AT 10 L/MIN ARGON

CONSTANTS

POWDER USED	= Al POWDER MIX
POWDER FLOW RATE	= 0.884 g/sec.
WEIGHT OF IRON USED	= 2000 (g)
WEIGHT LOSS OF IRON CORRECTED FOR CRUCIBLE	= 459 (g)
NUMBER OF LANCES USED FOR INJECTION	= 5

LANCE TYPE USED: TSL Aluminus Porcelain of ID 8 mm, OD 12 mm

For the injection of aluminium powder mixture into molten iron at 10 l/min, the total boron added (expressed as Total %B by weight of melt) and the Maximum %B in the melt have been calculated for comparison with analytical results. Calculation details for a few samples are presented in the following table.

SAMPLE NUMBER - EXPERIMENTAL		S1	S2	S3	S4
SAMPLE NUMBER - ANALYSIS		36	37	38	39
INJECTION OF Al POWDER MIX					
POWDER FLOW TIME	(sec)	15	23	33	41
POWDER WEIGHT ADDED	(g)	13.26	20.33	29.17	36.24
WATER IN POWDER	(g)	2.64	4.05	5.81	7.21
Al WEIGHT ADDED	(g)	3.70	5.67	8.14	10.11
Al_2O_3 FORMED IN [A5]	(g)	4.98	7.64	10.97	13.62
Al USED IN [A5]	(g)	2.64	4.05	5.81	7.21
Al LEFT FOR [A6]	(g)	1.06	1.63	2.33	2.90
B_2O_3 ADDED	(g)	5.60	8.58	12.31	15.29
B_2O_3 USED IN [A6]	(g)	1.37	2.10	3.01	3.74
BORON FORMED IN [A6]	(g)	0.42	0.65	0.93	1.16
MAXIMUM %B IN Fe	%	0.02	0.03	0.05	0.06
Al_2O_3 FORMED IN [A6]	(g)	2.00	3.07	4.41	5.48
Al_2O_3 FROM [A5] & [A6]	(g)	6.99	10.71	15.37	19.10
SLAG COMPOSITION					
B_2O_3 LEFT FROM [A6]	(g)	4.23	6.48	9.30	11.56
CaF_2 ADDED	(g)	0.95	1.46	2.10	2.61
% Al_2O_3 IN SLAG	%	57.41	57.41	57.41	57.41
% B_2O_3 IN SLAG	%	34.74	34.74	34.74	34.74
% CaF_2 IN SLAG	%	7.84	7.84	7.84	7.84
% B AS OXIDE IN SLAG	%	10.79	10.79	10.79	10.79
TOTAL % BORON wrt Fe	%	0.09	0.13	0.19	0.24
% B IN Fe - BY ANALYSIS	%	0.00	0.03	0.03	0.01

REFERENCES

Anantharaman, T. R., Metallic Glass: Production Properties and Applications, Aedermannsdorf, Switzerland, 1984.

Ast, D. G. and Krenitsky, D., Proc. 2nd Int. Conf. on Rapidly Quenched Metals, Sec. II, Mat. Sci. Eng., Vol 23, p 241, 1976.

Cargill III, G. S., in Solid State Physics, Vol. 30, F. Seitz, D. Turnbull and H. Ehrenreich, eds., Academic Press, New York, p 227, 1975.

Chen et al. U.S. Patent 3 856 513 , Dec. 1974.

Chen, H. S. and Miller, C. E., Rev. Sci. Ins., Vol. 41, (8) 1970.

Chipman, J; Alfred, R.M; Gott, L.W; Small, R.B.; Wilson, D.M.; Thomson, C.N.; Guernsey, D.L.; and Fulton, J.C., The Solubility of Carbon in Molten Iron and in Iron-Silicon and Iron-Manganese Alloys, Transactions of the A.S.M, Vol. 44, pp 1215-1230, 1952.

Conochie, D.S and Robertson, D.G.C, Institute of Mining and Metallurgy, Transactions Section C, Vol. 89, p 61 1980.

Davenport, W.G; Richardson, F.D and Bradshaw, A.V, Journal of the Iron and Steel Institute, Vol. 205, p 1034, 1967.

Davis, L. A., Metallic Glasses, Gilman and Leamy, eds., ASM, Metals Park, Ohio, p 190, 1977.

Davis, L. A.; DeCristofaro, N. and Smith, C. H., Proceedings of Conference: Metallic Glasses Science and Technology, ed. Hargitai, C., et al., Hungarian Academy of Science, Budapest, Hungary, 1980.

Davis, L. A.; Ray, R.; Chou, C. P. and O'Handley, R. C., Scripta Met., Vol. 10, p 541, 1976.

Davies, R.M and Taylor, G.I, Proceedings of the Royal Society, London, Series A Vol. 200, p 2285, 1950.

Duwaz, P.; Willens, R. H. and Klement, W., Journal of Applied Physics, Vol. 31, (6) p 1136, 1960.

Duwez, P. and Lin, S. C. H., J. Appl. Phys, Vol. 38, p 4096, 1967.

Duwez, P. and Willens, R. H.; TMS of AIME, Vol. 227, (2), pp 362-365, 1963.

Egami, T.; Flanders, P. J. and Graham, C. D. Jr., AIP Conf. Proc., Vol. 24, p 697, 1975.

Engh, T.A.; Sandberg, H; Hultkvist, A and Norberg, L.G., Si Deoxidation of Steel by Injection of Slags with Low SiO_2 Activity, Scandinavian Journal of Metallurgy, Vol. 1, pp 103-114, 1972.

Gilman, J. J., Phys. Today, pp 46-53, May 1975.

Grace, J.R., Transactions of the Institute of Chemical Engineering, Vol. 51, p 116, 1973.

Hamada, T., U.S. Patent 4 505 745, Mar 1986.

Hasegawa, R.; DeCristofaro, N. and Narasimhan, M. C., J. Appl. Phys., Vol. 49, 1712, 1978.

Hatta, S.; Egami, T. and Graham, C. D. Jr., IEEE Trans. Mag. MAG-14, 1013, 1978.

Hubert, J. C., Mollard, F. and Lux, B., Zeit. fur Metallkunde, Vol. 64, p 835, 1973.

Jones, H., Rapid Solidification of Metals and Alloys, The Institute of Metallurgists, Monologue No.8, 1983

Jones, H.; Rep. Prog. Phys., Vol. 36, p 1425, 1973.

Klement, W.; Willens, R. H. and Duwez, P., Nature, Vol. 187, (4740), pp 867-870, 1960.

Koster, U. and Herold, U., Scripta Met., Vol. 12, pp 75-77, 1978.

Kozakevitch P. and Leroy, P, Rev. Metall., Vol. 51, p 203, 1954.

Luborsky, F. E.; Becker, J. J. and McCary, R. O., IEEE Trans. Mag. MAG-11, 1640, 1975.

Luborsky, F. E.; Becker, J. J. and McCary, R. O., Proc. 2nd Int. Conf. on Rapidly Quenched Metals, Sec. I, MIT, Cambridge, p 467, 1976A.

Luborsky, F. E. and Walter, J. L., J. Appl, Phys., Vol. 47, p 3648, 1976B.

Luborsky, F. E.; Becker, J. J.; Walter, J. L. and Liebermann, H. H., IEEE Trans. Mag, MAG-15, 1146, 1979.

Luborsky, F. E., in Ferromagnetic Materials, Vol. 1, Ed. E. P. Wohlfarth), Amsterdam, North Holland, p 451, 1980.

Maringer, R. E. and Mobley, C. E., J. Vac. Sci. Tech., Vol. 11, p 1067, 1974.

Maringer, R. E., Mobley, C. E. and Collings, E. W., in Proc. Second Int. Conf. on Rapidly Quenched Metals, Section I, N. G. Grant and B. C. Giessen, eds, MIT Press, Cambridge, Mass., p 29, 1976.

Massumoto, T. and Maddin, R.; Materials Sci. Eng., Vol. 19, p 1, 1975.

Masumoto, T., Report 1673 of the Research Ins. for Iron, Steel and Other Metals, Tohoku University, Sendai, Japan, 1976.

Meshkot, A., M.Sc. Thesis Thames Polytechnic, London, 1985.

Metallic Glasses Science and Technology, Proceedings of Conference: ed. Hargitai, C., et al., Hungarian Academy of Science, Budapest, Hungary, 1980.

Minto, R and Davenport, W.G, Institute of Mining and Metallurgy, Transactions Section C, Vol. 81, p 36, 1972.

Nakagawa and Suzuki, Ann. CIRP, VOL 25, (1), P 55, 1977.

Narasimhan, M. C., U.S. Patent 4 142 571, Mar. 1979.

O'Handley, R. C.; Chou, C. -P. and DeCristofaro, N., J. Appl. Phys., Vol. 50, 3603, 1979.

Ohguchi, S., Ph.D. Thesis, Imperial College, London, 1983.

Poggi, D; Minto, R and Davenport, W.G, Journal of Metals, Vol. 21, p 40, 1969.

Polk, D. E. and Giessen, B. C. in Metallic Glasses, American Soc. of Metals, Papers Presented at a Seminar of the Materials Science Division, Sep.1976.

Polk, D. E., Scripta Met., Vol. 4, p 117, 1970.

Pompillo, C. A. and Polk, D. E., Mat. Sci. and Eng., Vol. 33, p 275, 1978.

Pond, R. and Maddin, R., Trans. Met. Soc. AIME, Vol. 245, p 2475, 1969.

Rapidly Quenched Metals III, proc. of the third int. conf., 1978.

Rapidly Quenched Metals, Proc. of the 5th Int. Conf., Deutsche, Forschungemeinschaft, Sep. 1984.

Rosenfelder, W. J.; Borax Holdings Ltd., Internal Report, 1983

Rosenfelder, W. J.; Int. Ferro-Alloys Congress (INFACON), 1986

Schile, R. D.; U.S. Patent 3 543 831, Dec. 1970.

Seki, K.; Hiromoto, T. and Inoue, T., INFACON 86.

Sinha, A. K. and Duwez, P., J. Phys. Chem. Sol. , Vol. 32, p 267, 1971.

Stewart, A. M., Metals Forum, Vol. 6, (12), pp 122-131, 1983.

Sussman et al., U.S. Patent 4 572 747, Feb. 1986A.

Sussman, R. C. and Evans, L. G., Presented at TMS-AIME meeting, Mar. 1986B.

Takayama, S.; J. Mater. Sci., Vol. 11, p 164, 1976.

Turkdogan, E.T. Physical Chemistry of High Temperature Technology, 1980.

Turkdogan, E.T. Physicochemical Properties of Molten Slags and Glasses, The Metals Society, London 1983.

U.S. Patent 3 845 805, Also in Chem. and Eng. News, p 24, Nov. 1973.

U.S. Patent 3 845 805, Reported in Chem. and Eng. News, p 24, Nov. 1973.

Urquhart, R.C and Davenport, W.G., Journal of Metals, Vol. 22, p 36, 1970.

Vogt, E., Informal Rapid Solidification Conference, University of Surrey, 18-19 Sep. 1986.

Vojtanik, P.; Kisdi-Koszo, E.; Lovas, A. and Potocky, L., Proceedings of Conference: Metallic Glasses Science and Technology, ed. Hargitai, C., et al., Hungarian Academy of Science, Budapest, Hungary, 1980.